MEASUREMENTS OF VISCOELASTIC PROPERTIES

BY NANOINDENTATION

By

GANG HUANG

Bachelor of Science in Mechanical Engineering
Huazhong University of Science and Technology
Wuhan, China
1997

Master of Science in Mechanical Engineering
Huazhong University of Science and Technology
Wuhan, China
2000

Submitted to the Faculty of the
Graduate College of the
Oklahoma State University
in partial fulfillment of
the requirements for
the Degree of
DOCTOR OF PHILOSOPHY
May, 2007

MEASUREMENTS OF VISCOELASTIC PROPERTIES

BY NANOINDENTATION

Dissertation Approved:

Dr. Hongbing Lu

Dissertation Adviser

Dr. Don. A. Lucca

Dr. Andrew S. Arena

Dr. Leticia Barchini

Dr. Demir Coker

Dr. A. Gordon Emslie

Dean of the Graduate College

ACKNOWLEDGEMENTS

I would like to express my sincere gratitude to my advisor, Dr. Hongbing Lu, for his supervision throughout my entire Ph.D. study. I appreciate his intelligent, perseverant, warmhearted, and inspiring guidance. I am also grateful for his generous financial support to allow me to complete my research work in the program. I would like to thank all other members of my thesis committee, Dr. Don A. Lucca, Dr. Andrew S. Arena, Jr. and Dr. D. Coker from the School of Mechanical and Aerospace Engineering, Dr. Leticia Barchini from the Department of Mathematics. My thanks also extend to the faculty and staff of the Mechanical and Aerospace Engineering. I would express respectful thanks to Dr. Bo Wang for his guidance and advice in my research work. I would also appreciate Dr. Rong Z. Gan from the School of Aerospace and Mechanical Engineering at the University of Oklahoma for her diligent supervision during my research work on nanoindentation of biological tissues.

I would also thank Dr. Jin Ma, Mr. Nitin Daphalapurkar, Ms. Haowen Yu, Dr. Huiyang Luo for their constructive suggestions and discussions during my research work. I would thank all other members in Dr. Hongbing Lu's research group for the compatible and enjoyable environment.

My research work was initially supported by the National Science Foundation under CMS-9985060, and was supported by NASA under grant NNL04AA4ZG with Dr. Thomas S. Gates, the technical manager, as the technical director since early 2005.

The work on nanoindentation of eardrum is supported by NIH (NIDCD R01DC006632).

I would express my sincere gratitude to my parents, my sister and my brother for their unconditional support, understanding, and confidence on me all the time. Without their endless and consistent support, none of my research work could be possible. This dissertation is dedicated to my whole family.

TABLE OF CONTENTS

Chapter Page

I. INTRODUCTION 1
II. FUNDAMENTAL THEORIES ON NANOINDENTATION 10
2.1 Elastic indentation problem 10
2.2 Local stress-strain analysis of indentation problem 14
2.3 Linear viscoelasticity 18
2.4 Linearly viscoelastic indentation problem 19
III. MEASUREMENTS OF CREEP COMPLIANCE (TIME-DOMAIN) USING NANOINDENTATION 21
3.1 Analytical prerequisites 21
3.2 A corrected method to obtain creep function under a step loading 24
3.3 Experiments 27
3.4 Result and discussion 28
IV. MEASUREMENTS OF COMPLEX CREEP COMPLIANCE (FREQUENCY DOMAIN) USING NANOINDENTATION 32
4.1 Introduction 32
4.2 Theoretical background 35
4.3 Experiments 41
4.3.1 DMA experiments 41
4.3.2 Nanoindentation experiments 42
4.4 Results and discussions 44
4.4.1 DMA results 44
4.4.2 Nanoindentation results 45
4.5 Conclusions 56
V. MEASUREMENTS OF TWO INDEPENDENT VISCOELASTIC FUNCTIONS BY NANOINDENTATION 58
5.1 Introduction 58
5.2 Analytical Background 59
5.2.1 Indentation by rigid axisymmetric indenters of arbitrary shape 60
5.2.2 Berkovich indenter 63
5.2.3 Viscoelastic solutions 66
5.3 Nanoindentation measurements 70
5.4 Results and discussions 72
5.5 Conclusions 80
VI. APPLICATION OF NANOINDENTATION TO MEASURING VISCOELASTIC FUNCTION FOR THIN FILMS I: SINGLE WALL CARBON NANOTUBE (SWNT) 82
6.1 Introduction 82

6.2 Analytical prerequisites 84
6.3 Experimental details 86
6.3.1 SWNT/ polyelectrolyte films preparation 86
6.3.2 Measurements 88
6.4 Results and Discussions 90
6.5 Conclusions 96
VII. APPLICATION OF NANOINDENTATION TO MEASURING VISCOELASTIC FUNCTION FOR THIN FILMS II: TYMPANIC MEMBRANE 98
7.1 Introduction 98
7.2 Analytical prerequisites 100
7.2.1 Measurements of the through-thickness properties using nanoindentation 100
7.2.2 Analytical solution for the measurement of in-plane viscoelastic properties of TM under a central concentrated load 100
7.3 Nanoindentation experiments 103
7.4 Results and discussions 107
7.4.1 Relaxation modulus measured from through-thickness nanoindentation tests 107
7.4.2 Analytical results of the Young's relaxation modulus from in-plane nanoindentation tests on TM 118
7.5 Conclusions 121
VIII. MEASUREMENTS OF RELAXATION MODULUS USING NANOINDENTATION 123
8.1. Analytical Prerequisite 124
8.2. Nanoindentation Measurements 129
8.3. Results and Discussions 132
8.4. Conclusions 142
IX. SUMMARY 144
REFERENCES 149

LIST OF TABLES

Table Page

6-1 Comparison of modulus data for the SWNT/polyelectrolyte and polyelectrolyte films determined from different approaches 94

7-1 Results of modulus (steady state) from nanoindentation measurements 121

LIST OF FIGURES

Figure Page

1-1 A schematic for the mechanism of nanoindentation 2
1-2 A schematic indentation using conical indenter (Oliver and Pharr, 1992).....2
1-3 A typical load-displacement curve of nanoindentation 3
2-1 Indentation of elastic layer by cylindrical indenter (Ling, Lai and Lucca, 2002) 13
2-2 Elastic indentation problem 15
3-1 A ramp loading history 25
3-2 Constant loading rate history and step loading history.....28
3-3 Load-displacement curves for Berkovich indenter and spherical indenter 29
3-4 Experiment curve and fitting curve for load-displacement 30
3-5 Creep compliance measured from nanoindentation 31
4-1 Comparison of storage compliance at 75 Hz computed by two methods (a) PC. (b) PMMA.....34
4-2 Geometry of the spherical indenter. (a) Schematic diagram of the indenter. (b) A TEM image of the spherical indenter tip. 36
4-5 Nanoindentation output from oscillation on a constant rate loading at 10 Hz. (a) Carrier load-depth curve. (b) History of amplitude of harmonic load. (c) Response of harmonic displacement amplitude. (d) Out-of-phase angle with correction 46
4-6 Comparison of contact radius results at 75 Hz using the Lee-Radok approach and the Ting approach. (a) Contact radius computed for PMMA under a harmonic load superimposed on a step loading. (b) Contact radius computed for PC under a harmonic load superimposed on a step loading. 47
4-7 Nanoindentation output from oscillation on a step loading at 75 Hz. (a) Carrier load-depth curve. (b) The history of harmonic load amplitude. (c) Response of harmonic displacement amplitude. (d) Out-of-phase angle with correction.....50

4-8 Complex compliance in shear from nanoindentation under a harmonic load superimposed on a constant rate loading. 53
4-9 Complex compliance in shear from nanoindentation under a harmonic load superimposed on a step loading. 54
5-1 A schematic of indentation on a half space by an axisymmetric indenter 61
5-2 Berkovich, conical and spherical indenters 63
5-3 FEM modeling 65
5-4 Nanoindentation load-displacement curves for PVAc 72
5-5 Minimization results of load-displacement curves for PVAc 74
5-6 Results of $K(t)$ and $\mu(t)$ for PVAc from nanoindentation 74
5-7 Nanoindentation load-displacement curves for PMMA 76
5-8 Minimization results of load-displacement curves for PMMA 77
5-9 Results of $K(t)$ and $\mu(t)$ for PMMA from nanoindentation 79
6-1 SEM and AFM images of SWNT/polyelectrolyte films. (a) SEM image of the cross section of a 100-layer SWNT/polyelectrolyte film; (b) AFM image of top surface of a monolayer SWNT/polyelectrolyte film. 87
6-2 Stress-strain curves of SWNT/polyelectrolyte and resin 90
6-3 Experimental and fitted nanoindentation load-displacement curves. (a) In-pane nanoindentation load-displacement curves for SWNT/polyelectrolyte films from nanoindentation measurements and the fitting method; (b) Through-thickness nanoindentation load-displacement curves for SWNT/polyelectrolyte films from experiments and fitting method; (c) Nanoindentation load-displacement curves of polyelectrolyte from experiments and fitting method. 91
6-4 Uniaxial relaxation modulus of SWNT/polyelectrolyte film and polyelectrolyte film measured by nanoindentation. (a) In-plane modulus measured by both fitting and differentiation methods for SWNT/polyelectrolyte films; (b) Out-of plane modulus measured by both fitting and differentiation methods for SWNT/polyelectrolyte films; (c) Modulus measured by both fitting and differentiation methods for polyelectrolyte films. 93
7-1 A schematic of a thin plate cconstant rateed at the perimeter and loaded with concentrated force at the center. 101

7-2 Image of the right TM (medial view). 104
7-3 Schematic of through-thickness and in-plane nanoindentation tests setup (a) through-thickness test; (b) In-plane test. 106
7-4 Through-thickness tests results for dry samples. (a) Load-displacement curves; (b) relaxation modulus E(t). 108
7-5 Through-thickness tests results for wet samples. (a) Load-displacement curves for the Posterior side of TM ; (b) Load-displacement curves for the Anterior side of TM; (c) The measured E(t). 110
7-6 Results for dry TMs from in-plane nanoindentation tests. (a) Load-displacement curves; (b) Correlation of load-displacement curves between finite element analysis and experiments; (c) E(t) determined from the analytical solution and finite element method..... 114
7-7 Load-displacement curves of wet TM from in-plane indentation tests. (a) Sample from posterior side of TM; (b) Sample form anterior side of TM. 115
7-8 Results for wet posterior and anterior samples from in-plane nanoindentation tests. (a) Correlation of load-displacement curves between finite element analysis and experiment; (b) E(t) determined from finite element method and the analytical solution…..……..116
8- 1 Schematic of conical indentation and the geometries of the Berkovich, conical and spherical indenters..... 125
8- 2 Displacement history for nanoindentation tests of PMMA, PC and PU using Berkovich indenter tip..... 131
8- 3 Nanoindentation load-displacement curves for PMMA, PC and PU using Berkovich indenter tip 132
8- 4 Fitted and measured curves for PMMA using Eq. (8-13) (Berkovich indenter tip) 134
8- 5 Results of $E(t)$ for PMMA measured from different methods..... 134
8- 6 Fitted and measured curves for PC using Eq. (8-13) (Berkovich indenter tip)..... 135
8- 7 Young's relaxation function $E(t)$ for PC measured from different methods..... 136
8- 8 Fitted and measured curves for PU using Eq. (8-13) (Berkovich indenter tip)..... 137
8- 9 Young's relaxation modulus $E(t)$ for PU measured from different methods 138

8- 10 Nanoindentation load-displacement curves for PMMA, PC and PU measured from nanoindentation tests using a spherical indenter tip, plotted with the fitted curve as described by Eq. (8-17). 141

CHAPTER I.

INTRODUCTION

Nanoindentation technique for measurements of mechanical properties has been developed since early 1980's. The areas of its applications have been growing in the past 15 years due to the commercial availability nanoindentation instrumentation and the ease of applying the technique to measure mechanical properties of very small amounts of materials, such as thin solid films, wires, components in MEMS and NEMS, for which it is a challenge to determine properties using conventional testing methods, such as tensile or tortional tests.

Nanoindentation is an extension of conventional indentation technique to micron and submicron scales. The conventional indentation tests have been established as a standard method to measure mechanical properties of materials for more than one century (Dieter, 1986). Fig. 1-1 shows a schematic setup for nanoindentation. In a typical nanoindentation test, or depth sensing test, a nanoidenter tip of certain geometry (usually, Berkovich, spherical, conical, or flat punch) indents into the workpiece, while the load applied and induced depth are recorded. The early understanding of indentation problem was attributed to Hertz (1896), hunter (1960), Boussinesq (1885) and Sneddon (1965). Hertz (1896) solved the problem of elastic contact between two spheres. The Hertzian problem was investigated by Hunter (1960) for viscoelastic materials. Boussineq (1885) derived

the solution for stress and strain distribution of concentrated force on half space of elastic materials. Sneddon (1965) generalized the relationship between load and depth of indentation for elastic axisymmetric indentation problems. These solutions laid the foundation for extracting mechanical properties (including viscoelastic properties) from nanoindentation data.

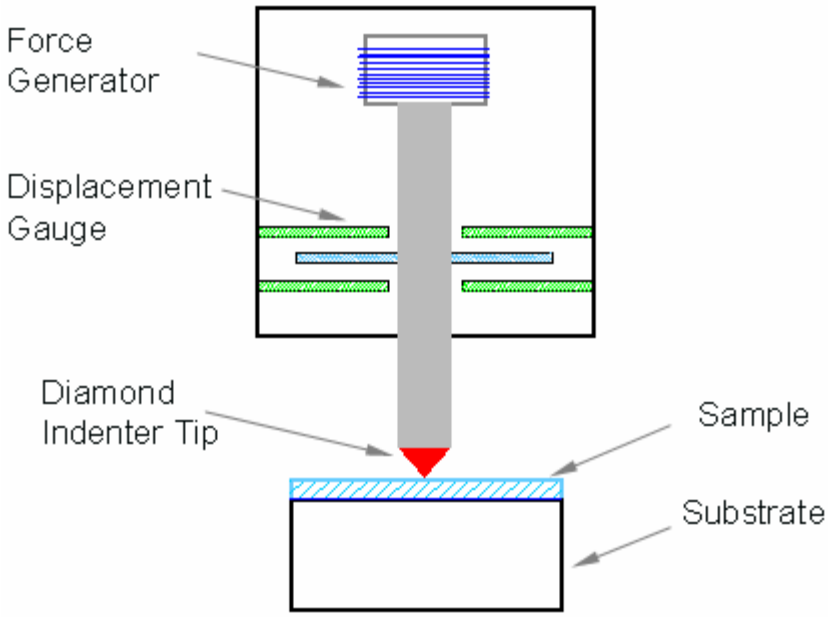

Fig. 1-1 A schematic for the mechanism of nanoindentation

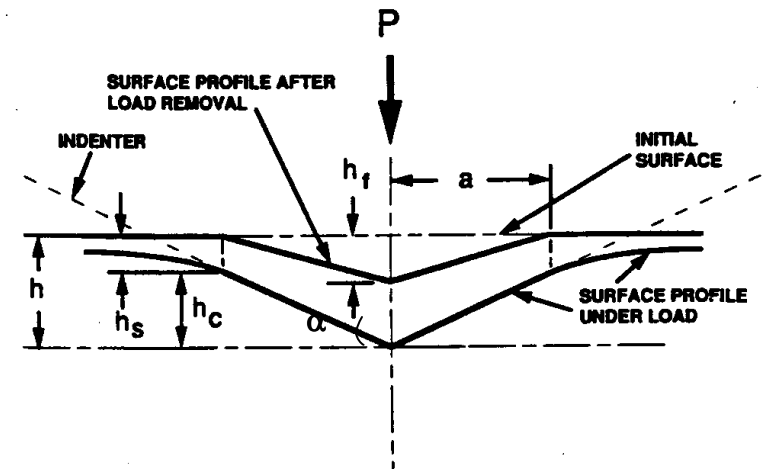

Fig. 1-2 A schematic indentation using conical indenter (Oliver and Pharr, 1992)

A contact profile from nanoindentation using a conical indenter is depicted in Fig. 1-2. In this figure, h is the indentation depth (the tip displacement) that is composed of h_s, the depth at perimeter of the free surface, and h_c, the contact depth, h_f is the depth of impression after load is fully removed and *a* is the contact radius. Fig. 1-3 shows a typical form of nanoindentation load- displacement data. Conventional indentation tests deal primarily with relatively large deformation. The hardness of a material is obtained by the maximum indentation force divided by the projected area of final impression measured optically after the load is removed (Pethica, Hutchings, Oliver 1983).

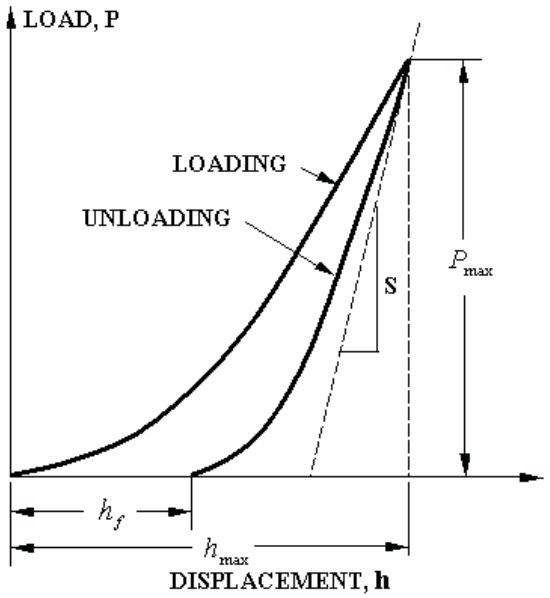

Fig.1-3

Fig. 1-3 A typical load-displacement curve of nanoindentation

With the increasing applications of very small structures, such as MEMES (Mirco-Electronic-Mechanical System), and very small amounts of material, such as thin film deposited on substrates, indentation technique was developed to provide an approach for

measuring properties at micron and sub-micron scales. Oliver, Hucthings and Pethica (1986) proposed a method to determine the hardness by calculating the contact area with the depth of impression obtained after indentation load is removed. Doerner and Nix (1991), Oliver and Pharr (1991, 1992) later refined the method to determine the contact area through indenter shape calibration. Using the contact area at maximum load and by considering Sneddon's solution for an elastic indentation problem, they developed methods to measure elastic modulus and hardness. In their improved methods, the contact area is measured at submicron resolution without the necessity to image optically the indent impression, as conventional indention tests did. Thus their improved methods have simplified nanoindentation testing procedures significantly on elastic-plastic materials.

While nanoindentation technique has been widely applied for elastic materials, it has attracted increasing attention for measuring mechanical properties of viscoelastic materials, such as polymers. Since the invention of synthetic polymers last century, they have been increasingly used in mechanical and chemical engineering. Due to their high specific strength, ease of fabrication and high corrosion resistance, they are anticipated to play an important role in some engineering areas, such as medical, automotive and aerospace industry. In these applications, how to measure reliably and effectively mechanical properties of polymers is critical to understand the deformation and failure of polymers and their components. In a variety of applications involving use of small amounts of polymers, such as filaments and fibers used in medical implants, polymer films deposited on substrates, the conventional methods are not suitable to measure some mechanical properties, such as Young's modulus in the through-thickness direction. Consequently, nanoindentation becomes an important technique in these situations.

Despite the fact that nanoindentation technique for measurements of some properties, such as Young's modulus and hardness for elastic-plastic materials, has been well established and used widely, nanoindentation on viscoelastic materials is not fully understood even in the regime of linear viscoelasticity. For nanoindentation on viscoelastic materials in the regime of linear viscoelasticity, the viscoelastic properties in both time domain and frequency domain are often of interest. In this dissertation, methods are presented to measure viscoelastic functions in both time and frequency domains for time-dependent materials using nanoindentation.

Solutions to linearly viscoelastic contact mechanics problems have been derived in the past. Radok (1960) found analytical solution to the viscoelastic contact problem involving a spherical indenter; some results have been reported on indentation on viscoelastic materials. Shimizu, Yanagimoto and Sakai (1999), Sakai and Shimizu (2001) investigated the viscoelastic response of soda lime silica glass through pyramidal indentation at glass transition temperature. Cheng et al. (2000) measured the relaxation modulus using a flat-ended cylindrical punch for a polymer that can be described by a three-element model. Vanlandingham et al. (2005) measured relaxation modulus under a near-step displacement and creep compliance using a near-step loading and investigated the applicability of linear viscoelasticity in nanoindentation on polymers. Cheng and Cheng (2005) derived an expression of unloading stiffness for a linearly viscoelastic solid under nanoindentation. These investigations are useful under their respective situations but are far from complete.

For measurement of viscoelastic properties in frequency domain using nanoindentation, Loubet et al. (1995) proposed a method based on analogy between

indention under cyclic loading and uniaxial counterpart, but there was no rigorous theory to support it. To use nanoindentation to find the viscoelastic properties of a general viscoelastic material in linear regime, consensus methods need to be developed, which is the objective of this work. In this dissertation (Chapter 4), from the original definition, an analytical method is derived to compute the complex creep compliance. And with the data provided by dynamic indentation experiments, the creep compliance for some solid polymer materials is obtained. They are compared with conventional counterparts to validate the method. The details will be presented later in this study.

Poisson's ratio, as one of two independent mechanical properties for isotropic linearly elastic (or viscoelastic) materials, plays a very important role in the deformation of materials, and is often assumed as constant in the measurement of some material properties, such as creep compliance in nanoindentation. While it is adequate to assume the Poisson's ratio as a known constant value for viscoelastic materials, such as polymers, well below the glass transition temperature, analysis based on assumption of a constant Poisson's ratio above glass transition temperature can induce considerable errors, since the Poisson's ratio of the viscoelastic material under this situation varies with time. In this dissertation, a method is developed to measure two independent viscoelastic functions using nanoindentation without recourse to the assumption of a constant Poisson's ratio.

This dissertation consists of nine chapters. In the first three chapters, background on the measurements of viscoelastic properties using nanoindentation is reviewed and methods for measuring linearly viscoelastic functions are developed and validated. In

the two chapters that follow, the developed methods are applied to two different films to determine the relaxation modulus. The dissertation is organized as follows.

In Chapter 2, previous methods from literature for measurements of elastic properties are reviewed; some theories on elastic and contact mechanics problems are summarized.

In Chapter 3, methods are developed for measuring creep compliance in time domain using nanoindentation under two quasi-static loading histories, namely, a constant rate loading and a step loading. Equations for determining creep compliance are derived and validated using two solid polymers, polymethyl methacrylate (PMMA) and polycarbonate (PC).

In chapter 4, a method is developed for measuring creep compliance in frequency domain using nanoindentation under dynamic loading histories which are achieved by superimposing a small oscillation upon a constant rate loading or step loading. Equations for determining complex creep compliance are derived and validated using PMMA and PC through comparing the nanoindentation data to data from Dynamic Mechanical Analysis.

In Chapter 5, a method is developed to measure two shear relaxation modulus and shear bulk modulus using nanoindentation assuming Poisson's ratio as functions of time. The method is validated on two bulk polymers, namely, poly(vinyl acetate) (PVAc) and PMMA above and below the glass transition temperatures, respectively.

In Chapter 6, methods for measuring in-plane and out-of-plane relaxation moduli are applied to single-wall carbon nanotube composite films made by layer by layer assembly.

In Chapter 7, the out-of-plane relaxation modulus of Tympanic Membrane is determined using the methods developed for measuring viscoelastic functions in time domain; the in-plane relaxation modulus is determined by a method based on the correlation between load-displacement results from finite element analysis and those from nanoindentation, and through the analytical analysis of the load-displacement data for a clamped circular film subjected to a central concentrated force.

In Chapter 8, methods are presented to measure uniaxial/shear relaxation modulus for linearly viscoelastic materials using nanoindentation. A constant rate displacement loading history is applied in nanoindentation tests. Based on viscoelastic contact analysis, uniaxial/shear relaxation modulus is extracted from nanoindentation load-displacement data from nanoindentation experiments. The methods for direct measurement of shear relaxation modulus can avoid the solution of an ill-posed problem in conversion from creep functions determined using load control in nanoindentation.

Chapter 9 gives a thorough summary for the dissertation.

In measurements of mechanical properties of viscoelastic materials, one of interesting and hardly-understood phenomena in nanoindentation is the appearance of negative slope in the unloading load-displacement curve for some polymers. To date, in literature there has been no quantitative explanation for this phenomenon. A rigorous approach to address the negative phenomenon is suggested for implementation in future work. Another work is to determine the master curves of viscoelastic properties for polymers using nanoindentation. Determination of the master curve for polymers is very important to predict the long-term behavior. In contrast from the measurements of viscoelastic properties at room temperature at which Poisson's ratio can normally be assumed as a

constant for polymers with much higher Tg than room temperature, the Poisson' ratio can no longer be assumed to be constant since in the development of master curves nanoindentation has to be conducted at a series of elevated temperatures at which Poisson's ratio changes with time. To analyze data at elevated temperatures the methods introduced in Chapter 5 for the measurements two independent viscoelastic functions can be applied, and shear relaxation modulus (or bulk modulus) functions can be measured at different temperatures to form master curves using the time-temperature superposition principle.

CHAPTER II.

FUNDAMENTAL THEORIES ON NANOINDENTATION

Some theories on elasticity, linear viscoelasticity, that form the foundation for nanoindentation technique, are summarized in this chapter. Linear elastic contact mechanics will be introduced, followed by linear viscoelastic analysis.

2.1 Elastic indentation problem

For an elastic problem of contact between a spherical indenter and a half-space, Hertz (1896) derived the pressure (the normal stress) in the contact region

$$-p = \frac{4\mu}{\pi R(1-\nu)}\sqrt{r_0^{\,2} - r^2}\,, \qquad 0 < r < r_0 \tag{2-1}$$

where μ is shear modulus, ν the Poisson's ratio, R the radius of the spherical indenter, and r_0 contact radius.

Integrating over the contact area yields the force applied by the indenter.

$$P = \frac{4\mu}{\pi R(1-\nu)}\int_0^{r_0} 2\pi r\sqrt{r_0^{\,2} - r^2}\,dr\,, \tag{2-2}$$

which leads to:

$$P = \frac{8\mu}{3(1-\nu)R}r_0^{\,3}\,. \tag{2-3}$$

According to Hunter (1960), for a rigid spherical indenter, if $h \ll R$

$$r_0^{\,2} = Rh\,, \tag{2-4}$$

where h is the displacement of tip of indenter.

From Eqs. (2-3) and (2-4), the relationship between loading and displacement for spherical indentation is:

$$P = \frac{8\mu\sqrt{R}}{3(1-\nu)} h^{\frac{3}{2}}. \tag{2-5}$$

Sneddon (1965) derived the general expressions for depth and loading in terms of indenter shape function. He also obtained relationship between loading and depth for several indenter tips. His equations for flat and conical indenters are widely used. For indentation by a flat-end circular indenter tip, the Sneddon's equation for load-displacement is:

$$P = \frac{4\mu R}{1-\nu} h\,, \tag{2-6}$$

where R is the radius of flat indenter.

For conical indenter, the equation is

$$P = \frac{4\mu \cot\alpha}{\pi(1-\nu)} h^2 \tag{2-7}$$

where α is denoted as shown in Fig. 1-2.

It is noted that above equations are limited to rigid indenter, with an elastic modulus assumed to be infinity. For the problem of a deformable indenter indenting into a half-space, the reduced modulus was introduced (Ficher-Cripps, 1999). For conical indention, the loading-depth equation is then

$$P = \frac{8E_r \cot\alpha}{\pi} h^2, \tag{2-8}$$

where E_r is reduced modulus, which is expressed as

$$\frac{1}{E_r} = \frac{1-v^2}{E} + \frac{1-v_i^{\ 2}}{E_i}, \tag{2-9}$$

where v and v_i are the Poisson's ratios of the sample material and the indenter, respectively, and E, E_i are the Young's modulus data of the sample material and the indenter, respectively.

A detailed derivation for solutions to indentation problem of elastic half space by rigid cylindrical, conical and spherical indenters, as well by elastic indenters was given by Ling, Lai and Lucca (2002). They also gave solutions to indentations of rigid indenters into an elastic layer supported by a rigid plane. For example, for indentation by a cylindrical indenter into a elastic layer with a height of h supported by a rigid substrate (Fig.2-1), Eq. (2-6) is changed into

$$\frac{P(1-v)}{4\mu Ha} = \int_0^1 \omega_1(\xi) d\xi, \tag{2-10}$$

where

$$\omega_1(\xi) = 1 - \frac{1}{\pi}\int_0^1 \omega_1(\beta)\left[K(\beta+\xi) + K(\beta-\xi)\right] d\beta, \tag{2-11}$$

and K is determined by

$$K(u) = \frac{a}{h}\int_0^\infty \frac{(3-4v)(\sinh\alpha)e^{-\alpha} - \left[\alpha(1+\alpha) + 4(1-v)^2\right]}{\alpha^2 + 4(1-v^2) + (3-4v)\sinh^2\alpha} \cos\left(\frac{a\alpha u}{h}\right) d\alpha. \tag{2-12}$$

This result is very conducive for the investigation of the mechanical behavior of solid thin film using nanoindentation.

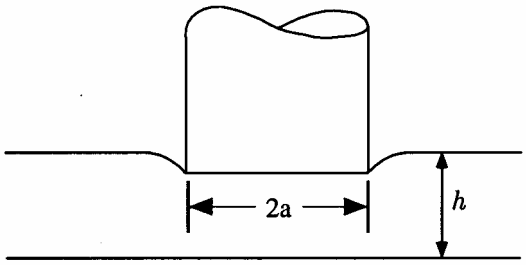

Fig. 2-1 Indentation of elastic layer by cylindrical indenter (Ling, Lai and Lucca, 2002)

Usually the indenters used are made of diamond so that they can be considered as rigid materials, especially for indentation on polymers as the difference in modulus data is two orders of magnitude. Consequently, in this dissertation, the equations for elastic indentation can be applied readily without considering deformation of the indenter.

In indentation on elastic-plastic materials, the contact area between indenter and sample material is needed to extract properties, such as elastic modulus and some other properties. Doerner and Nix (1986) found a linear relationship between contact stiffness and square root of projected contact area. King (1987) also found the same relationship through finite element simulation. Take spherical indentation as an example, differentiating Eq. (2-5) with respect to h leads to

$$S = \frac{dp}{dh} = \frac{4\mu\sqrt{R}}{1-\nu}\sqrt{h}\,, \tag{2-13}$$

where S is the contact stiffness. Considering $r_0^{\,2} = Rh$, we have

$$S = \frac{dp}{dh} = \frac{2\sqrt{A}E}{\sqrt{\pi}(1-\nu^2)}\,. \tag{2-14}$$

Pharr, Oliver and Brotzen (1992) demonstrated that above equation is the general relationship between contact stiffness, contact area and modulus for all kinds of

axisymmetric rigid indenters. Based on the above equation, Oliver and Pharr (1992) proposed an improved method to measure Young's modulus and hardness. In their method, the load-displacement curve at initial unloading is fitted with a power law equation. The power law equation is used to calculate the stiffness *S*. The contact areas which is function of the contact radius is determined by relating contact radius h_c to the indentation displacement h, based on Sneddon's solution to axisymmetric indentation problem. The contact area, taken as function of contact depth after indenter shape calibration, has such form as follows

$$A = a_0 h_c^{\,2} + a_1 h_c + a_2 h_c^{\,1/2} + a_3 h_c^{\,1/4} + a_4 h_c^{\,1/8} \cdots \tag{2-15}$$

The Young's modulus is then calculated through Eq. (2-14) after the contact area and contact stiffness are known. The method documented by Oliver and Pharr is regarded as a standard technique to measure elastic properties, and has been frequently quoted in nanoindentation. In this dissertation, some part of this method will also be applied and compared for indentation on polymers.

2.2 Local stress-strain analysis of indentation problem

Sneddon (1965) found the relation of indentation load and depth, and he also gave the pressure distribution in indentation direction. In this section, equations for the local surface stress of sample are derived based on displacement field proposed by Sneddon on elastic indentation problem.

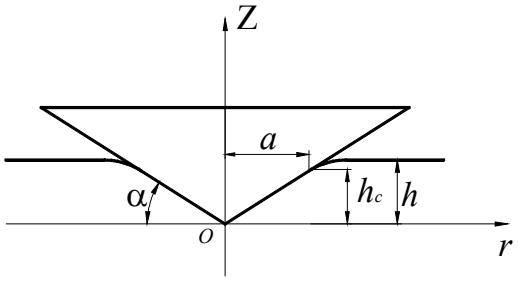

Fig. 2-2 Elastic indentation problem

Boundary condition:

$$\sigma_{rz}(r,0) = 0,$$

$$u_z(r,0) = h - f(r/a), \quad 0 \le r \le a \tag{2-16}$$

$$\sigma_{zz}(r,0) = 0, \quad r > a$$

where *f(r/a)* is the shape function, expressed as the depth of the tip to the cross section of radius of *r*.

Sneddon showed that displacement components fields could be specified as "dual integral equations" as follows

$$u_r(r,z) = -\frac{a}{2(1-\nu)}\hbar_1[(1-2\nu-\xi z)\xi^{-1}\psi(\xi a)e^{-\xi z}],$$

$$u_z(r,z) = \frac{a}{2(1-\nu)}\hbar_0[(2(1-\nu)+\xi z)\xi^{-1}\psi(\xi a)e^{-\xi z}], \tag{2-17}$$

$$(u_\theta = 0)$$

where $\hbar_\eta[f(\xi,z)] = \int_0^\infty \xi f(\xi,z) J_\eta(\xi r) d\xi$, is Hankel transform of order of η (η=0,1 in this case).

And among these equations, $\psi(\xi)$ can be represented as

$$\psi(\xi) = \int_0^1 \chi(t)\cos(\zeta t)dt\,. \tag{2-18}$$

Sneddon (1965) obtained the function $\chi(t)$ for different kinds of indenter. For conical indenter,

$$\chi(t) = \frac{2h}{\pi}(1-t)\,. \tag{2-19}$$

Substituting (2-19) into (2-18), one has

$$\psi(\zeta) = \frac{2h}{\pi}\frac{1}{\zeta^2}(1-\cos\zeta)\,. \tag{2-20}$$

Substituting (2-20) into (30-16), one has

$$\begin{aligned} u_r(r,0) &= -\frac{a}{2(1-v)}\hbar_1[(1-2v-\xi z)\xi^{-1}\psi(\xi a)e^{-\xi z}] \\ &= -\frac{a(1-2v)}{2(1-v)}\int_0^\infty J_1(\xi r)d\xi\int_0^1 \chi(t)\cos\xi a t dt \\ &= -\frac{a}{2(1-v)}\int_0^\infty J_1(\zeta x)d\xi\int_0^1 \chi(t)\cos\zeta t dt \qquad \left(x=\frac{r}{a},\ \text{and } x\geq t\right) \\ &= -\frac{1-2v}{2(1-v)}\int_0^1 \frac{1}{x}\frac{2h}{\pi}(1-t)dt \\ &= \frac{2v-1}{2(1-v)}\frac{ah}{r\pi}\quad, \end{aligned} \tag{2-21}$$

$$u_z(r,0) = h - f(r/a) = h - r\tan\alpha\,, \tag{2-22}$$

$$u_\theta = 0\,. \tag{2-23}$$

Next, strain is determined from Eqs. (2-17) and (2-21). Because of axisymmetric characteristic for nanoindentation problems, the strain field can be computed as following:

$$\varepsilon_z = \frac{\partial u_z}{\partial z}; \qquad \varepsilon_r = \frac{\partial u_r}{\partial r}; \qquad \varepsilon_\theta = \frac{u_r}{r}. \tag{2-24}$$

Then

$$\varepsilon_z = \frac{\partial u_z}{\partial z} = -\frac{a(1-2v)}{2(1-v)}\int_0^\infty J_0(\xi r)\psi(\xi a)\frac{\partial}{\partial z}\{[2(1-v)+\xi z]e^{-\xi z}\}d\xi, \tag{2-25}$$

$$\varepsilon_{z=0} = \frac{a(2v-1)}{2(1-v)}\int_0^\infty J_0(\xi r)\psi(\xi a)\xi d\xi$$

$$= \frac{2v-1}{2(1-v)a}\hbar_0[\psi(\zeta)]. \tag{2-26}$$

From Sneddon's solution for $\sigma_z(r,0)$,

$$\sigma_z(r,0) = -\frac{\mu}{a(1-v)}\hbar_0[\psi(\zeta)]$$

$$= -\frac{2\mu h}{\pi a(1-v)}\cosh^{-1}(a/r), \tag{2-27}$$

we can derive

$$\varepsilon_z = \frac{(2v-1)h}{\pi(1-v)a}\cosh^{-1}(a/r), \quad (z=0) \tag{2-28}$$

$$\varepsilon_r = \frac{\partial u_r}{\partial r} = \frac{1-2v}{2(1-v)}\frac{ah}{r^2\pi}, \qquad (z=0) \tag{2-29}$$

$$\varepsilon_\theta = \frac{u_r}{r} = -\frac{1-2v}{2(1-v)}\frac{ah}{r^2\pi}. \qquad (z=0) \tag{2-30}$$

Substituting Eqs. (2-28), (2-29) and (2-30) into Stress- Strain relationship, one can obtain stresses at the surface (z = 0),

$$\sigma_r = \frac{E}{1+v}\left(\frac{v}{1-2v}\varepsilon_{kk} + \frac{\partial u_r}{\partial r}\right)$$

$$= \frac{E(2v-1)}{1-v^2}\left[\frac{v}{1-2v}\frac{h}{\pi a}\cosh^{-1}\left(\frac{a}{r}\right) - \frac{1}{2}\frac{ah}{r^2}\right], \tag{2-31}$$

$$\sigma_\theta = \frac{E}{1+v}\left(\frac{v}{1-2v}\varepsilon_{kk} + \frac{u_r}{r}\right)$$

$$= \frac{E(2v-1)}{1-v^2}\left[\frac{v}{1-2v}\frac{h}{\pi a}\cosh^{-1}\left(\frac{a}{r}\right) + \frac{1}{2}\frac{ah}{r^2}\right], \tag{2-32}$$

$$\sigma_z = -\frac{2\mu h}{\pi a(1-v)}\cosh^{-1}(a/r)\,;\ \ \sigma_{rz} = \sigma_{r\theta} = \sigma_{\theta z} = 0\,. \tag{2-33}$$

According to Sneddon, for conical indenter, there are $P = \frac{\pi\mu a^2}{1-v}\tan\alpha$, $h = \frac{1}{2}\pi a\tan\alpha$.

Using these relationships, we can rewrite Eqs. (2-31) and (2-32) in another form,

$$\sigma_r = -\frac{\mu}{1-v}v\tan\alpha\cdot\cosh^{-1}\left(\frac{a}{r}\right) + \frac{(1-2v)}{2\pi r^2}P\,, \tag{2-34}$$

$$\sigma_\theta = -\frac{\mu}{1-v}v\tan\alpha\cdot\cosh^{-1}\left(\frac{a}{r}\right) - \frac{(1-2v)}{2\pi r^2}P\,. \tag{2-35}$$

These and Sneddon's result for σ_z ,

$$\sigma_z = -\frac{2\mu h}{\pi a(1-v)}\cosh^{-1}(a/r)\,, \tag{2-36}$$

give all the stress components in elastic contact problem at the interface of the contact surface and free surface, $r = a$. These stress components are

$$\sigma_{rr}' = \sigma_r = \frac{\pi(1-2v)}{2a^2}P\,, \tag{2-37}$$

$$\sigma_{\theta\theta}' = \sigma_\theta = -\frac{\pi(1-2v)}{2a^2}P\,, \tag{2-38}$$

$$\sigma_z' = \sigma_z = 0\,. \tag{2-39}$$

2.3 Linear viscoelasticity

The stress-strain relation can be described by convolution integral based on Boltzman

superposition principle, which takes stress (strain) prehistory into consideration. The linearly viscoelastic constitutive law is

$$\varepsilon_{ij}(t) = \int_{-\infty}^{t} D_{ijkl}(t-\zeta)\frac{d\sigma_{kl}(\zeta)}{d\zeta}d\zeta \,. \tag{2-40}$$

where D_{ijkl} are components of creep tensor, ε_{ij} and σ_{kl} are shear strains and shear stresses, respectively. For isotropic materials, the deviatoric stress- strain relations are

$$e_{ij}(t) = \frac{1}{2}\int_{-\infty}^{t} J(t-\zeta)\frac{dS_{ij}(\zeta)}{d\zeta}d\zeta \,, \tag{2-41}$$

and $$S_{ij}(t) = 2\int_{-\infty}^{t} \mu(t-\zeta)\frac{de_{ij}(\zeta)}{d\zeta}d\zeta \,, \tag{2-42}$$

where J and μ are creep compliance and relaxation modulus, respectively.

If time is defined as positive, one has

$$e_{ij}(t) = \frac{1}{2}J(t)S_{ij}(0^{+}) + \frac{1}{2}\int_{0}^{t} J_{ij}(t-\zeta)\frac{dS_{ij}(\zeta)}{d\zeta}d\zeta \tag{2-43}$$

and $$S_{ij}(t) = 2\mu(t)e_{ij}(0^{+}) + 2\int_{-\infty}^{t} \mu(t-\zeta)\frac{de_{ij}(\zeta)}{d\zeta}d\zeta \,. \tag{2-44}$$

2.4 Linearly viscoelastic indentation problem

Indentation into half space of a workpiece is a three dimensional problem. Because the contact stresses and strains are highly localized close to the contact area, and their magnitude decreased rapidly with distance from the point of contact, the deformation field is inhomogeneous. Therefore, with complexity of stress and strain distribution under the indenter, it is not practical to solve a viscoelastic indentation problem directly based

on the constitutive equations, such as Eqs. (2-40) and (2-41). It is noted that load and displacement are the only data output from nanoindentation. Thus, it is convenient to characterize the linearly viscoelastic behavior by examining load-displacement relationship.

For viscoelastic contact problems, Lee (1955) found his solution by applying inverse Laplace transformation of the corresponding elastic problem. However, such a method is valid only when the boundary conditions can be prescribed. For nanoindentation of viscoelastic materials, both the traction boundary and displacement boundary are changing with time as the contact between the indenter and the workpiece changes with time. It is not possible to predict explicitly the history of both traction boundary and displacement boundary. Therefore direct application of the correspondence principle is not appropriate for solving viscoelastic indention problem. Lee and Radok (1960) later proposed an approach applicable for viscoelastic contact problems with moving boundary conditions. They showed that the Hertzian contact problem in viscoelasticity could be solved by replacing the elastic constants in elastic problem with integral operators under condition of non-decreasing contact area, such that the corresponding viscoelastic problem could be expressed in hereditary form. Using the Hertzian solution to elastic indentation problem and assuming that the viscoelastic material is incompressible (Eq.2-5), the load-displacement relation follows for a spherical indenter,

$$\frac{1}{2}\int_0^t J(t-\tau)\frac{dP}{d\tau}d\tau = \frac{8}{3}\sqrt{R}h^{3/2}(t)\,. \tag{2-45}$$

In this dissertation, Lee and Radok's hereditary operator based on elastic indentation solution will be applied to develop a consensus method to measure viscoelastic properties of polymers.

CHAPTER III.

MEASUREMENTS OF CREEP COMPLIANCE (TIME-DOMAIN) USING NANOINDENTATION

3.1 Analytical prerequisites

In this section a method to measure local surface creep compliance for linearly viscoelastic materials is proposed and validated.

As introduced before, the load-displacement relationship for spherical indentation problem, i.e., Hertz problem is:

$$P = \frac{8\mu\sqrt{R}}{3(1-\nu)} h^{\frac{3}{2}}, \tag{3-1}$$

where μ is shear modulus, v Poisson's ratio, R the radius of the spherical indenter, and r_0 contact radius. Applying Lee and Radok's method, one has

$$h^{3/2}(t) = \frac{3(1-\nu)}{8\sqrt{R}} \int_{-\infty}^{t} J(t-\xi)\left[\frac{dP(\xi)}{d\xi}\right] d\xi, \tag{3-2}$$

Under a constant rate loading history, $P(t) = v_0 t H(t)$, with v_0 being loading rate, Eq. (3-2) becomes

$$h^{3/2}(t) = \frac{3(1-\nu)v_0}{8\sqrt{R}} \int_{0}^{t} J(\xi) d\xi, \tag{3-3}$$

where v_0 is loading rate. Differentiation of Eq.(3-3) with respect to time yields

$$J(t) = \frac{4\sqrt{R}\sqrt{h(t)}}{(1-\nu)v_0}\frac{dh}{dt}. \tag{3-4}$$

Sneddon's solution for elastic conical indentation problem, in terms of load-displacement relationship is

$$P = \frac{4\mu\cot\alpha}{\pi(1-\nu)}h^2 \tag{3-5}$$

where α is the angle between the cone generator and the substrate plane. Again applying Lee and Radok's method to Eq.(3-5) leads to:

$$h^2(t) = \frac{\pi(1-\nu)}{4\cot\alpha}\int_{-\infty}^{t} J(t-\xi)\left[\frac{dP(\xi)}{d\xi}\right]d\xi \tag{3-6}$$

Under a constant rate loading, $P(t) = v_0 tH(t)$, with $H(t)$ being Heaviside function, finally Eq.(3-6) becomes

$$J(t) = \frac{8h(t)}{\pi(1-\nu)v_0\tan\alpha}\frac{dh(t)}{dt} \tag{3-7}$$

Eq.(3-3) and Eq.(3-7) will be used for the computation of creep compliance in terms of derivative of displacement with respect to time under constant rate loading. Due to the fact that data from for displacement nanoindentation experiments are usually scattered, the derivative of displacement with respect to time based on experimental data can induce some error, even if the related curve is fitted. An alternative approach is proposed next.

The general representation of the creep function based on the generalized Kelvin model is

$$J(t) = J_0 + \sum_{i=1}^{N} J_i(1 - e^{-\frac{t}{\tau_i}}), \tag{3-8}$$

where $J_0, J_1, \cdots, J_N$ are compliance numbers, and $\tau_1, \tau_2, \cdots, \tau_N$ are retardation times.

For the Berkovich indenter, substituting Eq.(3-8) into Eq. (3-6) one has

$$h^2(t) = \frac{\pi(1-\nu)}{4\,ctg\ \alpha} v_0 [(J_0 + \sum_{i=1}^{N} J_i)t - \sum_{i=1}^{N} J_i \tau_i (1 - e^{-\frac{t}{\tau_i}})] \ . \tag{3-9}$$

Considering $P(t) = v_0 t$, Eq.(3-9) can be rewritten as

$$h^2(t) = \frac{\pi(1-\nu)}{4ctg\,\alpha}[(J_0 + \sum_{i=1}^{N} J_i)P(t) - \sum_{i=1}^{N} J_i (v_0 \tau_i)(1 - e^{-\frac{P(t)}{v_0 \tau_i}})] \ . \tag{3-10}$$

If we fit Eq. (3-10) into the experimentally measured load-displacement curve using the least square correlation, we can find a set of best-fit parameters $J_0, J_1, \cdots, J_N$ and $\tau_1, \tau_2, \cdots, \tau_N$. We may then substitute these constants to Eq. (3-8) to determine the creep function when the Berkovich indenter is used in nanoindentation.

The same method for data reduction to determine J(t) can be applied to a spherical indenter. For a spherical indenter, substitution of Eq. (3-5) into Eq. (3-3) leads to

$$h^{3/2}(t) = \frac{3(1-\nu)v_0}{8\sqrt{R}}[(J_0 + \sum_{i=1}^{N} J_i)t - \sum_{i=1}^{N} J_i \tau_i (1 - e^{-\frac{t}{\tau_i}})] \ , \tag{3-11}$$

Since $P(t) = v_0 t$, Eq.(3-11) can be rewritten as

$$h^{3/2}(t) = \frac{3(1-\nu)}{8\sqrt{R}}[(J_0 + \sum_{i=1}^{N} J_i)P(t) - \sum_{i=1}^{N} J_i (v_0 \tau_i)(1 - e^{-\frac{P(t)}{v_0 \tau_i}})] \ . \tag{3-12}$$

Similar to the approach for a conical indenter, we can fit Eq. (3-12) into the experimentally measured load-displacement curve to find a set of the best-fit parameters $J_0, J_1, \cdots, J_N$ and $\tau_1, \tau_2, \cdots, \tau_N$, we then substitute these parameters into Eq. (3-8) to determine the creep function when a spherical indenter is used in nanoindentation.

It is noted that applicability of the hereditary integral operator provided by Lee and Radok (1960) as shown in Eqs. (3-3) and (3-6) is based on the condition that contact area between indenter and workpiece is non-decreasing with time. It should be pointed out that in Eqs. (3-3) and (3-6) the Poisson's ratio is assumed to be constant.

3.2 A corrected method to obtain creep function under a step loading

Section 3.1 details the determination of creep function from indentation under ramp loading. Alternatively, under step loading the creep function could be also obtained. For a step loading suddenly applied in indentation, it could be expressed in terms of Heaviside function:

$$P(t) = P_0 H(t). \tag{3-13}$$

Substituting it into Eq.(3-6) , one can derive the creep function for Berkovich indenter:

$$J(t) = \frac{4h^2(t)}{\pi(1-\nu)P_0 \tan\alpha}. \tag{3-14}$$

Also substituting it into Eq.(3-2) , one has for spherical indentation:

$$J(t) = \frac{8\sqrt{R}h^{3/2}(t)}{3(1-\nu)P_0}. \tag{3-15}$$

Eqs. (3-14) and (3-15) are derived for theoretical step loading, however, such ideal step loading could never be realized in practice. On one hand, the sudden increase of loading will take some certain time, even though it is very short. On the other hand, even seemingly infinitesimal time of increase of sudden load will cause unfavorable impact on the instrument, which could induce error for experimental data. Thus, instead the creep test is implemented by applying ramp loading with short rise time (usually 1s in this

study) followed by constant loading hold for comparatively long time. According to conventional creep test, the beginning data for 10 times of the rising time are not reliable for computation, which means in creep indentation experiment, the initial data of 11 s cannot be taken for determination of creep function of linearly viscoelastic materials, i.e., the creep function for 11 s in the beginning is lost. Nonetheless, such a period of time is a considerable portion, if the whole time scale for experiment is not large. Lee and Knauss (2000) proposed a method to compute shear modulus for that period time of interest. They used Boltzman superposition principle to reformulate the relationship between stress and strain. To avoid the loss of the accurate data, this study took a method similar to that used by Lee and Knauss.

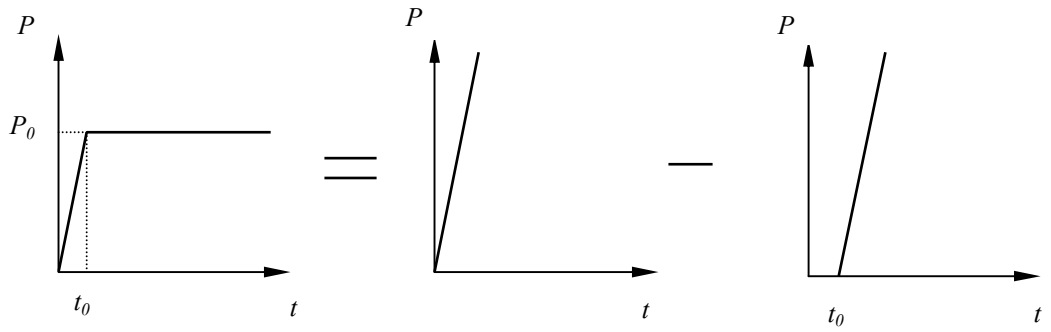

Fig. 3-1 A ramp loading history

The work presented by Lee and Knauss is on the data correction for uniaxial stress state, while indentation problem as discussed herein is a three dimensional stress state. Formulas need to be derived for data correction to determine the creep function using load-displacement relation in a viscoelastic indentation problem. As shown in Fig.(3-1), based on Boltzman superposition principle, a realistic loading, can be considered as the superposition of two different loading histories

$$P(t) = P_1(t) - P_2(t) = v_0 tH(t) - v_0(t - t_0)H(t - t_0), \tag{3-16}$$

where v_0 is the ramp loading rate.

For a conical indenter, substituting $P(t) = v_0 tH(t) - v_0(t - t_0)H(t - t_0)$ into Eq.(3-6), one has: When $t<t_0$,

$$h^2(t) = \frac{\pi(1-\nu)v_0 \tan\alpha}{4}\int_0^t J(\xi)d\xi; \tag{3-17}$$

and when $t>t_0$,

$$h^2(t) = \frac{\pi(1-\nu)v_0 \tan\alpha}{4}[\int_0^t J(t-\xi)d\xi - \int_{t_0}^t J(t-\xi)d\xi]$$

$$= \frac{\pi(1-\nu)v_0 \tan\alpha}{4}[\int_0^t J(\xi)d\xi - \int_0^{t-t_0} J(\xi)d\xi]. \tag{3-18}$$

Differentiation of Eqs.(3-17) and (3-18) with respect to time t yields

$$J(t) = \frac{8h(t)}{\pi(1-\nu)v_0 \tan\alpha}\frac{dh(t)}{dt} \qquad (t < t_0) \tag{3-19}$$

$$J(t - t_0) = J(t) - \frac{8h(t)}{\pi(1-\nu)v_0 \tan\alpha}\frac{dh(t)}{dt} \qquad (t \geq t_0) \tag{3-20}$$

Similarly, for a spherical indenter, the following results are obtained:

$$J(t) = \frac{4\sqrt{R}h^{1/2}(t)}{(1-\nu)v_0}\frac{dh(t)}{dt} \qquad (t < t_0) \tag{3-21}$$

$$J(t - t_0) = J(t) - \frac{4\sqrt{R}h^{1/2}(t)}{(1-\nu)v_0}\frac{dh(t)}{dt} \qquad (t \geq t_0) \tag{3-22}$$

Therefore, the procedure of data correction could be considered as reversed computation started at some point, for example, ten times of rise time. For a conical indenter, using

Eqs. (3-19) and (3-20), the data of the creep function determined by Eq. (3-14) can be corrected through the following steps:

(i) For $kt_0 \le t \le (k+1)t_0$, compute $J(t-t_0)$ at $t = kt_0 + m\lambda t_0$ by Eq. (3-20) and result of *J(t)* calculated with Eq. (3-14), where λ is some sufficiently small number, $0 < m \le 1/\lambda$, and k is a positive integer, usually $k \ge 10$.

(ii) For $(k-1)t_0 \le t \le kt_0$, compute $J(t-t_0)$ at $t = (k-1)t_0 + m\lambda t_0$ by Eq. (3-20) and result from (i).

(iii) Repeat the same step as (ii) for $(n-1)t_0 \le t \le nt_0$, where $n = k-1, k-2, \cdots, 3$.

(iv) For $0 \le t < t_0$, compute J(t) by Eq. (3-19).

For a spherical indenter, the same method can be used to correct the initial part of creep function. Simply replace Eqs. (3-14), (3-19) and (3-20) in (i)-(iv) for a conical indenter by Eqs. (3-15), (3-21) and (3-22), respectively.

3.3 Experiments

An MTS Nano Indenter XP system was employed in nanoindentation, where both Berkovich and spherical indenters were used. All the experiments were started after the indenter drift rate due to environment noise reached within 0.05nm/s. The room temperature and humidity were carefully monitored and maintained to be 22.5 ^{o}C and 50% respectively.

Two bulk polymers, Polycarbonate (PC) and Polymethyl Methacrylate (PMMA) were chosen as test materials. The glass transition temperature for PC and PMMA are 145 ^{o}C and 105 ^{o}C respectively. They were annealed for two hours at the temperature 5 ^{o}C above

their glass transition temperatures, and cooled down to room temperature at rate of 5 ^{o}C/hr. After annealing, the sample materials were stored at bell jar for 72 hours before the experiments were carried out.

3.4 Result and discussion

As shown in Fig.3-2, a ramp loading history and a step loading history were applied in the experiments. The resulted load-displacement curves at ramp loading for both Berkovich indenter and spherical indenter are shown in Fig.3-3.

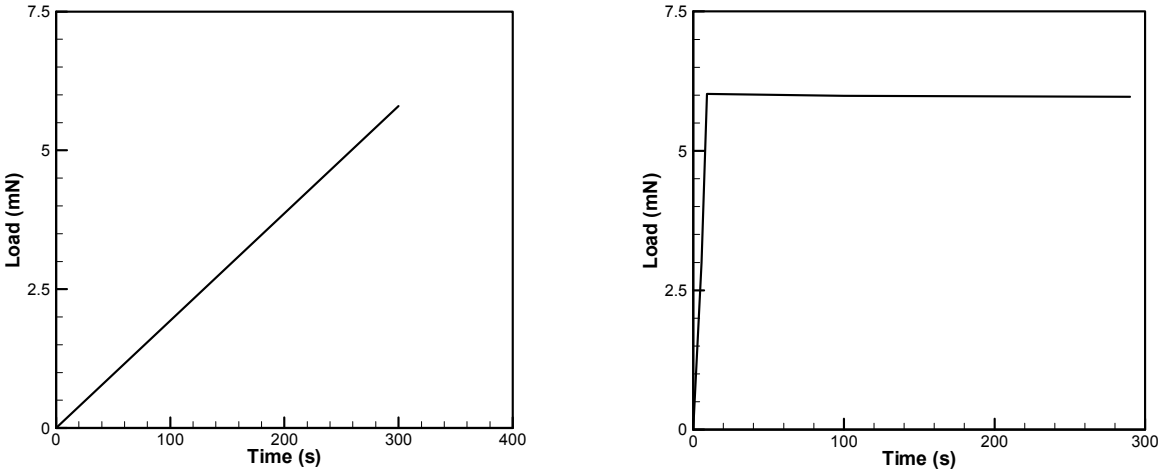

(a) Constant rate loading (b) Realistic step loading

Fig. 3-2 Constant loading rate history and step loading history

Because the measurement of creep function is based on linear viscoelasticity, it's critical that overall deformation in the course of indentation is within the limit of linearity. It is assumed that when the indentation depth is small enough, the displacement will be fully recovered some time after complete unloading, and it could be inferred that

the test materials should deform within the limit of viscoelastic linearity. One straightforward way to determine the linearity is to observe the impression after removal of the loading. After experiments, the material sample surface was observed with help of SEM (Scanning Electron Microscopy). It was found that for PMMA, when the depth was below 780 nm, no impression was observed. And also it was observed that for PC no impression left when the depth below 1123 nm. Thus approximately, the depth limit of linearity for PMMA and PC could be considered as 780 nm and 1123 nm respectively.

For experiment at ramp loading, the method in terms of derivative of displacement with respective to time and exponential fitting of load-displacement curve, i.e. Eqs.(3-4) and (3-7), were applied to retrieve the creep function for PMMA and PC. For curve fitting method, the load-displacement curve was fitted at displacement less than limit of linearity. Fig 3-4 shows the fitted curves for PMMA and PC.

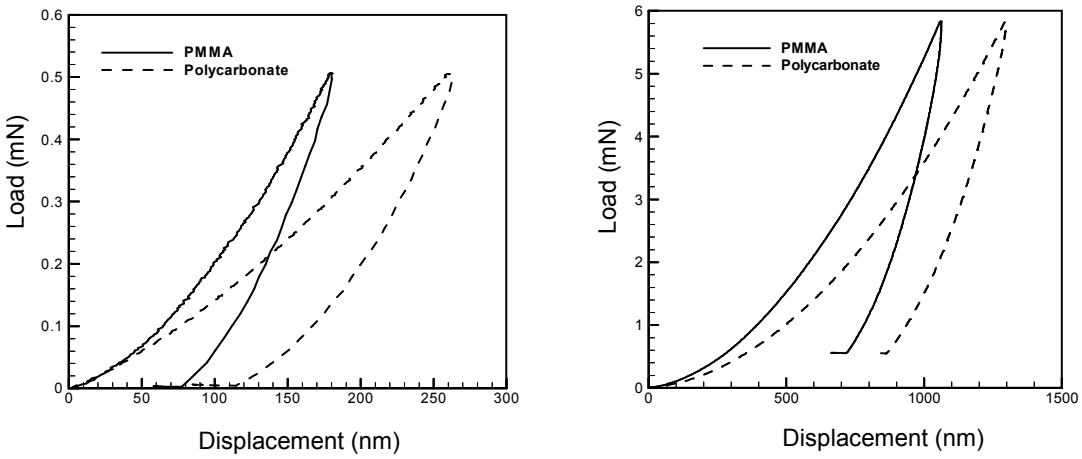

(a) Berkovich indenter (b) Spherical indenter

Fig. 3-3 Load-displacement curves for Berkovich indenter and spherical indenter

For experiment at step loading, the method introduced in Sec. 3.1.3 is used to correct data of creep function. Because of “fading effect” of viscoelastic materials, the creep

function after enough long time (here 20s) was computed using Eqs. (3-14) and (3-15), while the initial 20s of creep compliance data were computed from a reversed procedure described in Sec.3.2.

The final results for creep function from ramp loading experiment and step loading experiments are shown in Fig.3-5, where they were compared with conventional data.

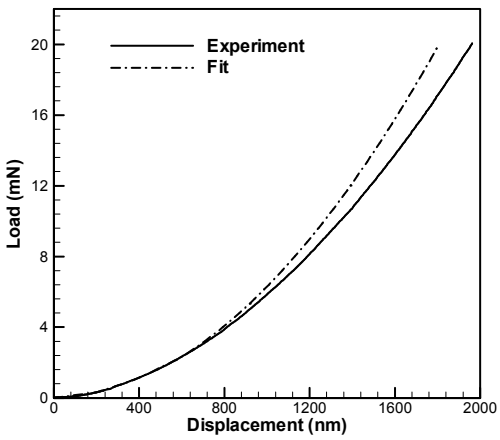

(a) PC using Berkovich indenter

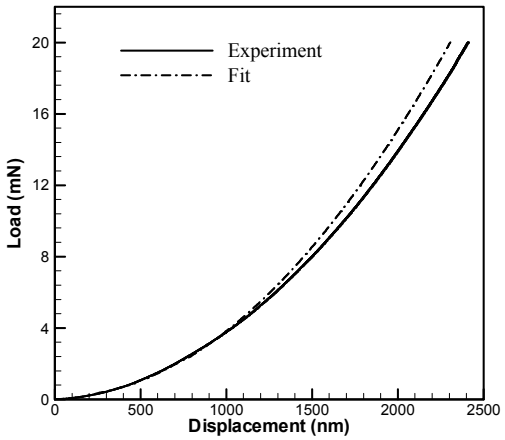

(b) PMMA using Berkovich indenter

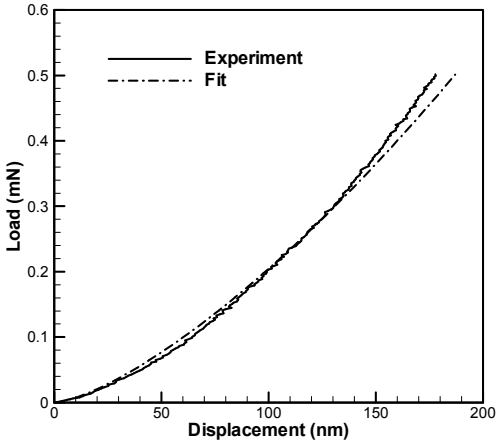

(c) PC using spherical indenter

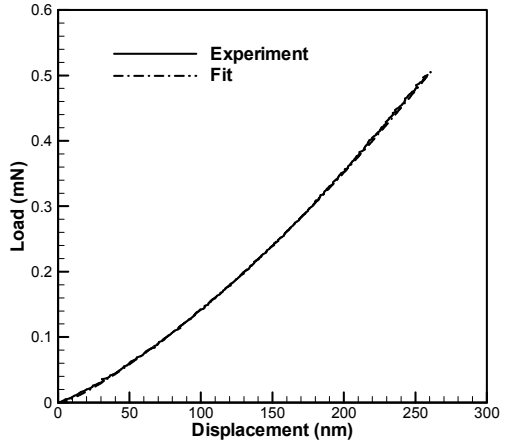

(d) PMMA using spherical indenter

Fig. 3-4 Experiment curve and fitting curve for load-displacement

Fig.3-5 shows that the measured creep compliance of represented solid polymers agree with well with the conventional data. Thus, within linear viscoelasticity, the introduced methods to compute creep function are validated to be appropriate for viscoelastic materials.

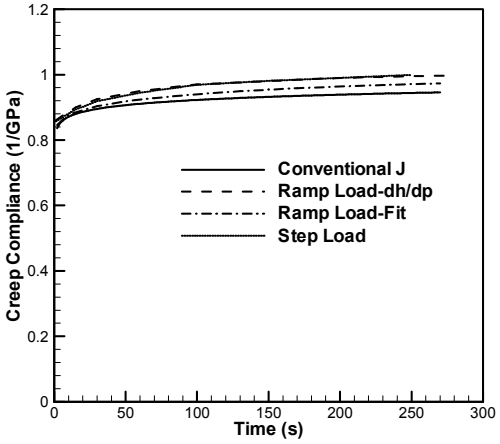

(a) PMMA using Berkovich indenter

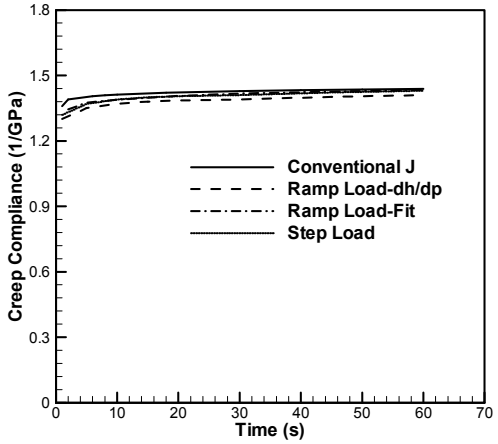

(b) PC using Berkovich indenter

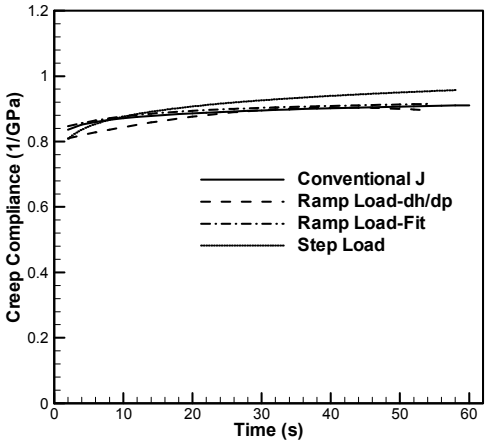

(c)PMMA using spherical indenter

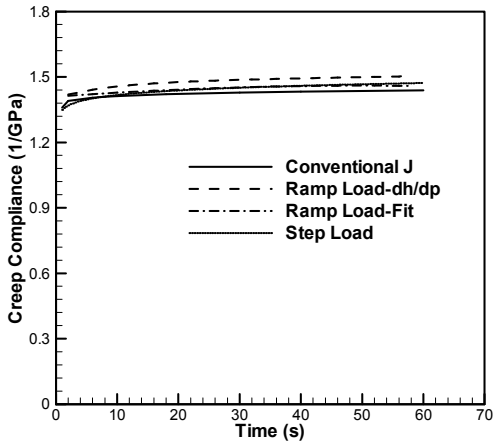

(d) PC using spherical indenter

Fig. 3-5 Creep compliance measured from nanoindentation

CHAPTER IV

MEASUREMENTS OF COMPLEX CREEP COMPLIANCE (FREQUENCY DOMAIN) USING NANOINDENTATION

4.1 Introduction

Methods for measuring the Young's modulus have been very well established for time-independent materials. Based on the assumption that unloading in the load-displacement curve induces only elastic recovery, Oliver and Pharr (1992) pioneered a method to determine basic material properties such as the Young's modulus. The method is based on Sneddon's solution (1965) for the relationship between the load and displacement for an axisymmetric indenter indenting into a half-space composed of a linearly elastic, isotropic and homogeneous material. While the methods work well for time-independent materials (metals, etc.), applying the methods directly to viscoelastic materials has experienced problems. For example, the unloading curve in viscoelastic materials sometimes has a negative slope (Oyen-Tiesma et al., 2001), under situations in which a small unloading rate and a relatively high load were used for a material with pronounced viscoelastic effects. Some work has been done in recent years to improve the methods proposed by Oliver and Pharr (1992) to determine the Young's modulus, or the Young's relaxation modulus. Cheng et al. (2000) derived the analytical solutions for

linear viscoelastic deformation, and provided a method to measure viscoelastic properties using a flat-punch indenter. Lu, et al. (2003) proposed methods to measure the creep compliance of solid polymers using either Berkovich or spherical indenter. Hutcheson and Mckenna (2005) analyzed the interaction between nanosphere particles and polymer surfaces using viscoelastic contact analysis by considering a time-dependent Poisson's function.

For a viscoelastic material, in addition to the representation of viscoelastic properties in the time-domain, the material properties can also be represented by complex material functions in the frequency-domain. A method was proposed by Loubet et al. (1995) for the computation of the complex modulus of viscoelastic materials. The method uses data acquired from an MTS Nano Indenter XP System installed with a Continuous Stiffness Module (CSM). The CSM allows cyclic excitation in load or displacement and the recording of the resulting displacement or load (Lucas, Oliver, and Swindeman, 1998). The indentation displacement response and the out-of-phase angle between the applied harmonic force and the corresponding harmonic displacement are measured continuously at a given excitation frequency. Loubet et al. presented the following equations to compute the complex modulus $E^*(\omega)$:

$$E^*(\omega) = E' + iE'', \text{ with } E' = \frac{\sqrt{\pi}S}{2\sqrt{A}} \text{ and } E'' = \frac{\sqrt{\pi}C\omega}{2\sqrt{A}}, \tag{4-1}$$

where E' and E'' are the uniaxial storage modulus and the loss modulus, respectively, S the contact stiffness, C the damping coefficient, and A the contact area between the indenter and the workpiece. This method was used to measure the complex modulus of polyisoprene. In an effort to examine the formulas in Eq. (4-1), we conducted

experiments using an MTS Nano Indenter XP system with CSM, and used the formulas in Eq. (4-1) to compute the complex modulus of polycarbonate (PC) and polymethyl methacrylate (PMMA) at 75*Hz*. Data are computed at all times at this frequency, and plotted in Fig. 4-1, but only steady state values represent the complex viscoelastic function. Also shown in Fig. 4-1 are the conventional data measured from Dynamic Mechanical Analysis (DMA) (for details, please see Sections 4.3 & 4.4) for the same batch of PC and PMMA. The uniaxial storage modulus of PC measured by DMA at 75 *Hz* is 2.29 *GPa*. However, the storage modulus computed using Eq. (4-1) is much higher than this value, indicating the difficulty associated with the method described in Eq. (4-1) for measurement of storage modulus for PC. Similar problem is evident for PMMA. Also shown in these figures are storage modulus data measured by the proposed method that will be discussed in Section 4.4.

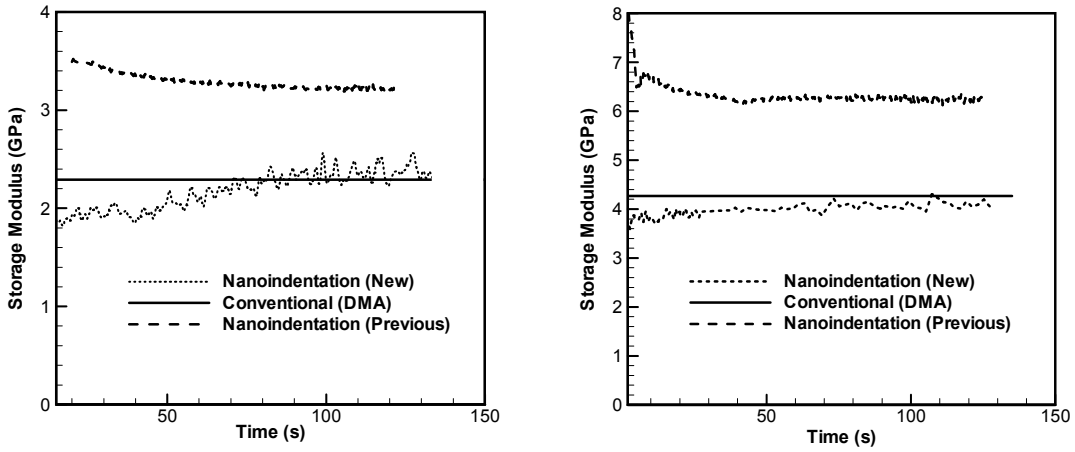

(a) (b)

Fig. 4-1 Comparison of storage compliance at 75 Hz computed by two methods (a) PC. (b) PMMA.

This study is intended to develop a method to measure the complex viscoelastic functions of time-dependent materials in the frequency-domain using nanoindentation with a spherical indenter. Based on solutions for the indentation of an axisymmetric indenter into a linearly elastic material, viscoelastic indentation under a time-harmonic loading condition is analyzed using a hereditary integral operator as proposed by Lee and Radok (1960). Formulas are derived to process the amplitudes of load and displacement as well as the out-of-phase angle between load and displacement to determine the storage and loss parts of the complex compliance (or modulus) function using a spherical indenter. The Lee-Radok approach is applicable to situations where the contact area between the nanoindenter and the workpiece does not decrease. When the condition of non-decreasing contact area is not satisfied, Ting's approach (1966) is used to estimate the difference between the approximation from Lee-Radok approach and the solution obtained from the Ting approach. Dynamic nanoindentation tests were conducted on PC and PMMA to determine the complex compliance, and results are compared with data obtained from DMA on the identical materials to validate the method presented.

4.2 Theoretical background

In this section, we present derivation of the formulas for the computation of complex compliance for a linearly viscoelastic material. The formula for the complex modulus is also presented, as it is simply the reciprocal of the complex compliance. Formulations will be given for a spherical indenter that will be used in experimental verification in this study.

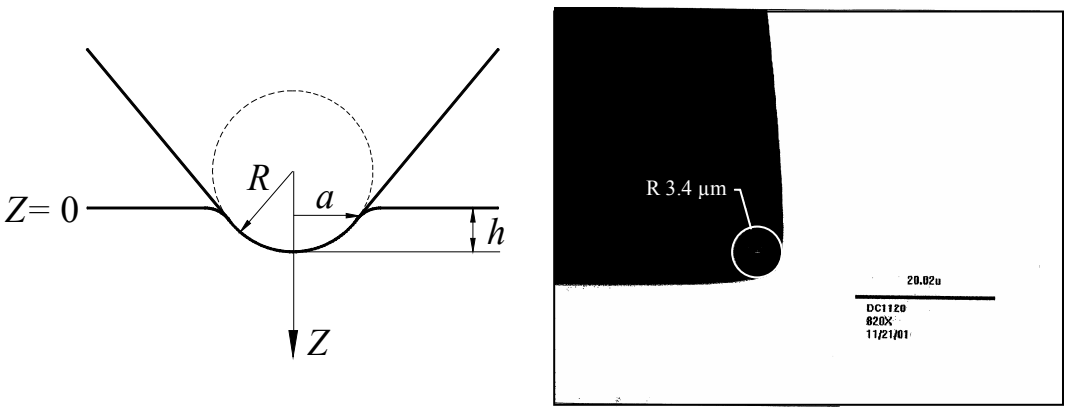

(a) (b)

Fig. 4- 2 Geometry of the spherical indenter. (a) Schematic diagram of the indenter. (b) A TEM image of the spherical indenter tip.

Fig. 4-2 shows the geometry of a spherical indenter. We first consider the problem of a spherical indenter indenting into a half space composed of a homogenous, linearly elastic, isotropic material. The diamond indenter is assumed to be a rigid because of the huge difference in the Young's modulus between the indenter and polymer samples; and the material occupies the half space ($z \geq 0$). The spherical indenter has a tip radius R. Based on the Hertzian solution, under the condition that the ratio of indentation depth to radius of indenter is not higher than 0.16 (Giannakopoulos, 2000), the relation between the applied indentation load and the indentation displacement can be expressed by (Hertz, 1881, Ling, 2002)

$$P = \frac{8\sqrt{R}}{3(1-\nu)} G h^{3/2}, \tag{4-2}$$

where G is the shear modulus, ν the Poisson's ratio, P the applied indentation load, and h the indentation displacement.

For the nanoindentation of a spherical indenter into a viscoelastic material, we assume a constant Poisson's ratio. During nanoindentation experiments in which a relatively short time (such as ~250 *s* used in this study) is involved, the Poisson's ratio (Lu et al., 1997) does not change significantly for some polymers in the glassy state, such as PMMA. Thus it is assumed that a constant Poisson's ratio will not cause much error in the complex compliance data.

For a half space composed of a linearly viscoelastic material, we consider first the case in which the contact area between the indenter tip and the work material is non-decreasing. The condition for non-decreasing contact area will be established at the end of the section. Using the hereditary integral operator proposed by Lee and Radok (1960) in Eq. (4-2), the indentation load-displacement relation is represented by

$$h^{3/2}(t) = \frac{3(1-\nu)}{8\sqrt{R}} \int_{-\infty}^{t} J(t-\theta) \frac{dP(\theta)}{d\theta} d\theta , \tag{4-3}$$

where $J(t)$ is the creep compliance function in shear in the time-domain, $P(t) = 0$ for $t < 0$.

Consider a sinusoidal nanoindentation load superimposed on a step loading, represented by

$$P(t) = P_m H(t) + \Delta P_0 \sin \omega t , \tag{4-4}$$

where $H(t)$ is the Heaviside unit step function, P_m is the carrier load, or main load, ΔP_0 is the amplitude of the harmonic load. Eq. (4-4) implies $P(t) = 0$ for $t < 0$.

Inserting Eq. (4-4) into Eq. (4-3), we have

$$h^{3/2}(t) = \frac{3(1-\nu)}{8\sqrt{R}}[P_m J(t) + \omega \Delta P_0 \int_0^t J(t-\theta)\cos\omega\theta d\theta]. \quad (4\text{-}5)$$

The contact radius is $a(t) = \sqrt{Rh(t)}$. Considering that the complex compliance is defined after the harmonic response has reached a steady state (or equivalently $t \to \infty$), we have

$$h^{3/2}(t) = \frac{3(1-\nu)}{8\sqrt{R}}\{P_m J(t) + \Delta P_0[J'(\omega)\sin\omega t - J''(\omega)\cos\omega t]\} \quad (4\text{-}6)$$

where $J'(\omega) = \omega\int_0^\infty J(t)\sin\omega t dt$ and $J''(\omega) = -\omega\int_0^\infty J(t)\cos\omega t dt$ are storage compliance and loss compliance in shear, respectively. Note that the complex compliance in shear is $J^*(\omega) = J'(\omega) - iJ''(\omega)$. On the other hand, the total displacement as output from a nanoindenter is expressed as

$$h(t) = h_m(t) + \Delta h_0 \sin(\omega t - \delta), \quad (4\text{-}7)$$

where $h_m(t)$ is the carrier displacement, and δ is the out-of-phase angle between the applied harmonic force and displacement. This representation is based on the fact that displacement is behind of load in phase in dynamic nanoindentation. Δh_0 is typically of the order of a few *nm* while $h_m(t)$ is of the order of a few hundreds *nm* under step loading so that $\Delta h_0 << h_m(t)$, Eq. (4-7) leads to

$$h^{3/2}(t) = h_m^{3/2}(t) + \frac{3}{2}h_m^{1/2}(t)\Delta h_0 \cos\delta \sin\omega t - \frac{3}{2}h_m^{1/2}(t)\Delta h_0 \sin\delta\cos\omega t + o(\Delta h_0), \quad (4\text{-}8)$$

where $o(\Delta h_0)$ represents high order terms of Δh_0, and they are negligible under condition of $\Delta h_0 << h_m(t)$. Comparing Eq. (4-6) with Eq. (4-8), we find that

$$h_m^{3/2}(t) = \frac{3(1-\nu)}{8\sqrt{R}} P_m J(t) \quad , \quad (4\text{-}9)$$

$$J'(\omega) = \frac{4\sqrt{R}}{1-\nu}\frac{h_m^{1/2}(t)\Delta h_0}{\Delta P_0}\cos\delta \text{ , and } J''(\omega) = \frac{4\sqrt{R}}{1-\nu}\frac{h_m^{1/2}(t)\Delta h_0}{\Delta P_0}\sin\delta \text{ .} \tag{4-10}$$

Under the loading condition in which a small sinusoidal load is superimposed upon a constant rate loading, i.e.,

$$P(t) = v_0 t + \Delta P_0 \sin\omega t \text{ ,} \tag{4-11}$$

where v_0 is the loading rate, following similar procedures as in deriving Eq. (4-10), the formulas to determine complex compliance can also be derived under the condition that the time *t* has evolved to a value such that $h_m(t) >> \Delta h_0$.

Substituting Eq. (4-11) into Eq. (4-3) for the spherical indenter, we have

$$h^{3/2}(t) = \frac{3(1-\nu)}{8\sqrt{R}}\left\{v_0\int_0^t J(t-\theta)d\theta + \Delta P_0\left[J'(\omega)\sin\omega t - J''(\omega)\cos\omega t\right]\right\}. \tag{4-12}$$

Comparing Eq. (4-12) with Eq. (4-8), the same formulas as in Eq. (4-10) for the complex compliance can be derived for a small oscillatory load superimposed upon a constant rate loading.

Eq. (4-10) is used to determine the complex compliance in shear from nanoindentation. The uniaxial complex compliance, $D(\omega)$, can be computed from

$$D^*(\omega) = D'(\omega) - iD''(\omega) = \frac{J'(\omega) - iJ''(\omega)}{2[1+\nu^*(\omega)]}, \tag{4-13}$$

where $D'(\omega)$ and $D''(\omega)$ are uniaxial storage modulus and loss modulus, respectively, $\nu^*(\omega)$ the complex Poisson's ratio. Assuming that $\nu^*(\omega)$ is a constant during short-time nanoindentation tests for glassy polymers, from Eqs. (4-10) and (13), $D'(\omega)$ and $D''(\omega)$ can be computed by

$$D'(\omega) = \frac{2\sqrt{R}}{1-\nu^2}\frac{h_m^{1/2}(t)\Delta h_0}{\Delta P_0}\cos\delta, \text{ and } D''(\omega) = \frac{2\sqrt{R}}{1-\nu^2}\frac{h_m^{1/2}(t)\Delta h_0}{\Delta P_0}\sin\delta. \quad (4\text{-}14)$$

Similarly, the complex modulus in shear can also be determined by $G^*(\omega) = 1/J^*(\omega)$, and the uniaxial complex modulus can be computed by $E^*(\omega) = 1/D^*(\omega)$.

It should be noted that Eq. (4-3) is valid only if the indentation contact area is non-decreasing (Lee and Radok, 1960). Under the oscillatory loading condition, indentation can possibly induce decreasing contact area, in which case, the Lee-Radok integral operator will cause a residual surface traction at points not in contact at current time but formerly within the contact region, thus violating the boundary condition that the surface traction should vanish outside the contact region. In the case of arbitrary contact area history, Ting (1966) developed an analytical approach to solve the problem of axisymmetric viscoelastic indentation by a rigid indenter. The Ting approach leads to the same results as those derived from the Lee-Radok approach when the contact area is non-decreasing. The Ting approach, however, is necessary in the case where decreasing contact area occurs in nanoindentation.

We next provide a condition under which non-decreasing contact area is maintained so that the solution derived from the Lee-Radok approach is valid. In terms of Eq. (4-8) and $a(t) = \sqrt{Rh(t)}$, for a small harmonic loading superimposed on a constant rate loading, if $v_0 \geq \Delta P_0 \omega$, as seen from Eq. (4-11) for a harmonic loading superimposed on a constant rate loading, the non-decreasing load leads to the non-decreasing contact area in the entire indentation history. For a harmonic loading superimposed on a step loading, when $\omega \leq \dot{h}_m / \Delta h_0$, from Eq. (4-7) the contact area will be non-decreasing during the whole process; as the frequency exceeds the critical value $\omega_c = \dot{h}_m / \Delta h_0$, the contact area

increases and decreases with time as a result of the applied harmonic load so that the Ting approach should be adopted. Nevertheless, as will be discussed in Section 4.2, under certain condition when $\omega > \omega_c$, the solutions derived from the methods by Lee & Radok and Ting are very close, even though the solution from the Lee-Radok approach is not justified. Since a closed-form solution derived from the Lee-Radok approach exists, while only numerical solution can be obtained using the Ting approach, the formulas derived for a harmonic superimposed on a step loading from the Lee-Radok approach could be used to estimate the complex viscoelastic functions in the regime of linear viscoelasticity.

4.3 Experiments

We conducted two independent tests, namely nanoindentation and DMA tests, to find the complex viscoelastic functions of the same materials. The results would be compared to examine the measurement technique by nanoindentation. We describe in this section first DMA experiments and then nanoindentation experiments.

4.3.1 DMA experiments

The conventional data of complex compliance were obtained by DMA tests. Dynamic Mechanical Analyzer, model RSA α (Rheometric Scientific), was employed in the measurements of complex compliance. In DMA three-point bending tests were conducted on both PC and PMMA, which have the dimensions of 50 × 13 × 1.7 *mm* and 50 × 13 × 1.4 *mm*, respectively. The PC material was made by GE Plastics. The PMMA was made by Rhom and Haas, which is the same batch of materials as used by Lu et al. (1997). The

glass transition temperatures for PMMA and PC are 105 ^{o}C and 144 ^{o}C, respectively. Before testing, all samples were annealed for two hours. The annealing temperatures for PMMA and PC samples were 110 ^{o}C and 150 ^{o}C, respectively. They were then cooled down slowly, at a cooling rate of about 5 $^{o}C/hr$, to room temperature. The annealed samples were further stored in a container with a constant relative humidity 50%, to allow the samples to be aged for about 72 *hrs* prior to DMA tests. These procedures are necessary to ensure property consistency as the behavior of polymers depends on a variety of conditions including previous stress history, aging time and moisture concentration.

For the comparison with the complex compliance data from nanoindentation conducted at 22 ^{o}C, the frequency range is 0 - 260 *Hz*. However, The DMA can only reach a frequency up to 16 *Hz*. In order to extend the frequency range for conventional data of complex compliance, temperature-frequency trade-off was applied (Ferry 1950). To implement this, DMA tests were performed at selected lower temperatures. The complex compliance data at these temperatures were shifted to obtain master curves that cover the frequency range of 0 - 260 *Hz* (see Section 4.1 for details).

4.3.2 Nanoindentation experiments

Nanoindentation tests were conducted using an MTS Nano Indenter XP system. The capacities of indentation depth and load with this system are 500 μm and 500 *mN*, respectively. The resolutions of displacement and load are 0.01 *nm* and 50 *nN*, respectively. A spherical indenter with a tip radius 3.4 μm was used on the XP module.

Fig. 4-2(b) shows a TEM micrograph of the spherical indenter tip. The tip is axisymmetric and has a spherical surface within the depth of indentation (up to ~500 *nm*) considered in this study. The same PC and PMMA in DMA tests (see Section 4.3.1) were used in nanoindentation experiments. The material preparation procedures were identical to those used in DMA experiments. All nanoindentation tests were performed at 22 ^{o}C. The surface roughness values as measured by an AFM (Digital Instruments Dimension 3100) were 2.859 *nm* for PC and 2.286 *nm* for PMMA, respectively. These small surface roughness values justify the consideration of smooth and flat sample surfaces in nanoindentation involving indentation depths up to a few hundreds *nm*; nanoindentation results under the same conditions were found to be repeatable. In order to reduce the drift caused by noise and temperature gradient during nanoindentation tests, the indenter system was enclosed in a chamber. All nanoindentation tests did not start until a thermal equilibrium state was reached and the drifting of the indenter tip dropped below a set value, typically 0.05 *nm/s*.

The CSM implemented in XP module was used to apply the dynamic excitation with a frequency range of 3 - 260 *Hz*. A prescribed harmonic displacement was set before each experiment. In experiments, the nanoindenter modulates the amplitude of harmonic force to produce the set target in harmonic displacement, typically with amplitude between a fraction of a *nm* and a few *nm*. After the indenter tip had made contact with the surface of test sample, the indentation load, depth, harmonic load amplitude, harmonic displacement amplitude, and out-of-phase angle between the harmonic load and the displacement were recorded simultaneously at a sampling rate of five data points per second. The loading history employed in the dynamic indentation test was small harmonic loading

superimposed on a quasi-static loading, i.e., either a step loading or a constant rate loading. The step loading was implemented by a constant rate load (at a short-rise time, e.g., 2 *s*) followed by a constant load. After the harmonic response had reached a steady state, data were used to determine the complex compliance of the material.

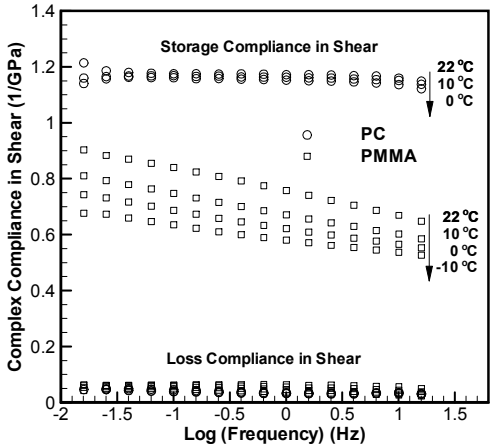

Fig. 4-3 Complex compliance from DMA tests at different temperatures.

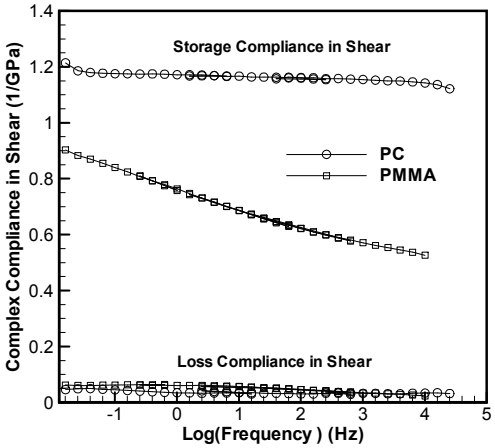

Fig. 4-4 Master curves of complex compliance in shear

4.4 Results and discussions

4.4.1 DMA results

DMA tests were performed at temperatures 22 ^{o}C, 10 ^{o}C, 0 ^{o}C and -10 ^{o}C for PMMA, and 22 ^{o}C, 10 ^{o}C and 0 ^{o}C, for PC. Fig. 4-3 shows the storage compliance and loss compliance in shear for PMMA and PC at different temperatures. As shown in Fig. 4-3, the complex compliance of PC does not change much in this range of temperature and frequency, while the complex compliance of PMMA presents considerable change. Based

on the curves of complex compliance at different temperatures, very smooth master curves are obtained using frequency-temperature superposition. The shift factors, in logarithmic scale referred to 22 ^{o}C, Log a_T, are 1.6 s and 3.2 s at 10 ^{o}C and 0 ^{o}C for PC, respectively; the Log a_T for PMMA are 1.2 s, 2.0 s and 2.8 s at 10 ^{o}C, 0 ^{o}C and -10 ^{o}C, respectively. Fig. 4-4 shows the master curves of complex compliance of PMMA and PC, reaching up to 10^4 Hz. The range is wide enough for the comparison with nanoindentation data. It is observed from Fig. 4-4 that there is no β - transition within the frequency range for both PC (Sane and Knauss, 2001, Knauss and Zhu, 2002) and PMMA (Lu et al., 1997).

4.4.2 Nanoindentation results

Results on the complex compliance from nanoindentation measurements are presented and discussed in this section. Two types of loading histories were applied in the indentation tests; they were: (1) a small harmonic load superimposed on a constant rate loading; and (2) a small harmonic load superimposed on a step loading. We first present the input and output of nanoindentation tests under the two loading histories.

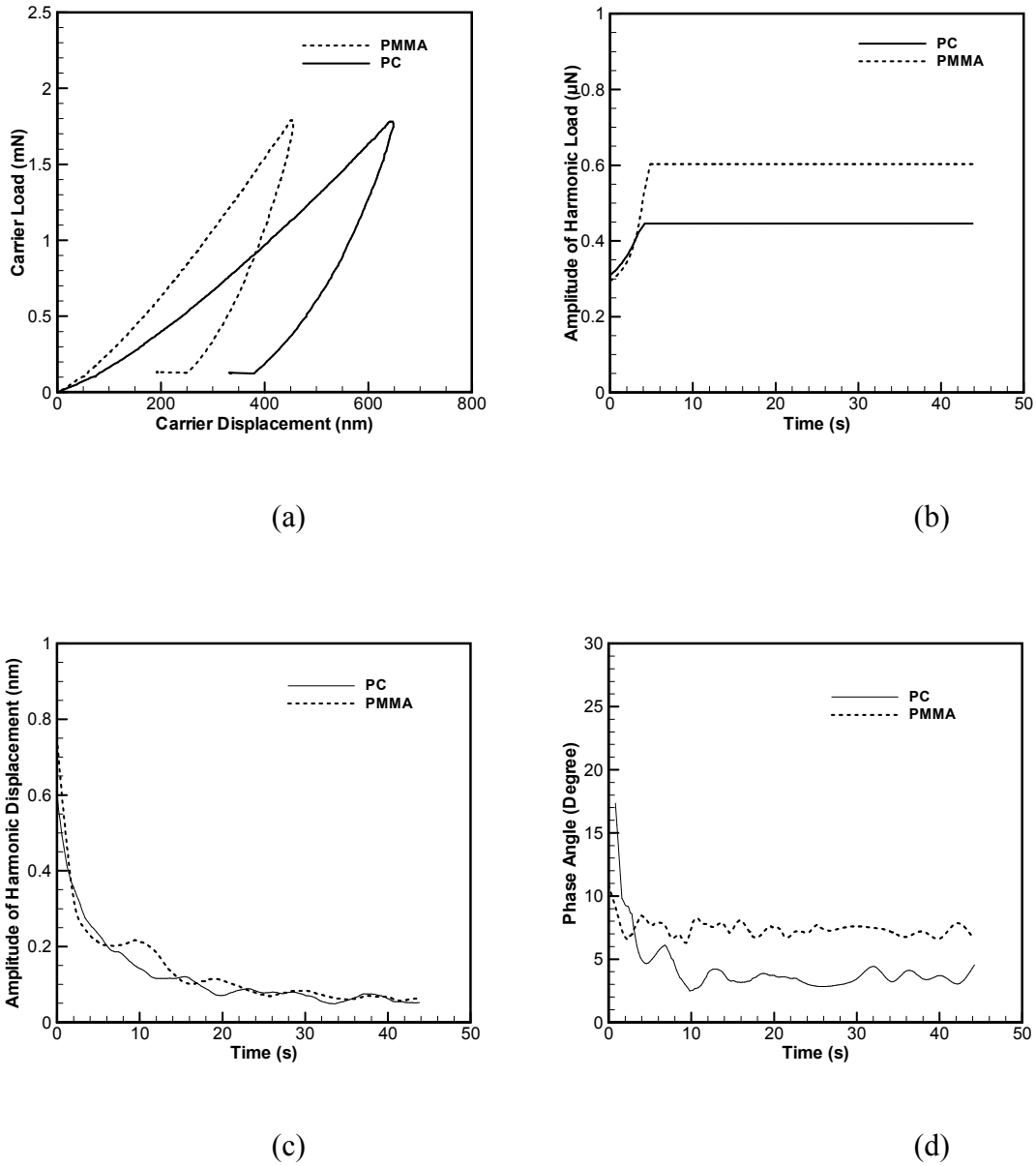

Fig. 4-5 Nanoindentation output from oscillation on a constant rate loading at 10 *Hz*. (a) Carrier load-depth curve. (b) History of amplitude of harmonic load. (c) Response of harmonic displacement amplitude. (d) Out-of-phase angle with correction

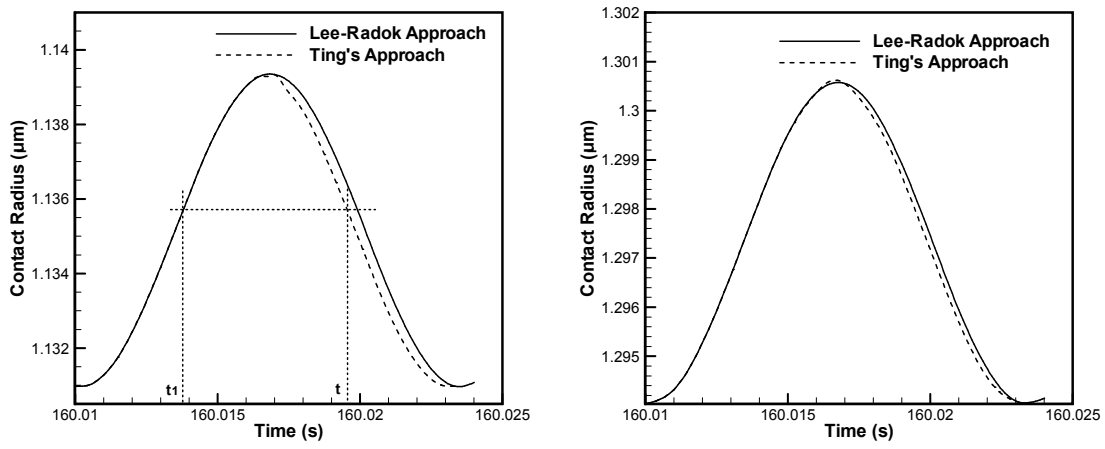

(a) (b)

Fig. 4-6 Comparison of contact radius results at 75 Hz using the Lee-Radok approach and the Ting approach. (a) Contact radius computed for PMMA under a harmonic load superimposed on a step loading. (b) Contact radius computed for PC under a harmonic load superimposed on a step loading.

Constant rate carrier loading was used in the first type of dynamic indentation. When the loading rate v_0 is greater than $\Delta P_0 \omega$, the contact area will be non-decreasing under dynamic loading so that the Lee-Radok approach is applicable.

The loading rate used for both PC and PMMA is 0.04 *mN*/*s*. Fig. 4-5(a) shows the quasi-static component of load-depth curve. Fig. 4-5(b) shows the harmonic load amplitude as the input, and Fig. 4-5(c) shows the harmonic displacement in response to the harmonic load. The steady values of ΔP_0 for PC and PMMA are 0.445 μN and 0.602 μN, respectively. Therefore the condition, $v_0 \geq \Delta P_0 \omega$, is satisfied, resulting in non-decreasing contact area. It is noted that the condition for non-decreasing contact area can be satisfied at all frequencies, up to 135 *Hz*, in nanoindentation with the use of appropriate loading rate v_0 so that the formulas in Eq. (4-10) can be applied to find the

complex compliance in shear. In addition to the requirements in non-decreasing contact area, it is necessary to ensure that the harmonic displacement is much smaller than the carrier displacement. As the carrier displacement increases with time to larger values, for example, 200 *nm* for PMMA and PC, the contribution from higher order terms of $\Delta h_0 / h_m$ is well less than 1% so that the use of Eq. (4-10) is justified. The out-of-phase angle between harmonic load and harmonic displacement is shown in Fig. 4-5(d).

The second dynamic loading condition is a harmonic load is superimposed on a step loading. As discussed in Section 4.2, if $\omega \le \dot{h}_m / \Delta h_0$, the contact area will be non-decreasing, indicating that when the creep rate is high and the amplitude of harmonic displacement is small, the non-decreasing contact area condition can be still satisfied at some frequencies, so that the solutions in Eq. 4-10 using the Lee-Radok hereditary operator are applicable. For example, with the indentation input shown in Figs. 4-7(a) and (b) (details of Fig. 4-7 will be discussed later), the frequency limits, ω_c, below which the condition of non-decreasing area holds, are 2.4 *Hz* for PC, and 6.5 *Hz* for PMMA, respectively. If $\omega > \dot{h}_m / \Delta h_0$, the contact area will decrease. In this case, Lee-Radok approach seems not applicable. However, considering the loading condition in this study, the resulting harmonic displacement for both PC and PMMA is very small compared to the carrier displacement, normally, $\Delta h_0 << 0.006 h_m$. Therefore, the variation in the contact area between the indenter and the sample surface is always less than ~1% after a steady state in oscillatory response has reached, so that the effect of change in the contact area is not significant. To demonstrate this, the viscoelastic indentation problem is solved numerically using the Ting approach. With a periodical displacement output in the form of Eq. (4-7), it suffices to consider only one cycle of the history in the steady state. We

present results on contact radius only; other results, such as the indentation displacement, can be obtained in the similar way. In the first half cycle starting from the valley (lowest point in a cycle) in the steady state, the contact area is increasing; the Ting approach gives the same results as those obtained from the Lee-Radok approach, that is

$$a^3(t) = \frac{3(1-\nu)R}{8}\int_0^t J(t-\tau)d(P(\tau)) \tag{4-15}$$

where $P(t)$ is given by Eq. (4-4). For the second half of the cycle, in which the contact area is decreasing, the solution derived from the Ting approach is

$$a(t) = a(t_1), \tag{4-16}$$

where t_1 is obtained by

$$P(t) = \frac{8R}{3(1-\nu)}\int_0^{t_1} G(t-\tau)d\left(a^3(\tau)\right), \tag{4-17}$$

where $G(t)$ is the shear relaxation modulus. Using the creep functions of PC and PMMA, the contact radius in one cycle can be determined after the sinusoidal response has reached the steady state. Fig. 4-6 shows the results of contact radius for PC and PMMA materials at 75 *Hz*, under a harmonic load superimposed on a step loading. At 75 *Hz*, the frequency limit for non-decreasing contact area condition has been exceeded. The results, however, indicate that the contact radius computed by the Lee-Radok approach correlates well with those obtained by the Ting approach. The correlation coefficients for PMMA and PC are 0.939 and 0.993, respectively. At frequencies higher than ω_c, Eq. (4-10) and its variants should be considered as an approximation for the viscoelastic functions in the frequency-domain.

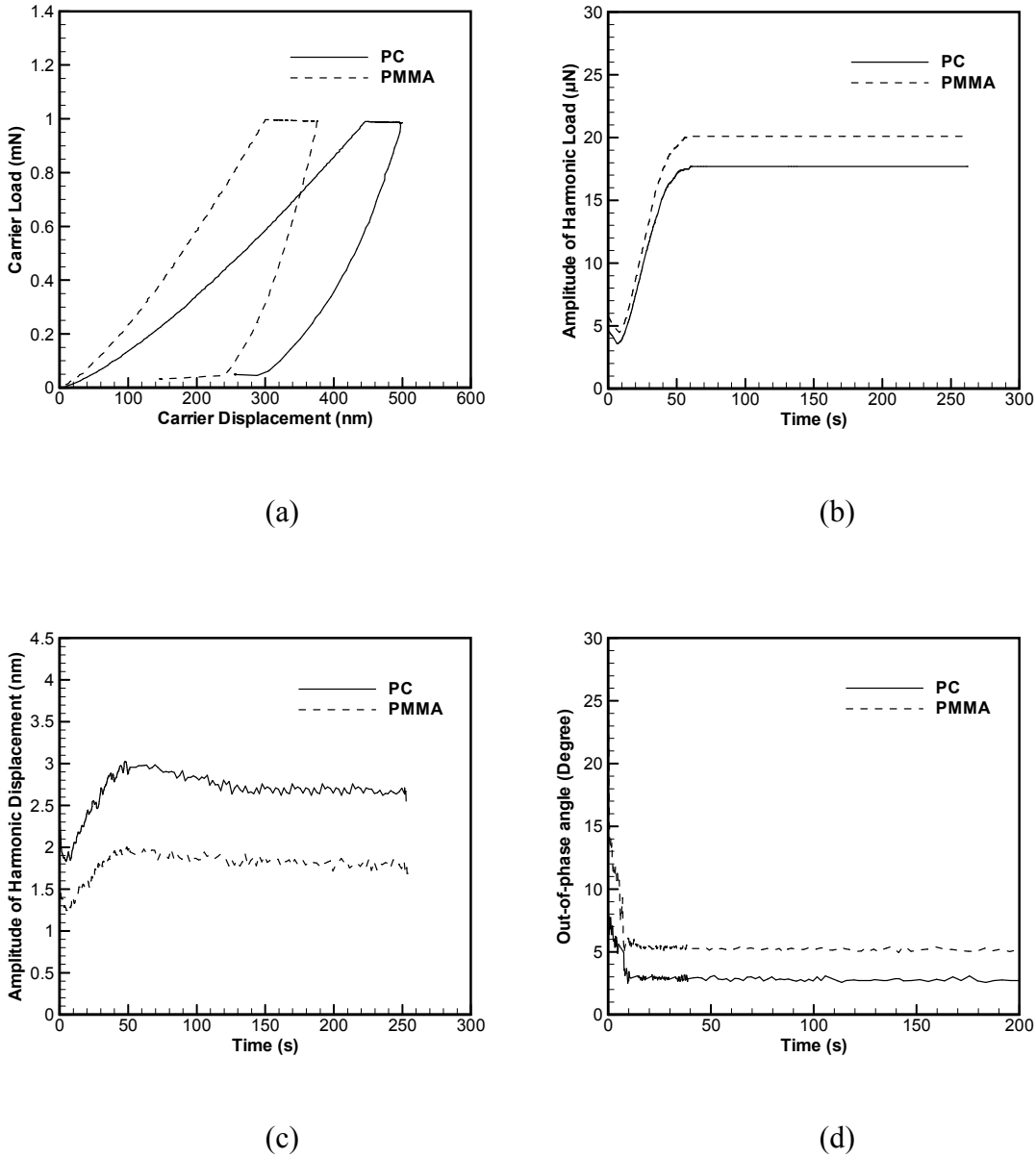

Fig. 4-7 Nanoindentation output from oscillation on a step loading at 75 *Hz*. (a) Carrier load-depth curve. (b) The history of harmonic load amplitude. (c) Response of harmonic displacement amplitude. (d) Out-of-phase angle with correction.

In the context of presentation of complex compliance in this work, Eq. (4-10) is used at all frequencies under a harmonic loading superimposed on a step loading, but results in nanoindentation at frequencies higher than ω_c should be understood as a very good

approximation to the actual values due to the high correlation between approximate and accurate solutions.

The nanoindentation results of input and output under the second dynamic loading at 75 *Hz* are shown in Fig. 4-7. Fig. 4-7(a) records the corresponding quasi-static carrier load-depth curve (without the harmonic component) for both PC and PMMA. Figs. 4-7(b) and (c) illustrate the amplitudes of harmonic load and displacement at 75 *Hz* for PC and PMMA. As shown in Fig. 4-7(b), at initial stage of the contact between the indenter and sample surface, the amplitude of harmonic load generally increased until $t = 50\ s$, and was maintained constant thereafter. Accordingly, as shown in Fig. 4-7(c), there was an increase in amplitude of harmonic displacement before $t = 50\ s$. So the condition of Eq. (4-4) is precise after about 50 *s*. A steady state was reached at about $t = 150\ s$. As shown in Fig. 4-7, after $t = 150\ s$, $\Delta h_0 / h_m$ is much less than 1%, thus the condition of using Eq. (4-10) is satisfied. Fig. 4-7(d) shows the out-of-phase angle between harmonic load and harmonic displacement for both PC and PMMA.

In order to ensure that the deformation of the polymer samples is in the linearly viscoelastic regime, the indentation depth into the sample surface for PC and PMMA materials was controlled to within the limit of linearity. According to Lu, et al, (2003), the limits of linearity in indentation depth were determined as 1123 *nm* for PC, and 780 *nm* for PMMA, respectively, for a spherical indenter with a radius of 3.4 μm. It was found that in indentation within the limit of linearity, the deformation of PC and PMMA is linearly viscoelastic, indicated by the fact that complex compliance is independent of the magnitude of indentation carrier load.

For time-dependent materials under dynamic loading, the out-of-phase angle between the harmonic load and displacement plays an important role in the computation of complex compliance. Consequently, we discuss next the correction on out-of-phase angle.

As presented by Pethica and Oliver (1992), the out-of-phase angle between the force and displacement ϕ can be computed by

$$\tan\phi = \frac{\omega(C_i + C_c)}{k - m\omega^2}, \tag{4-18}$$

where k is system stiffness, C_c is the damping inside capacitor gauge measuring displacement of the indenter, and C_i is the damping resulting from the contact between indenter and sample. If the sample material is ideally elastic, there is no out-of-phase angle between harmonic indention load and harmonic indentation depth. For an elastic material, however, from Eq. (4-18), $C_i = 0$, but $C_c \neq 0$, so that $\phi \neq 0$, which is not physically reasonable. It should be noted that the air damping resulting from the gauge capacitor gives apparent out-of-phase angle that does not necessarily represent the damping behavior of the material. Therefore, ϕ is not exactly the out-of-phase angle between harmonic indentation load and harmonic depth and must be corrected. If the contribution in ϕ from the nanoindentation instrument is removed, we can determine the out-of-phase angle, δ, representing the damping of viscoelastic material by

$$\tan\delta = \frac{\omega C_i}{k - m\omega^2}. \tag{4-19}$$

As an example, the out-of-phase angles for PC and PMMA using spherical indenter are shown in Fig. 4-5(d) and Fig. 4-7(d).

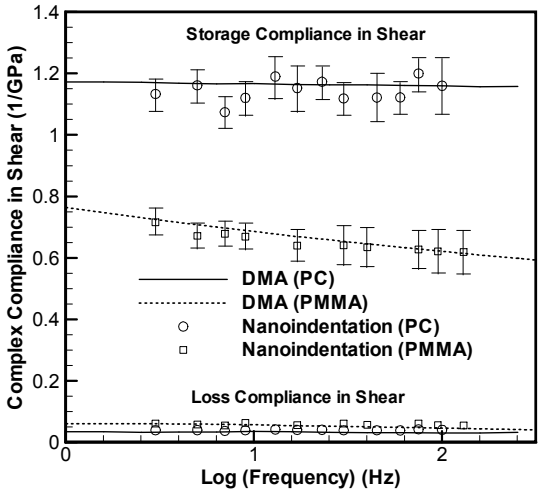

Fig. 4-8 Complex compliance in shear from nanoindentation under a harmonic load superimposed on a constant rate loading.

To determine the complex compliance from nanoindentation tests using the spherical indenter, Eq. (4-10) is used. The complex compliance curves of PC and PMMA materials are shown in Figs. 4-8 and 4-9. Error bars are shown for storage compliance. Error bars for loss compliance are about 1/3 size of the symbols. The complex compliance shown in Fig. 4-8 was measured from nanoindentation under a constant rate loading superimposed by a harmonic load. Fig. 4-9 shows the complex compliance measured from nanoindentation under a step loading superimposed by a harmonic load. The complex compliance measured from both types of nanoindentation tests were compared with DMA results. These two sets of results are in good agreement. The average percent error for the storage compliance of PC and PMMA at these discrete experimental data is less than 6%, indicating a very good agreement. The maximum errors for the storage compliance of PC and PMMA are 9.1% and 5.1%, respectively. Figs. 4-8 and 4-9 show that the loss compliances for both PC and PMMA are much smaller than the storage compliances, which implies that the material damping of the two polymers is very small.

For PC, both storage and loss compliances remain almost constant within 3 - 200 *Hz*. The reductions in storage and loss compliance for PC are only 0.8% and 3.8%, respectively, while for PMMA, the storage compliance decreases by 16.6%, and loss compliance decreases by 35.4% between 3 *Hz* and 260 *Hz*.

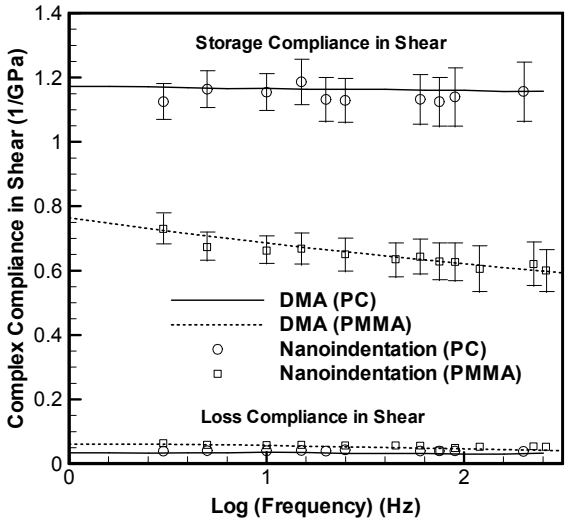

Fig. 4-9 Complex compliance in shear from nanoindentation under a harmonic load superimposed on a step loading.

In the computation of both storage compliance and loss compliance, Poisson's ratio is usually time-dependent for polymeric materials. In these experiments, the time-scale is not large; the maximum time duration is less than 300 seconds. Within this time period, it has been demonstrated that the Poisson's ratio does not change significantly (Lu, et al, 1997). Therefore, we assumed a constant Poisson's ratio ($\nu = 0.3$) in the computation of the complex compliance for both PC and PMMA materials. The natural frequency of the indentation system is 180 *Hz*, thus we avoided testing near the resonant frequency.

We turn next to the comparison in results from Loubet et al. and the new method proposed in this study. The method by Loubet et al. (1995) on measurement of the

uniaxial complex modulus is based on the analogy between dynamic indentation and uniaxial dynamic analysis. Nanoindentation on viscoelastic materials, however, is a complex viscoelastic problem involving moving contact interface, and needs to be analyzed to derive formulas for the computation of viscoelastic functions in the frequency-domain. Based on their method, the uniaxial storage modulus at 75 *Hz* for both PC and PMMA were computed using the data of stiffness, damping and contact area from nanoindentation experiments, as shown in Fig. 4-1. During the tests, a constant rate loading superimposed by a small harmonic loading was applied. Since tests were under a single frequency (75 *Hz*) within a time frame less than 250 *s*, the storage modulus computed using Eq. (4-1) was plotted with respect to time. Also plotted in Fig. 4-1 are the DMA data of uniaxial storage modulus at 75*Hz*, which is a horizontal line since it is a single value representing material behavior. The uniaxial storage modulus measured from this method is generally much higher than DMA data. As shown in Fig. 4-1, the minimum errors in storage modulus are 40% for PC and 46% for PMMA, respectively, indicating that the approach based on the analogy between uniaxial dynamic tension test and dynamic nanoindentation is not appropriate for measuring viscoelastic functions for polymers. Also plotted in Fig. 4-1 are the storage modulus data using the new method presented. Eq. (4-13) was used to convert shear data to uniaxial data. For PC in steady state, the average storage modulus obtained from the new method is consistent with the DMA data, which is 2.29 *GPa*, and the error is 6.1%. For the average storage modulus of PMMA in steady state, the error, compared with the conventional data from DMA, is 2.5%. The indentation results using the new method for time-dependent materials, such as polymers, can recover complex viscoelastic functions determined from conventional

tests with good accuracy. The complex compliance in shear measured using the proposed method at all frequencies shows a good agreement with those obtained from conventional tests. This study has thus provided a method to measure viscoelastic functions in the frequency-domain for time-dependent materials.

4.5 Conclusions

A method to measure the complex compliance has been presented using nanoindentation with a spherical indenter for linearly viscoelastic materials. Following the Hertzian solutions for indentation in linear elasticity and the consideration of the Lee-Radok approach for a moving boundary problem in linear viscoelasticity, formulas for the components of the complex compliance function in the frequency-domain have been derived based on the load-displacement relation for linearly viscoelastic materials under harmonic loading. The formulas should be used under the conditions that $h/R < 0.16$ and the nanoindentation depth is below the limit of linearity. When a constant rate loading is used as the carrier load, the formulas are exact under the condition that the loading rate is high enough so that the condition of non-decreasing contact area is satisfied. While a step loading is used as the carrier load, the formulas are considered to be approximate when the frequency is higher than a critical value such that decreasing contact area occurs; in the case of decreasing contact area, the Ting approach was used to find the solution in the steady state at a selected frequency to estimate the difference between solutions obtained using the Lee-Radok approach and the Ting approach. Very close correlation was found for the test conditions used in this study. Dynamic nanoindentation tests on PC and PMMA materials were performed, using a spherical indenter, to determine the amplitudes

of oscillating load and displacement, as well as the out-of-phase angle of displacement with respect to the harmonic force output. The complex compliance functions in the frequency-domain were determined using the proposed method and results were compared with conventional data obtained from DMA tests for PC and PMMA materials. The condition for non-decreasing contact area, $v_0 \geq \Delta P_0 \omega$, is satisfied under a constant rate carrier load so that the complex compliance formulas derived from the Lee-Radok approach are appropriate. Under a step carrier load, the condition of non-decreasing contact is satisfied up to the frequency limit, $\dot{h}_m / \Delta h_0$; at frequencies higher than the frequency limit, complex compliance data could be considered to be an approximation. In both constant rate and step carrier loading conditions, a good agreement between nanoindentation results and conventional data has been reached, indicating the validity of the proposed method for measuring the complex compliance function in the frequency domain using dynamic nanoindentation.

CHAPTER V

MEASUREMENTS OF TWO INDEPENDENT VISCOELASTIC FUNCTIONS BY NANOINDENTATION

5.1 Introduction

In measurements of elastic properties, Poisson's ratio is often of interest; however it is hardly thoroughly studied. Lucas, Hay and Oliver (2004) applied a lateral load to determine the Poisson's ratio through the measurements and analysis of both normal contact stiffness and tangential contact stiffness. Various methods have been developed to measure the Poisson's ratio for a linearly viscoelastic material at the macroscale. Vlassak and Nix (1992) used bulge tests on both square and rectangular membranes, and measured both Young's modulus and Poisson's ratio for silicon nitride; Ma and Ravi-Chandar (2000) used a cylinder polymer sample under confined compression to measure both bulk and shear relaxation functions. These techniques are successful in their respective areas of application.

To date, methods are not available to measure two independent *viscoelastic functions*, such as bulk and shear relaxation functions at micro/nano scale using nanoindentation. In all the current nanoindentation techniques for measurements of viscoelastic functions, a constant Poisson's ratio is often assumed, and nanoindentation measures only one viscoelastic function(Cheng et al., 2000; Lu et al., 2003; Huang et al., 2004; Odegard et

al., 2005; VanLandingham et al.; 2005, Cheng and Cheng, 2005), such as the creep compliance in shear. However, for very small amounts of materials with viscoelastic behavior different from a bulk material, all viscoelastic functions are unknown. In addition, for a material with pronounced viscoelastic effects, such as a polymer near its glass transition temperature, any pair of independent viscoelastic functions (e.g., bulk and shear relaxation functions) would change with time. Assuming a constant Poisson's ratio could potentially cause significant error. Consequently, a method is needed to measure two independent viscoelastic functions using nanoindentation for very small amounts of viscoelastic materials.

In this chapter, a method is presented to measure two independent viscoelastic functions, namely bulk and shear relaxation functions for an isotropic, linearly viscoelastic material using nanoindentation. Equations are derived for the viscoelastic contact mechanics problems for both Berkovich and spherical indenters. The bulk and shear relaxation functions are determined through minimizing the difference between nanoindentation data and analytical results. The results from nanoindentation will be compared with viscoelastic property data determined from conventional tests for the same batch of materials to examine the method.

5.2 Analytical background

In this section we present formulas for the indentation load-displacement relation from linearly elastic contact mechanics analysis, and then use the approach developed by Lee-Radok (1960) to write down the indentation load-displacement relation for a linearly viscoelastic material.

5.2.1 Indentation by rigid axisymmetric indenters of arbitrary shape

For the Boussinesq problem of a rigid axisymmetric indenter tip indenting into a half-space composed of a homogeneous, linearly elastic and isotropic material, Sneddon (1965) derived solution for the indentation load *P* given as

$$P = \frac{4\mu a}{1-\nu}\int_0^1 \frac{x^2 f'(x)}{\sqrt{1-x^2}}dx\,, \tag{5-1}$$

where μ is the shear modulus, ν is the Poisson's ratio, a is the contact radius and $z = f(x)$ is the shape function of the indenter with $x = r/a$ as defined in Fig. 5-1. Sneddon's solution for the indentation displacement *h* is

$$h = \int_0^1 \frac{f'(x)}{\sqrt{1-x^2}}dx\,. \tag{5-2}$$

Since $x = r/a$, Eq. (5-2) gives the relationship between displacement of the axisymmetric indenter tip, *h*, and the contact radius, *a*. The relationship between *h* and *a* is uniquely determined by the geometry of the indenter. Combining Eqs. (5-1) and (5-2), and expressing ν in terms of bulk modulus, *K* and shear modulus, μ, one has

$$P = \frac{(3K+\mu)\mu}{3K+4\mu}F(h)\,, \tag{5-3}$$

where $F(h)$ is a function determined by Eqs. (5-1) and (5-2), and depends on the geometry of the axisymmetric indenter. For example, for a conical indenter, $F(h) = 8h^2/(\pi\tan\alpha)$, where α is the angle between the cone generator and the surface of the half space.

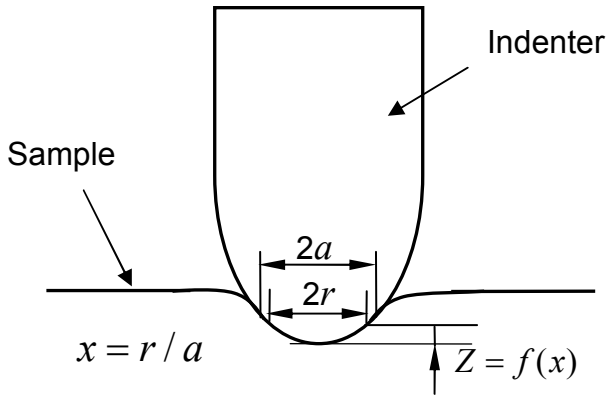

Fig. 5-1 A schematic of indentation on a half space by an axisymmetric indenter

When a rigid axisymmetric indenter indents into a half space composed of a homogeneous, isotropic and linearly viscoelastic material, following the approach by Lee-Radok (1960), under the condition of non-decreasing contact area between the indenter and the workpiece, the load-displacement relation in the Laplace domain can be written in the form

$$\frac{3\overline{K}(s)+4\overline{\mu}(s)}{s\overline{\mu}(s)[3\overline{K}(s)+\overline{\mu}(s)]}=\frac{\overline{F}(h(s))}{\overline{P}(s)}, \tag{5-4}$$

where s is the complex variable in Laplace domain, the notation $\overline{Q}(s)$ represents the Laplace transform of function $Q(t)$, for example, $\overline{K}$, $\overline{\mu}$, are the Laplace transform of bulk relaxation function $K(t)$ and shear relation function $\mu(t)$, respectively. It is noted that $\overline{K}(s)$ and $\overline{\mu}(s)$ can only be determined to the extent as shown on the left hand side of Eq. (5-4) when an axisymmetric nanoindenter is used, the two functions cannot be separated further. In other words, both $\overline{K}$ and $\overline{\mu}$ can only be determined in terms of their ratio in Laplace domain when any combinations of axisymmetric indenters are used. For example,

for a conical indenter that has the shape function, $f(x) = ax\tan\alpha$, the following relation in the Laplace domain holds

$$\frac{3\overline{K}(s)+4\overline{\mu}(s)}{s\overline{\mu}(s)[3\overline{K}(s)+\overline{\mu}(s)]} = \frac{8\overline{h^2}(s)}{\pi\overline{P}(s)\tan\alpha}. \tag{5-5}$$

For a circular flat punch indenter, the following relation holds,

$$\frac{3\overline{K}(s)+4\overline{\mu}(s)}{s\overline{\mu}(s)[3\overline{K}(s)+\overline{\mu}(s)]} = \frac{8R\overline{h}(s)}{\overline{P}(s)}, \tag{5-6}$$

and for a spherical indenter, the shape function is $f(x) = a^2x^2/(2R)$ under condition $ax<<R$, the following relation in the Laplace domain holds

$$\frac{3\overline{K}(s)+4\overline{\mu}(s)}{s\overline{\mu}(s)[3\overline{K}(s)+\overline{\mu}(s)]} = \frac{16\sqrt{R}\overline{h^{3/2}}(s)}{3\overline{P}(s)}. \tag{5-7}$$

It is seen on the left hand sides of Eqs. (5-5) - (5-7) that, with the use of one or more equations in Eqs. (5-5) - (5-7), one can only determine $\frac{3\overline{K}(s)+4\overline{\mu}(s)}{s\overline{\mu}(s)[3\overline{K}(s)+\overline{\mu}(s)]}$, and cannot separate $\overline{K}(s)$ from $\overline{\mu}(s)$. Consequently, using any two different axisymmetric indenters cannot determine two independent viscoelastic functions. To separate and determine the two independent functions, we need another independent asymmetric nanoindentation problem.

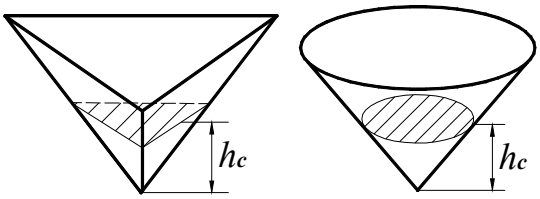

(a) Berkovich and conical indenters

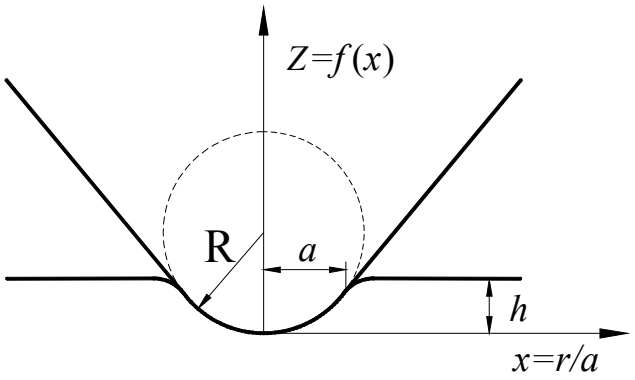

(b) Spherical indenter

Fig. 5-2 Berkovich, conical and spherical indenters

5.2.2 Berkovich indenter

Berkovich indenter is usually used in nanoindentation due to primarily its self-similarity in geometry. Berkovich indenter is often modeled as a conical indenter based on approximately the same height-area relationship of the two indenter tips. However, the Berkovich indenter has a flipped three-face pyramidal shape, as shown in Fig. 5-2, and is

not axisymmetric. Consequently Berkovich indenter is not a rigorously axisymmetric indenter, and represents some difference from an axisymmetric conical indenter.

Since the nanoindentation by Berkovich indenter is not an axisymmetric problem, it is necessary to determine the load-displacement relation for indentation by Berkovich indenter to establish a second equation independent of Eq. (5-4) (with special cases given in Eqs. (5-5) - (5-7)). However, an analytical solution for the viscoelastic contact problem using an asymmetric Berkovich indenter is not available. Consequently, a semi-empirical approach is taken to determine the load-displacement relation when the material is considered linearly viscoelastic. To this end, the nanoindentation by a Berkovich indenter on a linearly elastic material is modeled first, and then the linearly elastic solution is extended to linearly viscoelastic solution. To determine a semi-empirical linearly elastic solution, the indentation by Berkovich indenter tip was simulated using ABAQUS/Standard (2004) on different elastic materials with a series of Poisson's ratios and fixed Young's modulus. The simulations were also conducted on elastic materials with different Young's moduli and fixed Poisson's ratio, and it was found that the load P is proportional to Young's modulus or shear modulus at the same indentation displacement. Therefore it is possible to fit the numerical results on the relation between P and h into an analytic representation. The load-displacement curves at some Poisson's ratios with a fixed Young's modulus are shown in Fig. 5-3(a), and the curves were fitted numerically, to the following equation

$$P = 2.0837 \frac{(1 - 0.2202\nu)\mu}{1 - \nu} h^2 . \tag{5-8}$$

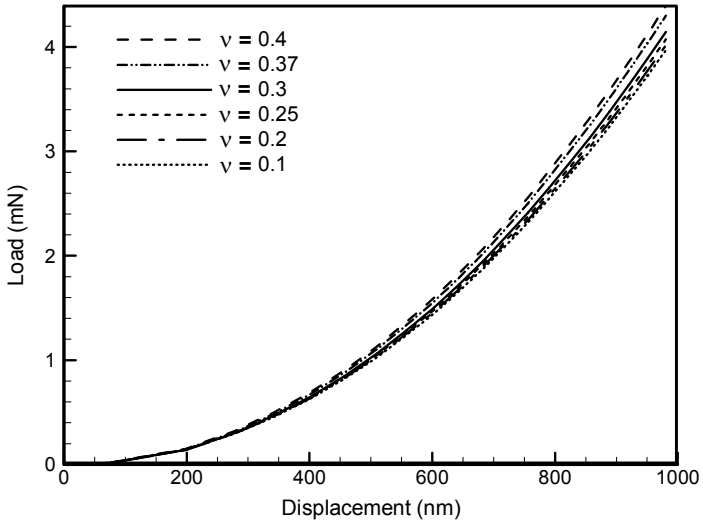

(a) FEM results of load-displacement curves at different Poisson's ratios

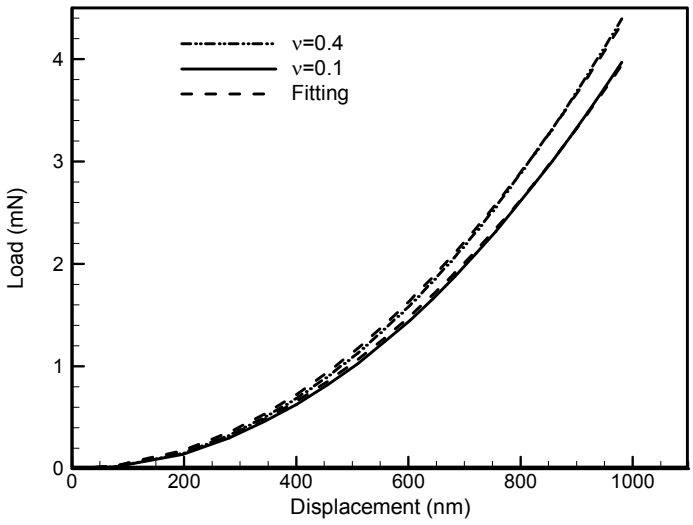

(b) Curve fitting of load-displacement data from FEM

Fig. 5-3 FEM modeling

As an example, both finite element results and fitted curves, indicated by Eq. (5-8), are plotted in Fig. 5-3(b). The two sets of results are very close to each other, with the minimum value of cross-correlation coefficient being 0.99992 for all Poisson's ratios. It

is noted that in the parenthesis of Eq. (5-8), only linear term of Poisson's ratio is used for purpose of simplifying the viscoelastic analysis in the sequel. Nonlinear terms in the parenthesis of Eq. (5-8) can provide slightly higher accuracy, but will lead to higher level of complexity in viscoelastic analysis, and are not used in this analysis.

5.2.3 Viscoelastic solutions

Eq. (5-8) shows that Berkovich indenter has a load-displacement relationship different from a conical indenter which is

$$P = \frac{4}{\pi \tan\alpha} \frac{\mu}{1-\nu} h^2 . \tag{5-9}$$

The representations in terms of elastic parameters are different in equations for indentations by Berkovich and spherical indenters. The situation is similar in the solutions to viscoelastic indentations by two indenters using hereditary integral operators (Lee and Radok, 1960). Consequently, using both Berkovich indenter and an axisymmetric indenter would potentially lead to the measurements of two independent viscoelastic functions. In this study, a spherical indenter is used, however, the similar approach can be used for a conical indenter or a circular flat punch indenter.

The Hertzian solution (Hertz, 1881) for indentation load-displacement relation by a spherical indenter indenting into a homogeneous, isotropic and linearly elastic material is

$$P = \frac{8\sqrt{R}}{3(1-\nu)} \mu h^{3/2} . \tag{5-10}$$

Eq. (5-8) can be re-written in terms of bulk modulus K and shear modulus μ for the Berkovich indenter as

$$(3K+4\mu)P_1 = 8.3348(2.6694K\mu + 1.2202\mu^2)h_1^{\,2}, \tag{5-11}$$

where P_1 and h_1 are the indentation load and displacement, respectively, under indentation by a Berkovich indenter. For indentation by a spherical indenter, Eq. (5-12) can be re-written as

$$(3K+4\mu)P_2 = \frac{8\sqrt{R}}{3}(6K\mu + 2\mu^2)h_2^{\,3/2}, \tag{5-12}$$

where P_2 and h_2 are the indentation load and displacement, respectively, under indentation by a spherical indenter. It is noted that viscoelastic indentations using either a Berkovich indenter or a spherical indenter involves varying contact area between an indenter and the work material. Consequently, the correspondence principle, requiring a fixed (i.e., time-independent) displacement boundary, cannot be applied directly. For the time-varying displacement boundary problem as in nanoindentation of a linearly viscoelastic material, Lee and Rodok (1960) developed an approach to use the hereditary integral operators to determine the relation between indentation load and displacement. Using the Lee-Radok approach for indentations by Berkovich and spherical indenters the load-displacement relations are

$$\int_0^t 3K(t-\xi)\frac{dP_1(\xi)}{d\xi}d\xi + \int_0^t 4\mu(t-\xi)\frac{dP_1(\xi)}{d\xi}d\xi = 22.2489\int_0^t \mu(t-\xi)\frac{d}{d\xi}\int_0^\xi K(\xi-\theta)\frac{dh_1^{\,2}(\theta)}{d\theta}d\theta d\xi + 10.1718\int_0^t \mu(t-\xi)\frac{d}{d\xi}\int_0^\xi \mu(\xi-\theta)\frac{dh_1^{\,2}(\theta)}{d\theta}d\theta d\xi, \tag{5-13}$$

$$\int_0^t 3K(t-\xi)\frac{dP_2(\xi)}{d\xi}d\xi+\int_0^t 4\mu(t-\xi)\frac{dP_2(\xi)}{d\xi}d\xi=16\sqrt{R}\int_0^t \mu(t-\xi)\frac{d}{d\xi}\int_0^\xi K(\xi-\theta)\frac{dh_2{}^{3/2}(\theta)}{d\theta}d\theta d\xi$$
$$+\frac{16\sqrt{R}}{3}\int_0^t \mu(t-\xi)\frac{d}{d\xi}\int_0^\xi \mu(\xi-\theta)\frac{dh_2{}^{3/2}(\theta)}{d\theta}d\theta d\xi. \quad (5\text{-}14)$$

It is noted that a non-decreasing contact area between the indenter and the workpiece should be maintained for Eqs. (5-13) and (5-14) to be valid.

Under constant rate loading histories, $P_1=V_1t$ and $P_2=V_2t$, with V_1 and V_2 being constant loading rates, Eqs. (5-13) and (5-14) are simplified to

$$\int_0^t [22.2489K(t-\theta)+10.1718\mu(t-\theta)]\frac{dh_1{}^2(\theta)}{d\theta}d\theta=V_1\int_0^t 3J(t-\xi)K(\xi)d\xi+4V_1t, \quad (5\text{-}15)$$

$$\frac{16\sqrt{R}}{3}\int_0^t [3K(t-\theta)+\mu(t-\theta)]\frac{dh_2{}^{3/2}(\theta)}{d\theta}d\theta=V_2\int_0^t 3J(t-\xi)K(\xi)d\xi+4V_2t, \quad (5\text{-}16)$$

where $J(t)$ is creep compliance in shear.

Under a constant rate loading history, both $h_1(t)$ and $h_2(t)$ can be measured from nanoindentation. Solving Eqs. (5-15) and (5-16) should lead to the determination of two independent viscoelastic functions $K(t)$ and $\mu(t)$. However, Eqs. (5-15) and (5-16) are difficult to solve directly. To circumvent this difficulty, a least squares correlation approach between experimentally measured displacements $h_1(t)$ and $h_2(t)$ and the corresponding analytical values is taken and described as follows.

The bulk and shear relaxation functions can be represented by the generalized Maxwell model:

$$K(t) = K_\infty + \sum_{i=1}^{N} K_i e^{-t/\tau_i} \text{ and } \mu(t) = \mu_\infty + \sum_{i=1}^{N} \mu_i e^{-t/\tau_i}, \tag{5-17}$$

where μ_i and K_i are relaxation numbers, τ_i the relaxation times and N the number of exponential terms in the Prony series.

Define a least squares correlation coefficient, C,

$$C = \frac{\sum_{i=1}^{M} \left(h_{1,i}^{\exp} - h_{1,i}^{th}\right)^2}{\sum_{i=1}^{M} \left(h_{1,i}^{\exp}\right)^2} + \frac{\sum_{i=1}^{M} \left(h_{2,i}^{\exp} - h_{2,i}^{th}\right)^2}{\sum_{i=1}^{M} \left(h_{2,i}^{\exp}\right)^2}, \tag{5-18}$$

where $h_{1,i}^{\exp}$ and $h_{2,i}^{\exp}$ are the measured displacement data at time t_i for Berkovich indentation and spherical indentation, respectively; $h_{1,i}^{th}$ and $h_{2,i}^{th}$ are analytical results of displacements computed from Eqs. (5-15) and (5-16), respectively, and can be represented in terms of the parameters in Eq. (5-17) after equations in Eq. (5-17) are substituted into Eqs. (5-15) and (5-16). When the measured displacements can be fully described by displacements computed by Eqs. (5-15) and (5-16) using appropriate parameters in Eq. (5-17), ideally C would be zero. In reality, however, C will not reach zero; instead, it must be minimized with the use of appropriate parameters in Eq. (5-17). During the minimization process, the best-fit parameters in Eq. (5-17) are iteratively searched until the coefficient C is minimized. The minimization of C will converge when two minimizations, one for the Berkovich indentation and the other for the spherical indentation, as shown in Eq. (5-18) are simultaneously achieved, indicated by the best correlations between nanoindentation load-displacement curves determined from both nanoindentation data and analytical results for each indenter. Thus, minimizing C leads to

a set of appropriate parameters in Eq. (5-17) for determining two independent viscoelastic functions, $K(t)$ and $\mu(t)$.

5.3 Nanoindentation measurements

An MTS Nano Indenter XP system was used in nanoindentation tests to acquire load-displacement data. The nanoindenter can reach a maximum indentation depth of 500 μm and a maximum load of 500 mN. The displacement resolution is 0.2 nm and the load resolution is 50 nN. Both the Berkovich and spherical indenters are made of diamond; their schematic geometries are as shown in Fig. 5-2. The Berkovich indenter has a three-faced pyramidal tip, and the spherical indenter has a tip radius of 10 μm. In all nanoindentation with the spherical indenter, the maximum indentation depth was below 620 nm.

The materials used in these tests were poly(vinyl acetate) (PVAc) and poly(methyl methacrylate) PMMA. The PVAc resin was the same as used in the work by Knauss and Kenner (1980), and by Deng and Knauss (1997); the resin was stored in an air-tight container, and was molded using the same procedures as in their work. The PMMA samples were made from the same PMMA plate as used in the work by Lu, *et al*. (1997) and by Sane and Knauss (2001). The PVAc specimen has a glass transition temperature of 29 ^oC and the PMMA specimen has a glass transition temperature of 105 ^oC. The dimensions of PVAc and PMMA specimens were $20mm \times 20mm \times 6mm$ and $20mm \times 10mm \times 5mm$, respectively. The PVAc specimen was annealed at 34 ^oC and PMMA specimen was annealed at 110 ^oC for two hours, and they were cooled down

slowly to room temperature at a cooling rate of approximately 5 ºC /hr. Samples were then stored in an enclosed desiccator with approximately 50% relative humidity produced by placing a saturated salt solution in this enclosed environment. The specimens were then carefully mounted on aluminum holders. All specimens had ageing time of nearly 75 hours. The humidity in the room was maintained at ~ 50% relative humidity.

The nanoindentation tests on PVAc were performed in air at 30 ºC. An infrared bulb placed close to the floor inside the nanoindenter chamber was used to heat the enclosed nanoindentation system to the desired temperature. The temperature was monitored and controlled by a temperature controller (Chromalox Instruments and Controls, Model 1604) with a resolution of ±0.1 ºC. Proper thermal insulation was used on the MTS Nano Indenter XP system to maintain the temperature stability during nanoindentation. The nanoindenter was calibrated with the use of a fused silica sample to ensure that load-displacement outputs were accurate at 30 ºC. The nanoindentation tests on PMMA were conducted at room temperature (23 ºC). Each test did not start until the drift rate of the indenter tip had dropped below a set value (typically 0.05 *nm*/*s*) to ensure that a thermal equilibrium condition for the specimen and nanoindenter system had been reached. This procedure is necessary as the precision of the nanoindenter depends on the temperature gradient of the instrumentation. After the indenter tip had made contact with the specimen surface, a constant rate indentation load was applied, and both the indentation load and indentation depth were recorded simultaneously at a sampling rate of five data points per second.

5.4 Results and discussions

Results on bulk and shear relaxation moduli are reported and discussed in this section from nanoindentation measurements using both Berkovich and spherical indenter tips. Constant rate loading histories were used in all nanoindentation tests.

For PVAc, nanoindentation tests were carried out at 30 ^{o}C, right in the glass transition region (T_g = 29 ^{o}C). A constant rate loading at a loading rate of 19.8 $\mu N/s$ was applied for both Berkovich and spherical indenters. The entire nanoindentation duration was less than 120 s in order to ensure thermal stability during each test. The load-displacement curves for PVAc from nanoindentation using both Berkovich and spherical tips are shown in Fig. 5-4. Data scattering from different tests are indicated by the error bars. As shown in Fig. 5-4, the repeatability of load-displacement data was high.

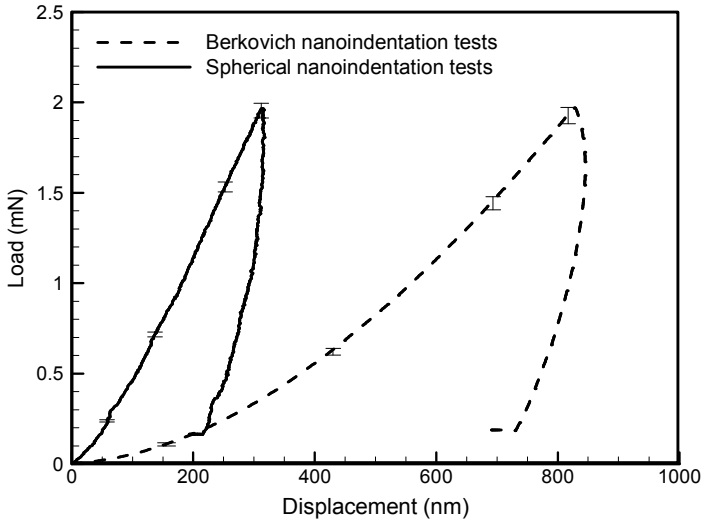

Fig. 5-4 Nanoindentation load-displacement curves for PVAc

The load-displacement data obtained from nanoindentation were analyzed using Eqs. (5-15) - (5-18) to determine both bulk and shear relaxation functions. An iterative algorithm was applied to extract two independent relaxation functions from minimization of the least squares coefficient C in Eq. (5-18). The bulk and shear relaxation functions were determined when the best correlation between load-displacement curves from nanoindentation and analysis was achieved. Both the measured and analytical load-displacement curves are plotted in Fig. 5-5(a) and Fig. 5-5(b) for indentations by Berkovich indenter and spherical indenter, respectively. The cross- correlation coefficients between the two load-displacement curves for Berkovich indenter and spherical indenter are 0.9998 and 0.9999, respectively. The good correlations were reached simultaneously in the two sets of P-h curves for both indenters, indicating the convergence of the overall minimization of C. The minimum C as computed from Eq. (5-18) is 0.000992.

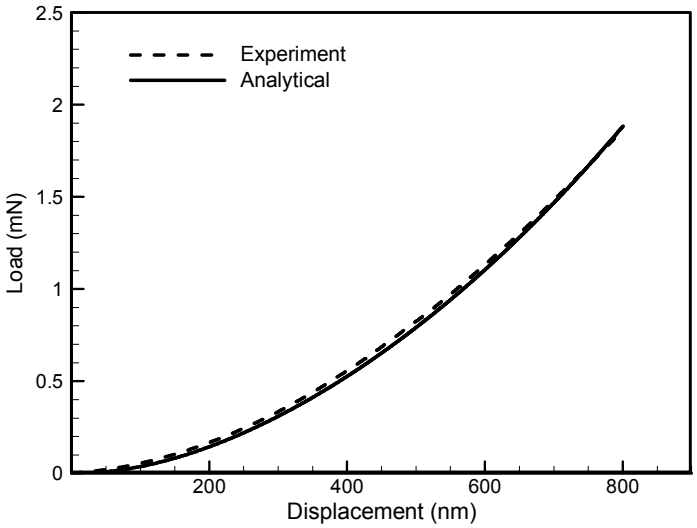

(a) Berkovich indenter

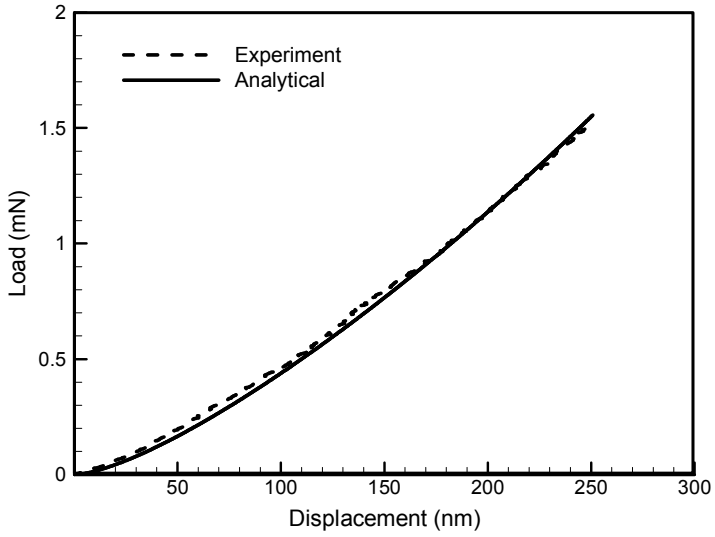

(b)Spherical indenter

Fig. 5-5 Minimization results of load-displacement curves for PVAc

Minimizing *C* leads to the following bulk and shear relaxation functions for PVAc

$$K(t) = 2.801 + 0.448e^{-0.05t} + 0.252e^{-0.1t}\ GPa, \tag{5-19}$$

$$\mu(t) = 1.102 + 0.331e^{-0.05t} + 0.165e^{-0.1t}\ GPa. \tag{5-20}$$

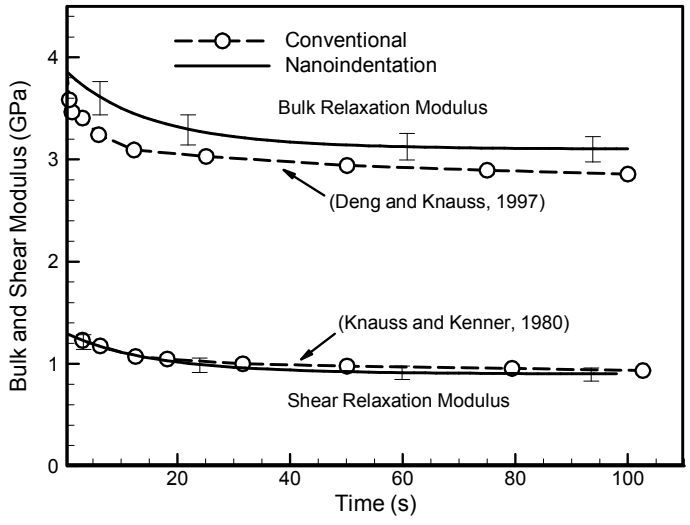

Fig. 5-6 Results of $K(t)$ and $\mu(t)$ for PVAc from nanoindentation

The bulk and shear relaxation functions given by Eqs. (5-19) and (5-20) are shown in Fig. 5-6. Also plotted in Fig. 5-6 are the conventional data. The conventional bulk relaxation modulus for PVAc are converted from complex bulk compliance data obtained by Deng and Knauss (1997), and the shear relaxation modulus data were measured by Knauss and Kenner (1980) on PVAc samples made of the same PVAc resin following the same molding procedures. An approximation method for data conversion as described by Emri *et al*. (2005) was used to convert complex bulk modulus (reciprocal of complex bulk compliance) in the frequency domain to bulk relaxation modulus in the time domain. As shown in Fig. 5-6, the bulk and shear relaxation functions are in a reasonably good agreement with data obtained from conventional tests. The average errors for bulk and shear relaxation moduli are 9.54% and 2.64%, respectively. The following sources could contribute to the discrepancy in the data from nanoindentation in this work and from conventional tests: (1) the conventional bulk relaxation modulus was not measured directly in the time domain, and was converted from complex bulk modulus in the frequency domain. Using an approximate method to convert data in the frequency domain to the time domain could cause error; and (2) nonlinear deformation in a small area in the workpiece close to indenter was not considered in the model.

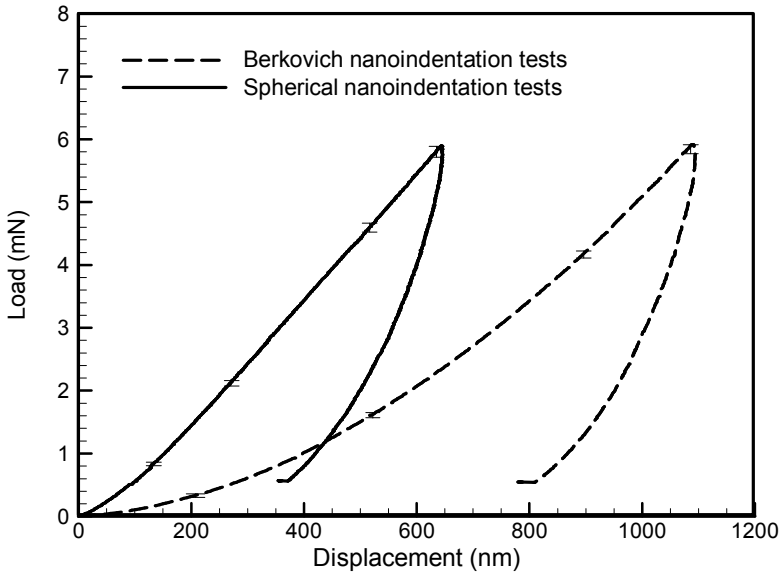

Fig. 5-7 Nanoindentation load-displacement curves for PMMA

Nanoindentation on PMMA was conducted at 23 ºC. A constant rate loading at a loading rate 33.0 $\mu N/s$ was used for nanoindentation using both Berkovich and spherical indenters. The load-displacement curves from nanoindentation measurements are shown in Fig. 5-7; the results were very reproducible for each indenter, indicated by the error bars showing data scattering. The load-displacement data were analyzed using Eqs. (5-15) - (5-18) to minimize the least squares correlation coefficient defined in Eq. (5-18) so that a best set of parameters in the Prony series in Eq. (5-17) can be determined to allow the analytical load-displacement data to correlate with data from nanoindentation measurements. The best set of parameters in the Prony series are then used in Eq. (5-17) to determine the two independent viscoelastic functions, bulk and shear relaxation functions. The results on nanoindentation load-displacement data for the use of Berkovich and spherical indenters are shown in Fig. 5-8(a) and Fig. 5-8(b), respectively. The cross correlation coefficient between analytical results and the data from

nanoindentation measurements is 0.9991 for indentation by a Berkovich indenter, and is 0.9997 for indentation by a spherical indenter. The good correlation for both indenters, as shown in Fig. 5-8, leads to the minimization of C, which is 0.000699, as computed from Eq. (5-18).

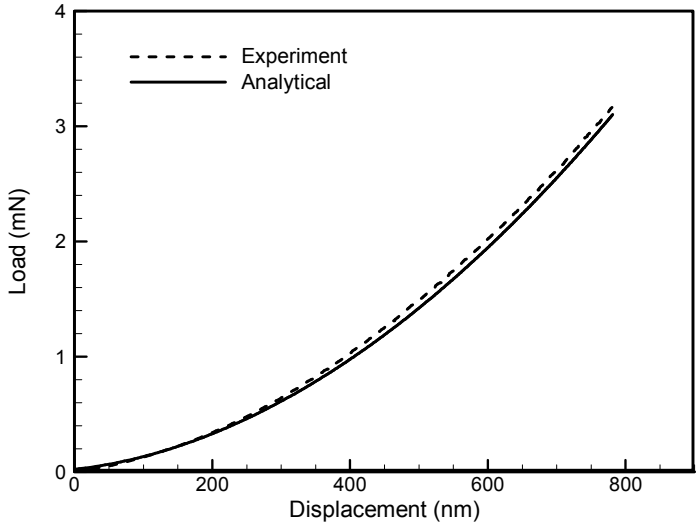

(a) Berkovich indenter

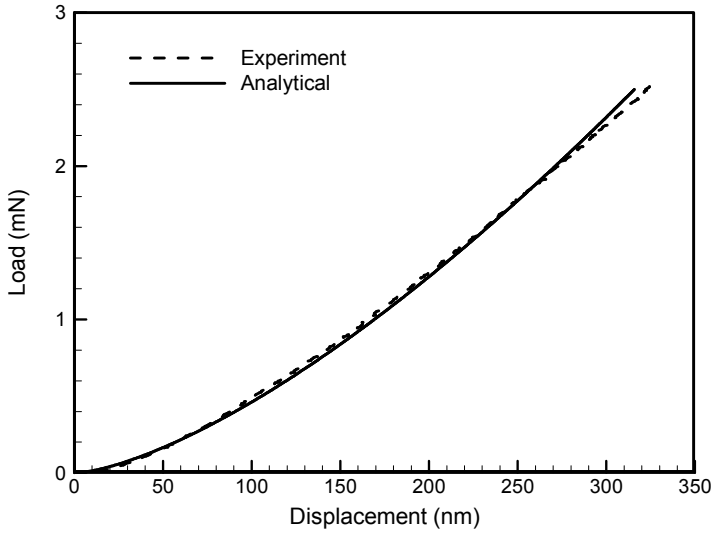

(b) Spherical indenter

Fig. 5-8 Minimization results of load-displacement curves for PMMA

Results of the bulk and shear relaxation functions for PMMA as determined from this approach are

$$K(t) = 4.800 + 0.336e^{-0.01t} + 0.288e^{-0.1t}\ GPa, \tag{5-21}$$

$$\mu(t) = 1.001 + 0.075e^{-0.05t} + 0.060e^{-0.1t}\ GPa. \tag{5-22}$$

The bulk and shear relaxation functions are shown in Fig. 5-9, and are compared with conventional data. The conventional data of bulk relaxation modulus were converted from the complex bulk compliance measured by Sane and Knauss (2001), and the conventional shear relaxation data were measured by Lu, Zhang and Knauss (1997). As shown in Fig. 5-9, the data measured using the nanoindentation agree reasonably well with conventional data. The average errors for the measured bulk and shear relaxation moduli are 4.8% and 5.9%, respectively.

Since the temperature for nanoindentation on PVAc was 30 ºC, slightly higher than its glass transition temperature (T_g = 29 ºC), the PVAc was in the glass transition region, so that relaxation was significant. For example, as shown in Fig. 5-6 the measured shear relaxation modulus decreased by 30.9% for PVAc within 100 *s* from the beginning of tests, representing a very pronounced viscoelastic behavior. For PMMA, nanoindentation was conducted at 23 ºC, much lower than its glass transition temperature (T_g = 105 ºC). The shear relaxation modulus decreased by 11.9% within 100 *s*, as shown in Fig. 5-9, indicating that the relaxation behavior of PMMA in the glassy state is present, but not as significant as that of PVAc in the glass transition region.

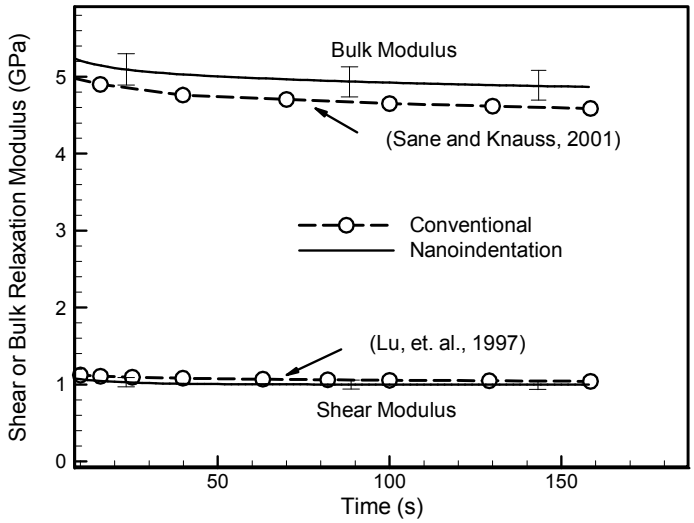

Fig. 5-9 Results of $K(t)$ and $\mu(t)$ for PMMA from nanoindentation

It is noted that for nanoindentation using spherical indenter, the Hertzian solution holds only when the ratio of indentation depth to the radius of spherical indenter is small, for example, less than ~ 0.16 (Giannakopoulos, 2000). For all spherical indentations in this study, the maximum indentation depth used was less than 350 *nm*, so that $h < 0.05R$, thus the use of Herzian solution was justified.

In order to ensure that the deformation of the polymer samples is in the linearly viscoelastic regime, the maximum indentation depth into the sample surface for PMMA and PVAc materials was controlled to within the limit of linearity. According to Lu, *et al*. (2003), the limit of linearity in indentation depth under constant rate loading condition was determined as 780 *nm* for PMMA for Berkovich indentation. It was found that in indentation within the limit of linearity, the deformation of PMMA is (nearly) linearly viscoelastic. For PVAc, since the specimen was in the rubbery state (above glass transition temperature) in nanoindentation, the limit of linearity was considered to be

higher than that of glassy state (below glass transition temperature). Consequently, by the use of a maximum indentation displacement of ~ 800 *nm* for PVAc, the PVAc would stay within limit of linearity.

Measurements of two independent viscoelastic functions are a well-known challenging problem, even at macroscale, due to excessive accuracy needed to acquire two independent sets of time-dependent data (Lu et al., 1997; Tschoegl et al., 2002) The method presented here has potential for measurements of two independent viscoelastic functions at submicron scale. Recently the commercially available nanoindenter can reach a temperature range between -10 °*C* and 200 °*C*. The method presented here can be applied to this range of temperatures so that both bulk and shear relaxation functions can be determined over a wide range of temperatures to form master curves as necessary information for the prediction of long-term viscoelastic behavior necessary for the investigation of long-term durability of very small amounts of time-dependent materials such as coatings in medical devices, MEMS and NEMS.

5.5 Conclusions

A method has been developed to extract two independent viscoelastic functions from nanoindentation data. Based on the difference of representations of two independent viscoelastic functions in the load-displacement relations between the Berkovich (non-axisymmetric) and spherical indenter (axisymmetric, or any other axisymmetric indenter), two independent viscoelastic functions can be separated and determined from load-displacement data from nanoindentation measurements. To determine the

viscoelastic load-displacement relation for an asymmetric Berkovich nanoindenter, finite element simulations were conducted for a linearly elastic material, and the results were fitted into a unified equation for all Poisson's ratios. The fitted elastic relation for a Berkovich indenter was then extended to a viscoelastic load-displacement relation using hereditary integral operator developed by Lee and Radok (1960). The viscoelastic load-displacement relations for both Berkovich and spherical indenters provide two independent equations for solving two independent viscoelastic solutions. Under constant rate loading conditions, the nanoindentation load-displacement relationships can be fitted into analytical equations with the use of appropriate parameters in the Prony series for the two material functions through minimizing a least squares correlation coefficient between measurement and numerical data. The best set of parameters are then used to determine the two independent viscoelastic functions. Two bulk polymers (PVAc and PMMA) were used in the validation. The methods, however, are expected to be applicable to very small amounts of material and heterogeneous materials where homogeneity is assumed locally. Both bulk and shear relaxation functions determined for PVAc and PMMA have a reasonably good agreement with the data measured from conventional tests on bulk materials, providing validation for the method presented.

CHAPTER VI

APPLICATION OF NANOINDENTATION TO MEASURING VISCOELASTIC FUNCTION FOR THIN FILMS I: SINGLE WALL CARBON NANOTUBE (SWNT)

6.1 Introduction

With the discovery of the excellent mechanical properties of single-wall carbon nanotube (SWNT), fabrication of SWNT/polymer composites has received increasing attention. SWNT/polymer composites prepared by typical hybrid process, such as blending, polymerization, extrusion, and surface modification, have such problems as poor matrix-SWNT connectivity and phase segregation, leading to the premature mechanical failure. Recently Mamedov *et al.* (2002) used the layer-by-layer assembly (LBL) technique to fabricate SWNT/polymer composites, and successfully mitigated the problems of connectivity and phase segregation. In this study, layer-by-layer assembly is used to prepare SWNT/polyelectrolyte nanocomposite films.

In the material development phase, the amounts of materials obtained from LBL technique are small, leading to difficulty in measuring the in-plane and the through-thickness mechanical properties of SWNT/polymer composite films using the conventional testing techniques, such as tensile tests and compression of stacking films. The nanoindentation technique (Oliver and Pharr, 1992) should provide an alternative approach to measure the properties of small amounts of materials such as SWNT/polymer

nanocomposite films. Methods for measuring the Young's modulus have been very well established for time-independent materials. Oliver and Pharr (1992) proposed a method todetermine the basic material properties such as Young's modulus. The method is based on Sneddon's solution (Sneddon, 1960) for the relationship between the load and displacement for an axisymmetric indenter indenting into a half-space composed of a linearly elastic, isotropic and homogeneous material. While the method works well for time-independent materials, such as metals well below their melting points, applying the methods directly to viscoelastic materials has experienced problems. For example, the unloading curve in viscoelastic materials sometimes has a negative slope, under situations where a small unloading rate and a relatively high load were used for a material with pronounced viscoelastic effects. Some work in recent years has improved the methods proposed by Oliver and Pharr (1992) for the determination of Young's modulus, or Young's relaxation modulus. Cheng et al. (2000) derived the analytical solutions for linearly viscoelastic deformation under flat-punch indentation, and provided a method to measure viscoelastic as well as instantaneous elastic properties using a flat-punch indenter. Lu et al. (2003) proposed methods to measure the creep compliance of solid polymers using either the Berkovich indenter or the spherical indenter and they also proposed a new method to measure the viscoelastic functions in frequency domain using a spherical indenter (2004). The methods are applicable to arbitrary linearly viscoelastic materials characterized by the generalized Kelvin's model.

This chapter presents methods for measuring the viscoelastic properties of polyelectrolyte films with and without SWNTs through the consideration of the viscoelastic indentation solution. In each nanoindentation test, a loading history was

prescribed to a film and the resulting response was recorded, subsequently the experimental load-displacement curve was analyzed to determine the viscoelastic properties as a function of time. Both in-plane and through-thickness properties of the nanocomposite films were investigated using nanoindentation.

6.2 Analytical prerequisites

In this section we provide formulas used for extracting the linearly viscoelastic properties from nanoindentation data in the time domain. The Berkovich indenter is considered herein, and is modeled as a rigid conical indenter. For the indentation problem in which a rigid conical indenter is indenting into an elastic half-space, Sneddon (1965) derived relationship between load and displacement,

$$h^2 = \frac{\pi(1-\nu)\tan\alpha}{4G} P, \tag{6-1}$$

where P, h are load and displacement, respectively; α the angle between the cone generator and the substrate plane, ν the Poisson's ratio, and G the shear modulus.

If the half-space is composed of a linearly viscoelastic material, the indentation involves a time-dependent contact area between the indenter and the workpiece. For this moving boundary problem, Lee and Radok (1960) proposed a hereditary integral operator to determine the time-dependent stresses and deformations in the case where the contact area between the indenter and the workmaterial does not decrease with time. Applying this technique to Eq. (6-1) leads to the following time-dependent indentation depth under a prescribed arbitrary indentation loading history *P(t)* in a linearly viscoelastic material

$$h^2(t) = \frac{\pi(1-\nu)\tan\alpha}{4}\int_0^t J(t-\xi)\left[\frac{dP(\xi)}{d\xi}\right]d\xi\,, \tag{6-2}$$

where $J(t)$ is the creep compliance in shear at time *t*. Under a constant rate loading, $P(t) = v_0 t$, differentiation of Eq. (6-2) leads to

$$J(t) = \frac{8h}{\pi(1-\nu)v_0\tan\alpha}\frac{dh(t)}{dt}\,, \tag{6-3}$$

where v_0 is the loading rate. Eq. (6-3) provides a direct differentiation method to determine the creep compliance in shear.

We next provide another method to determine the creep compliance. The creep compliance of a linearly viscoelastic material can be expressed by the generalized Kelvin model

$$J(t) = J_0 + \sum_{i=1}^{N} J_i(1-e^{-t/\tau_i})\,, \tag{6-4}$$

where J_0, J_i are compliance numbers, τ_i retardation times.

Under $P(t) = v_0 t$, substituting Eq. (6-4) into Eq. (6-2) leads to

$$h^2(t) = \frac{1}{4}\pi(1-\nu)\tan\alpha[(J_0 + \sum_{i=1}^{N} J_i)P(t) - \sum_{i=1}^{N} J_i(v_0\tau_i)(1-e^{-\frac{P(t)}{v_0\tau_i}})]\,. \tag{6-5}$$

After fitting Eq. (6-5) to the load-displacement curve from nanoindentation, all parameters, J_0, J_i (*i=1, ..., N*) and τ_i can be obtained. The creep compliance can be subsequently determined using Eq. (6-4). Once *J(t)* is obtained, other viscoelastic functions, such as the uniaxial relaxation modulus *E(t)*, can be determined. For example, the creep function in shear, *J(t)*, can be converted to *E(t)* through the following relation

$$\int_0^t E(\tau)J(t-\tau)d\tau = 2(1+\nu)t\,. \qquad (6\text{-}6)$$

6.3 Experimental details

6.3.1 SWNT/ polyelectrolyte films preparation

Poly(dimethyldiallylammonium chloride) (PDDA) and Poly(acrylic acid) (PAA) were used as organic components of LBL assembly. Single wall carbon nanotubes in the form of 15mg/g aqueous gel with lengths between 600-700 nm have been oxidized according to procedures described elsewhere (Mamedov et al., 2002; Hammond,2004; Lui et al, 1998). The nutshell procedures are as follows: 0.7 g of gel material was refluxed in 10 ml of 2.6 M HNO3 solution at 850C for 45 hours; then, the solution was centrifuged at 900 rpm and the black precipitate was washed by de-ionized water (DI-water) and centrifuged again.

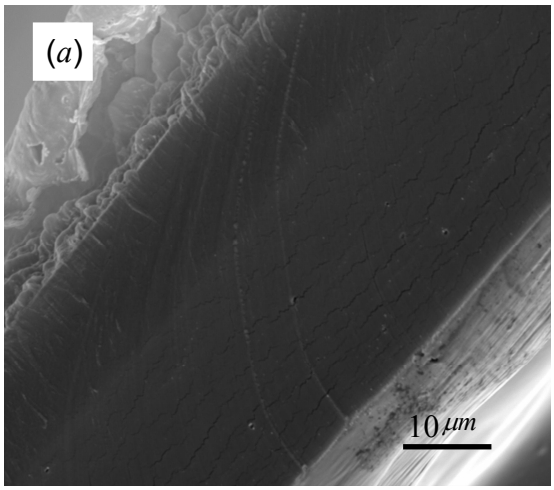

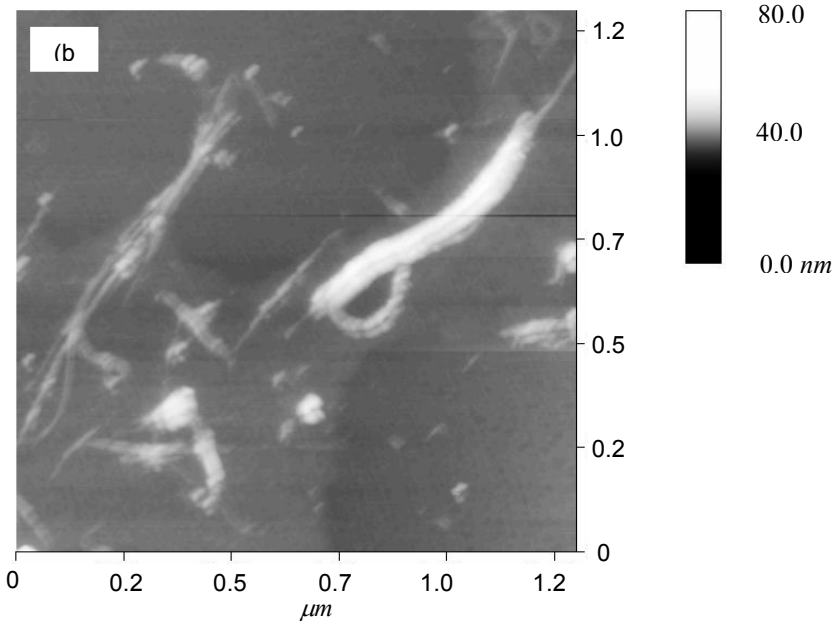

Fig. 6-1 SEM and AFM images of SWNT/polyelectrolyte films. (a) SEM image of the cross section of a 100-layer SWNT/polyelectrolyte film; (b) AFM image of top surface of a monolayer SWNT/polyelectrolyte film.

This procedure was repeated 2 or 3 times. After titration of supernatant to pH=8.0 with 1M NaOH, it was shaken with the precipitate and centrifuged again. The resulted precipitate was separated and re-dispersed in 100 ml of DI-water by bath-sonication for 50 min. The resulted solution was centrifuged at 5,000 rpm for 4 hours to remove un-dispersed SWNT bundles and impurities. Supernatant solution, containing ca. 0.1% oxidized SWNTs was used for layer-by-layer deposition. A typical deposition cycle consisted of: (1) deposition of PDDA for 10 minutes; (2) rinsing; (3) deposition of PAA/SWNT mixture for 30 minutes; and (4) final rinsing. Both rinsing steps consisted of several flushes of deposition chamber for a total of 3 minutes. The concentrations of

deposited species were 0.5% for both polymers and ca. 0.1% for oxidized SWNTs. When the desired film thickness was obtained (usually 80-100 deposition cycles), nanocomposites were air-dried. Images of SWNT/Polyelectrolyte films were acquired by a scanning electronic microscope (SEM) and an atomic force microscope (AFM). A JOEL JXM 6400 SEM was used to observe the cross-section of a 100-layer SWNT/Polyelectrolyte film; the accelerate voltage and working distance used in imaging were 25 kv and 45 *mm*, respectively. An SEM image of the cross section of a 100-layer film is shown in Fig. 6-1 (a). The top surface of a monolayer SWNT/polyelectrolyte film was observed using an AFM (Digital Instruments, Multimode Scanning Probe Microscope with controller Nanoscope III a) under tapping model. The cantilever used has a spring constant of 40 *N/m* and tip radius of 5 *nm*. Fig. 6-1 (b) shows an AFM top surface image of monolayer SWNT/polyelectrolyte film. The SWNT loading in the nanocomposite in this investigation is 4.75%.

6.3.2 Measurements

Nanoindentation measurements

An MTS Nano Indenter XP system with a Berkovich indenter tip was used for nanoindentation measurements. The resolutions for load and displacement are 50 *nN* and 0.01 *nm*, respectively. The Berkovich indenter was molded as a conical indenter with a half-cone angle of 70.3° based on the relation between the cross sectional area and depth. Nanoindentation was conducted at 23°*C* under a relative humidity around 50%. In all indentation experiments conducted in this work, the measured indenter tip drift rate was

within $\pm 0.02\ nm/s$. Indentation tests were performed on both the free surface of the films and the cross sections of films to measure both in-plane and through-thickness properties. For measurements of the through-thickness properties, each film was glued to an aluminum substrate using an epoxy (Loctite, Quick Set). In applying the adhesive, the top surface of the film was pressed slightly by a glass slide to flatten the entire film surface for nanoindentation. The smooth film surface facing the glass substrate in LBL process was used for nanoindentation; for measurements of in-plane properties, a film was embedded into polybed matrix and then sectioned by ultramicrotome to reveal the cross section. Film samples were annealed at $80°C$ to reduce the effects from prior thermal/mechanical history. Several locations in each film were chosen; and the results were found to be very reproducible.

Small scale tension measurements

The in-plane properties of the SWNT/polyelectrolyte multilayer nanocomposite film were also characterized in tension using small scale tensile measurements (SSTM). A film sample complying with the American Standard Test Methods (ASTM) D1708 standard was used. The dumb-bell shaped tensile specimens, with a gage length 21.75 *mm*, a width 4.75 *mm* and a thickness 0.056 *mm*, were die-cut from the multilayer nanocomposite films. All samples were prepared in identical procedures as the samples used in nanoindentation. All tensile tests were performed in a lab with a temperature of 23 $°C$ and a relative humidity of around 50%.

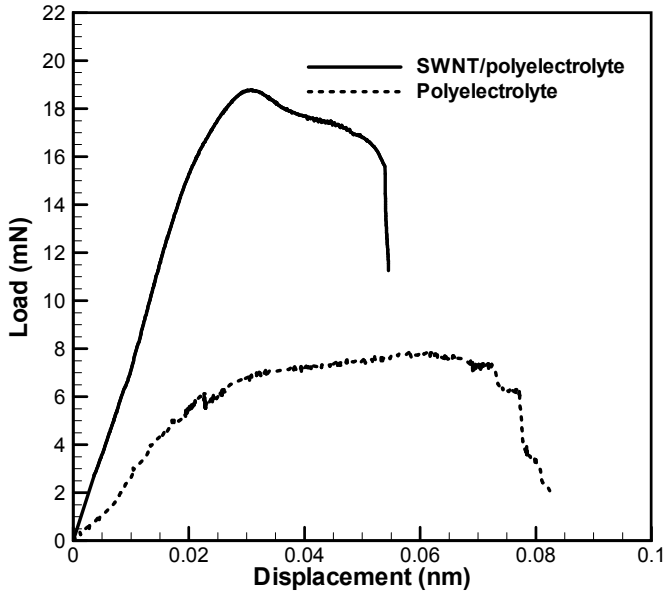

Fig. 6-2 Stress-strain curves of SWNT/polyelectrolyte and resin

6.4 Results and Discussions

The stress-strain curves for SWNT/polyelectrolyte multilayer composites and the resin material (PAA+PDDA) are shown in Fig. 6-2 from small scale tensile testing. From Fig. 6-2, the Young's moduli of the multilayer polyelectrolyte and the SWNT/polyelectrolyte multilayer nanocomposite are determined as 300 *MPa* and 770 *MPa*, respectively. The tensile strengths for the neat LBL polyelectrolyte and the SWNT/polyelectrolyte films are 6.6 *MPa* and 18.6 *MPa*, respectively. With the use of 4.75% of SWNT in polyelectrolyte, the Young's modulus and tensile strength have been enhanced by 2.57 times and 2.82 times over the near polyelectrolyte film, respectively.

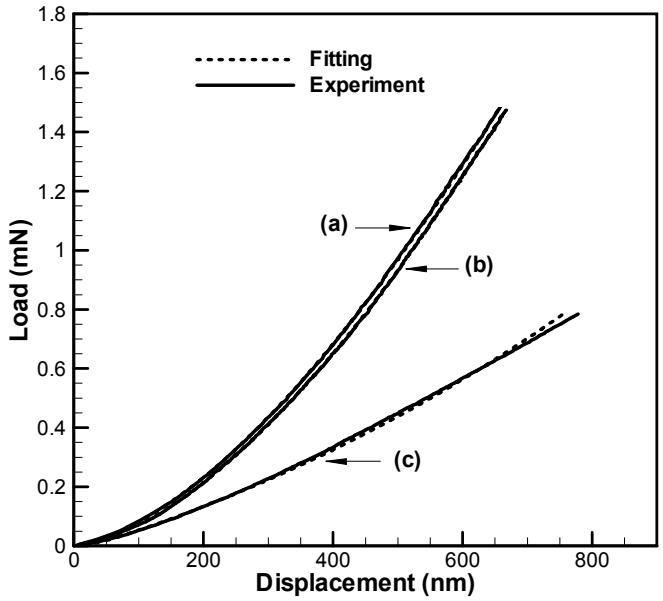

Fig. 6-3 Experimental and fitted nanoindentation load-displacement curves. (a) In-pane nanoindentation load-displacement curves for SWNT/polyelectrolyte films from nanoindentation measurements and the fitting method; (b) Through-thickness nanoindentation load-displacement curves for SWNT/polyelectrolyte films from experiments and fitting method; (c) Nanoindentation load-displacement curves of polyelectrolyte from experiments and fitting method.

We next present results from nanoindentation tests. In all nanoindentation tests on the SWNT composite films and polymer films, a constant rate loading history was applied. The load-displacement curves of polyelectrolyte film (PAA+PDDA) and SWNT/polyelectrolyte films (SWNT+PAA+PDDA) are shown in Fig. 6-3. It can be seen that nanoindentation load-displacement curve in the through-thickness direction is very close to the in-plane curve, indicating that the multilayer films have very similar linearly viscoelastic behavior in these two directions. The experimental load-displacement data were fitted into Eq. (6-5), and the fitted curves are also plotted in Fig. 6-3. It is seen that Eq. (6-5) can describe the nanoindentation data very well. In the computation, the Poisson's ratio for both films is assumed to be 0.3. With the compliance numbers and

retardation times determined from correlating Eq. (6-5) to nanoindentation data, the creep function is computed using Eq. (6-4), and the uniaxial relaxation modulus $E(t)$ is determined from Eq. (6-6). The in-plane relaxation modulus of SWNT/polyelectrolyte film is

$$E(t) = 0.787 + 0.325e^{-0.1t} + 0.254e^{-0.01t} + 0.208e^{-0.001t} \ GPa; \tag{6-7}$$

the through-thickness uniaxial relaxation modulus of SWNT/polyelectrolyte film is

$$E(t) = 0.725 + 0.3053e^{-0.1t} + 0.2984e^{-0.01t} + 0.197e^{-0.001t} \ GPa; \tag{6-8}$$

and the relaxation modulus of the neat polyelectrolyte film is

$$E(t) = 0.357 + 0.45016e^{-0.1t} + 0.390e^{-0.01t} \ GPa. \tag{6-9}$$

From Eqs. (6-7) and (6-8) the in-plane and through-thickness moduli of SWNT/polyelectrolyte approach 0.787 *GPa* and 0.725 *GPa*, respectively, as time t increases to 33 *s*. The maximum difference in linearly viscoelastic properties in the two directions is 8.6%. The Young's modulus data in these two directions agree with the modulus of 0.77 *GPa* as determined from SSTM. Similarly, from Eq. (6-9), the Young's modulus of polyelectrolyte determined from nanoindentation is 0.357 *GPa*, close to the Young's modulus of 0.3 *GPa* as determined from small scale tensile measurement.

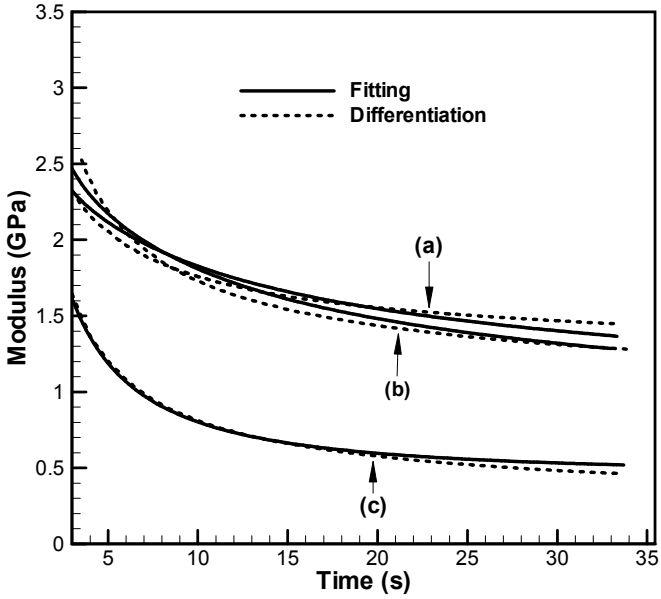

Fig. 6-4 Uniaxial relaxation modulus of SWNT/polyelectrolyte film and polyelectrolyte film measured by nanoindentation. (a) In-plane modulus measured by both fitting and differentiation methods for SWNT/polyelectrolyte films; (b) Out-of plane modulus measured by both fitting and differentiation methods for SWNT/polyelectrolyte films; (c) Modulus measured by both fitting and differentiation methods for polyelectrolyte films.

The uniaxial relaxation moduli for both SWNT/polyelectrolyte and polyelectrolyte films are shown in Fig. 6-4. It is seen that the in-plane modulus of SWNT composite film is 2.46 times of that for PAA+PDDA film at t= 33 s, indicating significant reinforcement effects of SWNTs. The relaxation curves for the in-plane modulus and through-thickness modulus are very close to each other, implying that the linearly viscoelastic properties are very close to each other, and the film can be modeled as isotropic in the regime of linear viscoelasticity. The modulus depends primarily on the composition of the films when the SWNTs are relatively straight. In this case, the SWNTs are in general oriented within the film plane, and the orientation of SWNTs within the plane is random. The volume fraction as determined from any in-plane direction and through-thickness direction is

approximately the same, leading to very close linearly viscoelastic properties. If should be noted, though, the material strength is expected to be much higher in the in-plane direction than in the through-thickness direction due to the such effects as high strength and interlocking of the SWNTs oriented within the film plane.

Table 6-1 Comparison of modulus data for the SWNT/polyelectrolyte and polyelectrolyte films determined from different approaches

	In-plane modulus of SWNT/polyelectrolyte (*GPa*)	Through-thickness Modulus of SWNT/polyelectrolyte (*GPa*)	Modulus of polyelectrolyte (*GPa*)
Tensile test	0.770	N/A	0.300
Nanoindentation (this study)	0.787	0.725	0.357
Default output value from Nano XP (MTS)	4.258	3.471	0.894

The MTS Nano Indenter XP system also gave Young's modulus based on analysis in software TestWorks 4.06 for time-independent materials. These data for the SWNT/polyelectrolyte film and the polyelectrolyte film, together with the nanoindentation data obtained from linearly viscoelastic analysis described here are summarized in Table 1. The default values provided by TestWorks 4.06 software on MTS Nano Indenter XP system is based on elastic/plastic analysis of unloading curves, which did not take into account of the time-dependent behavior of polymers and can cause significant error in the measurements of properties of polymers using nanoindentation (Lu et al., 2003). The direct output modulus from the nanoindenter is based on the elastic-plastic analysis on indentation using the approach developed by Oliver and Pharr (Ref. 2 in the References list). The modulus is determined from

unloading portion of the nanoindentation load-displacement curve and the contact area measured at the maximum nanoindentation load. While the method has been very effective and robust for elastic-plastic materials (without time-dependency), measurements of viscoelastic properties using this method have experienced problems (Lu, et al., 2003). The method tends to overestimate significantly the Young's modulus for a viscoelastic material such as polymers. The major reason is that during unloading, the displacement does not follow closely with the decreased load (as in the case for an elastic-plastic materials) in unloading due to prior increasing of the applied nanoindentation load and the memory effect of the time-dependent materials. As a result even when the load decreases during initial unloading, the displacement does not decrease at the same pace as the force, and sometimes could even increase during the initial stage of unloading, causing some high unloading slope, or negative slope in the initial unloading load-displacement curve, and leading the output of higher modulus than the actual value. Consequently a method appropriate for a viscoelastic material needs to be used for nanoindentation measurements of properties of time-dependent materials such as polymers. Since 95.25% (by weight) of the SWNT/polyelectrolyte in this study is polymer, consequently it is necessary to use viscoelastic analysis to measure its properties. As shown in Table 1, the values of modulus provided by default output from the nanoindentation system are much larger than those determined using both approaches presented in this study, indicating that the direct output from the nanoindenter on a viscoelastic film is not appropriate.

For nanoindentation of a film deposited on a substrate, the effect of substrate on the measurement of properties of the film is an issue of concern. An empirical estimation is

that the substrate is nearly negligible when the indentation depth is less than 10% of the thickness of the film, and the nanoindentation can be considered to be made on a half-space. However, it was found the critical value at which the substrate will affect varies with different combinations of film/substrate. Finite element analysis (Cai and Bangert, 1995) showed that for a hard film on a soft substrate, the critical penetration is about 7% of the thickness of the film; while for soft film on a hard substrate, the critical value is about 20% (Bhattacharya and Nix, 1988). In this study, the SWNT composite film was placed on a glass slide. The film thickness is around 35 μm while the maximum indentation depth is less than 1000 *nm*, thus the penetration is less than 3% of the thickness of the film. On the other hand, the nanoindentation hardness test shows that the hardness of the SWNT/substrate is 1 *GPa* and that of substrate is 10 *GPa*, thus the film/substrate combination can be treated as a soft film on a hard substrate. Therefore it is reasonable to assume that the effect of substrate on the measurement of properties of SWNT composite films is negligible, and the previous analysis assuming that the workmaterial is a linearly viscoelastic half space is justified.

6.5 Conclusions

Nanoindentation tests were performed on SWNT/ polyelectrolyte films prepared from layer-by-layer assembly. Using linearly viscoelastic analysis of nanoindentation, relaxation functions in the time domain were determined for in-plane and through-thickness directions, and found to be within 10%, so that the film can be modeled as an isotropic material in the regime of linear viscoelasticity. It was found that the modulus of

the SWNT/ polyelectrolyte film with 4.75% of SWNTs is nearly 2.46 times of the modulus of the neat polyelectrolyte film. Small scale tensile tests were also conducted, and determined the stress-strain relations of the two films. The modulus determined from SSTM for each of the two films is very close to the modulus of the corresponding film from nanoindentation data, indicating the validity of the methods used for linearly viscoelastic materials.

CHAPTER VII

APPLICATION OF NANOINDENTATION TO MEASURING VISCOELASTIC FUNCTION FOR THIN FILMS II: TYMPANIC MEMBRANE

7.1 Introduction

The human middle ear, including tympanic membrane (or eardrum), three ossicular bones (i.e., malleus, incus and stapes), and suspensory ligaments (or muscle tendons), transfers the sound from the external ear canal to cochlea (or inner ear). The tympanic membrane (TM) initiates this acoustic-mechanical transmission by converting the acoustic wave (pressure wave) into vibrations of the middle ear ossicular bones (Gan et al., 2004). The changes of structure and mechanical properties of the TM in middle ear diseases, such as the TM retraction, middle ear infection, otitis media with effusion, and perforation of the TM, can affect directly sound transmission and lead to conductive hearing loss (Gan et al., 2006).

The human TM is a membrane soft tissue composed of a series of collagen fiber layers. Understanding the mechanical behavior of the TM is of considerable importance in the research of ear biomechanics for sound transmission. Efforts have been made to measure the elastic properties of the TM. von Békésy (1960) conducted bending tests on human cadaver TM sample and reported the Young's modulus of 20 MPa. At almost the

same time, Kirikae (1960) measured the elastic modulus by performing longitudinal dynamic tension tests on human TM sample and obtained the Young's modulus of 40 MPa. The data from these tests are often quoted in literature and used in modeling sound transmission in human ears. Recently, Ladak et al. (2004) investigated the response of a cat eardrum to cyclical static pressures, and measured the displacement of eardrums. Fay et al. (2005) presented methods to estimate the elastic modulus of both human TM and cat TM based on composite laminate theory and dynamic measurements. Despite the viscoelastic behavior in TM, to date, the study on viscoelastic properties is very sparse in open literature. Since the human TM is viscoelastic, measurements of elastic properties should be considered as the first-order approximation of the time-dependent behavior of such a membrane material. Need exists to measure directly the viscoelastic properties of the TM. It has been observed that TM collagen fibers are oriented in multiple layers in both radial and circumferential directions (Lim, 1995). Consequently the viscoelastic properties in the through-thickness direction can be different from those in the in-plane direction; and it is also necessary to characterize material properties of TM in at least two different directions.

The human TM is a soft tissue with small dimensions (approximately 60 μm in thickness and 8 mm in diameter), as a result, it is a challenge to use conventional techniques such as tensile tests to determine the viscoelastic properties. With the successful development of nanoindentation techniques for measurements of viscoelastic functions, it becomes possible to measure the viscoelastic properties of human ear tissue using nanoindentation. In this study, measurements were conducted on fresh human cadaver TM samples in both through-thickness (or out-of-plane) and in-plane directions.

The nanoindentation data were analyzed to extract the relaxation moduli of human TM in both directions. The relaxation modulus in the through-thickness direction was determined using the method developed by Lu et al., (2003); the in-plane relaxation modulus was determined by solving an inverse problem in nanoindentation using finite element method (FEM) through correlating the numerical load-displacement data with the nanoindentation data, and by solving an in-plane viscoelastic nanoindentation problem analytically.

7.2 Analytical prerequisites

7.2.1 Measurements of the through-thickness properties using nanoindentation

The schematic of through-thickness nanoindentation using conical and spherical indenters are shown in Fig. 5-1. Methods for measuring through-thickness are presented in Chapter 3 (Section 3.1). Eq. (6-6) will be used for the conversion from creep compliance to relaxation modulus.

7.2.2 Analytical solution for the measurement of in-plane viscoelastic properties of TM under a central concentrated load

When a TM sample is suspended on a circular hole and is subjected to a concentrated load at the center of the hole, its deformation is primarily induced by in-plane bending and membrane stresses, both of which are the results of the in-plane properties of the TM and the applied loads. Solving this viscoelastic problem, in connection to experimental data as obtained for such a situation, can provide an approach to measure the in-plane

viscoelastic function. To this end, the elastic solution is extended to the linearly viscoelastic solution in this section.

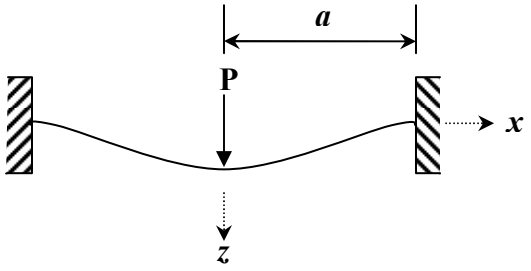

Fig. 7-1 A schematic of a thin plate cconstant rateed at the perimeter and loaded with concentrated force at the center.

Consider a homogeneous, isotropic and linearly elastic film clamped at a circular hole; The film is subjected to a concentrated force at its center, as shown in Fig. 7-1, and the film is thin compared with its diameter, so that it can be modeled as a thin plate. The plate (or film) has thickness *b,* radius *a*; its center is subjected to a force *P* perpendicular to the initial plate plane. For this problem, Timoshenko (1940) derived the following representation for the deflection, *W*, of the plate:

$$W = \frac{Pr^2}{8\pi D}\log\frac{r}{a} + \frac{P}{16\pi D}(a^2 - r^2), \tag{7-1}$$

where *r* is the radial coordinate, and *D* is the flexural rigidity given as

$$D = \frac{Eb^3}{12(1-\nu^2)},$$

with *E* being the Young's modulus of the plate.

The displacement at the center of the plate, determined by setting $r \to 0$ in Eq. (7-1), is

$$W_{\max} = \lim_{r \to 0} \left[\frac{Pr^2}{8\pi D} \log \frac{r}{a} + \frac{P}{16\pi D}(a^2 - r^2) \right] = \frac{Pa^2}{16\pi D}. \tag{7-2}$$

Rewriting Eq. (7-2) leads to

$$E = \frac{3Pa^2(1-\nu^2)}{4\pi W_{\max} b^3}. \tag{7-3}$$

Eq. (7-3) can be used to determine E for an elastic material.

We next extend the Timoshenko solution for the elastic problem to find the solution for a viscoelastic problem. Consider a circular plate composed of a homogeneous, linearly viscoelastic, and isotropic material. The plate is subjected to a concentrated force at its center. This problem has fixed displacement boundary condition so that the correspondence principle between a linearly elastic solution and its corresponding linearly viscoelastic solution applies. Applying the correspondence principle, with the consideration of a constant Poisson's ratio, ν, leads to

$$W_{\max}(t) = \frac{3a^2(1-\nu^2)}{4\pi b^3} \int_0^t J_D(t-\zeta) \frac{dP}{d\zeta} d\zeta, \tag{7-4}$$

where $J_D(t)$ is the uniaxial creep compliance.

When a constant rate loading history, $P(t) = V_0 t$ (V_0 is a constant), is applied. Differentiation of Eq. (7-4) with respect to time t gives

$$J_D(t) = \frac{4\pi b^3}{3a^2(1-\nu^2)} \frac{dW}{dP}. \tag{7-5}$$

This equation can potentially be used to determine the uniaxial creep compliance of the circular plate. However, since the load-displacement data from experiment are discrete data and scattered, differentiation of $\frac{dW}{dP}$ can lead to undesirable errors in the

measurement of $J_D(t)$. To circumvent this difficulty, a curve fitting approach, similar to the method described in Section 3.1 is introduced.

Consider now to represent the uniaxial creep compliance by the generalized Kelvin model,

$$J_D(t) = J_{D0} + \sum_{i=1}^{N} J_{Di}(1 - e^{t/\tau_i}). \tag{7-6}$$

where J_{D0} and J_{Di} are creep numbers for uniaxial creep compliance. Substituting Eq. (7-6) into Eq. (7-4), one has

$$W_{\max}(t) = \frac{3a^2(1-\nu)}{4\pi t^3}\left[(J_{D0} + \sum_{i=1}^{N} J_{Di})P(t) - \sum_{i=1}^{N} J_{Di}\tau_i V_0(1 - e^{-P(t)/(V_0\tau_i)})\right]. \tag{7-7}$$

Fitting Eq. (7-7) into the load-displacement curve obtained from experiments, the best-fit parameters, J_{D0}, J_{Di} and τ_i can be determined, which will then be substituted into Eq. (7-6) to determine the uniaxial creep compliance. Consequently, the Young's relaxation modulus $E(t)$ can be computed by solving the integral equation

$$\int_0^t E(\tau)J_D(t-\tau)d\tau = t. \tag{7-8}$$

7.3 Nanoindentation experiments

An MTS Nano Indenter XP was employed for nanoindentation on human TMs. Both Berkovich and spherical indenters were used in nanoindentation tests. The nanoindenter has a resolution of 0.2 nm in displacement and 50 nN in nanoindentation load. The full capacities in nanoindentation load and displacement are 500 mN and 500 μm, respectively. The Berkovich indenter is modeled as a conical indenter with a half-cone

angle 70.3º that has approximately the same relation between the cross-sectional area and height of the apex as measured from the cross-section, as illustrated in Fig. 5-2.

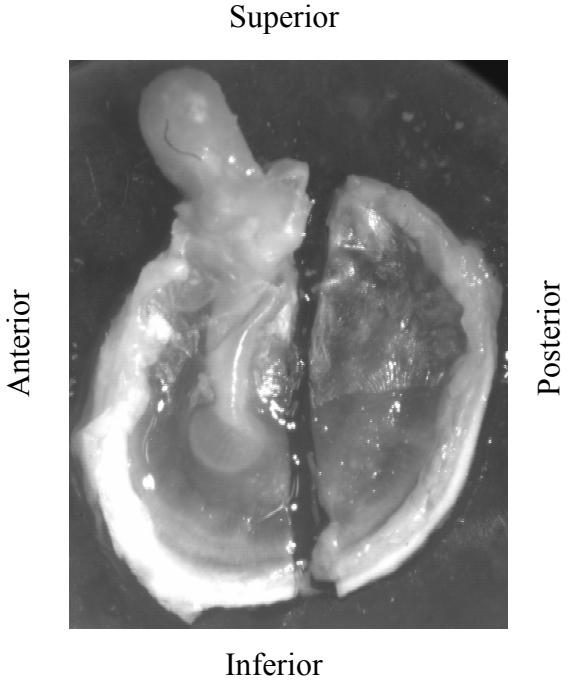

Fig. 7-2 Image of the right TM (medial view).

The specimens of the TM were harvested from fresh or fresh frozen human temporal bones (cadaver ears) through the Willed Body Program at the University of Oklahoma Health Science Center. All the experiments were performed within 6 days after obtaining the bones. Proper informed consent was obtained prior to experiments on TM specimens. The tympanic annulus of the TM was first separated from the bony ear canal, and then taken out with malleus attached and placed in normal saline solution (Fig. 7-2).

Before experiments the TM samples were stored in a freezer at –40 ºC. The TM was defrosted for approximately 20 minutes prior to sectioning using a scalpel. Fig. 7-2 shows a right TM which was cut into two parts, the posterior and anterior parts. A TM sample was mounted on top of a flat aluminum substrate. The mount was designed to allow

nanoindentation tests of TM in both dry and wet conditions. The medial side of the TM is rougher than the lateral side. Nanoindentation was made on the lateral side in all nanoindentation measurements. In physiological condition, the medial side is saturated with fluid so that it remains in wet condition. To emulate this condition, we allowed the medial side of the TM sample in contact with the aluminum substrate. The medial surface of TM sample was in contact with normal saline at its perimeter to remain wet in nanoindentation. Fig. 7-3(a) shows a schematic diagram for sample mounting method for nanoindentation in the through-thickness direction; the bottom of the TM sample was in full contact with the substrate. Fig. 7-3(b) shows a schematic of the method for sample mounting in nanoindentation to determine the in-plane viscoelastic properties. A sample was mounted on an orifice with diameter of around 1.4 mm, and was clamped at the perimeter of the orifice using an Epoxy glue. Care was taken to prevent the epoxy from flowing to the free sample surface to affect the measurements. For testing under low moisture condition, referred to as dry condition later, an initially wet sample was first mounted on the substrate, but no saline was added to the groove located at the perimeter. Consequently, the sample became dry during the preparation process for nanoindentation. For nanoindentation tests under wet condition, saline solution was placed in a circular groove located in contact with the sample to allow the moisture to diffuse to the sample to emulate the normal physiological environment of the TM.

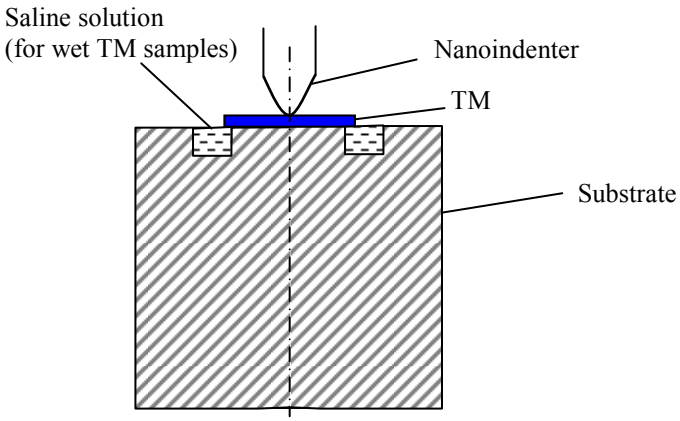

(a)

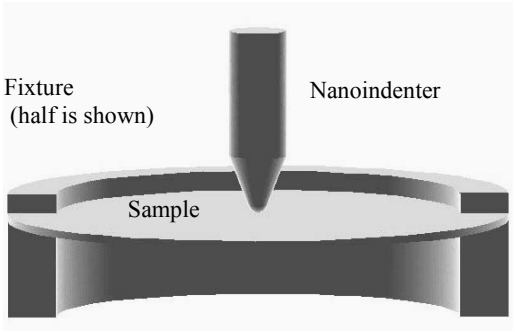

(b)

Fig. 7-3 Schematic of through-thickness and in-plane nanoindentation tests setup (a) through-thickness test; (b) In-plane test.

All nanoindentation tests were conducted at room temperatures (23 ºC) in a thermally insulated chamber. Before each test, a waiting time was used to allow the thermal equilibrium to be reached between the sample and the instrument to reduce the effect of temperature gradient on the properties measurement of the sample. In nanoindentation, the tip drift rate was controlled to be smaller than a limiting value, typically 0.2 nm/s for soft tissues, before nanoindentation was conducted. After the indenter had made contact

with the sample surface, the displacement and load were recorded simultaneously at a sampling rate of five data points per second.

7.4 Results and discussions

7.4.1 Relaxation modulus measured from through-thickness nanoindentation tests

Nanoindentation tests for the measurements of through-thickness properties were conducted on two posterior samples and two anterior samples. Both dry samples and wet samples were tested. The samples in dry condition were harvested from a left ear (male, age 81). The samples in wet condition were from both right and left ears (female, age 50) and a left ear (female, age 63). In all nanoindentation tests, a constant rate loading history was used for loading phase. After the load had reached a peak value, the load was reduced at the same constant rate until it reached zero. For dry samples, a Berkovich indenter was used, and for wet samples a spherical indenter of radius 10 μm was employed, so that the indenter was in good contact with the TM sample. The nanoindentation load-displacement curves for the dry samples are shown in Fig. 7-4 (a). Each curve for two samples is the average from at least three measurements at three locations on the same sample. Fig. 7-5 shows the nanoindentation load-displacement curves for wet samples; three individual results for each of the posterior (Fig. 7-5 (a)) and anterior TM samples (Fig. 7-5 (b)) are included.

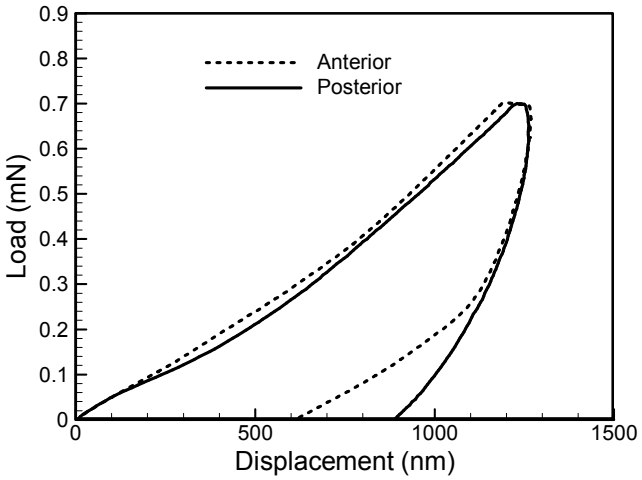

(a)

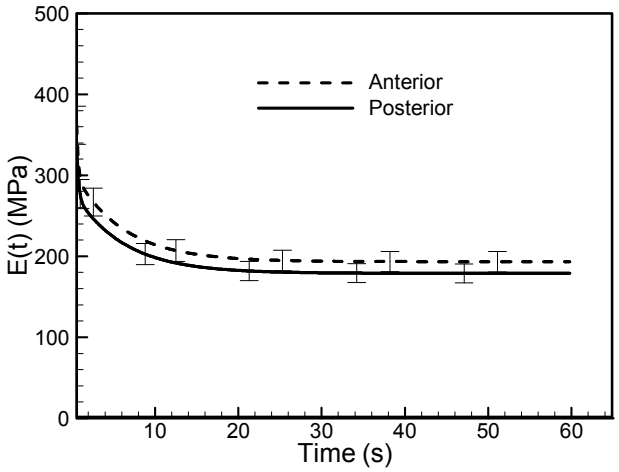

(b)

Fig. 7-4 Through-thickness tests results for dry samples. (a) Load-displacement curves; (b) relaxation modulus $E(t)$.

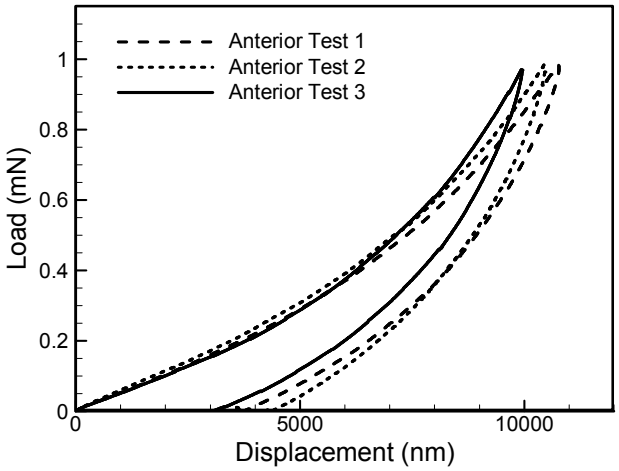
Anterior Test 1
Anterior Test 2
Anterior Test 3
Load (mN)
Displacement (nm)
0
0.2
0.4
0.6
0.8
1
0
5000
10000

(a)

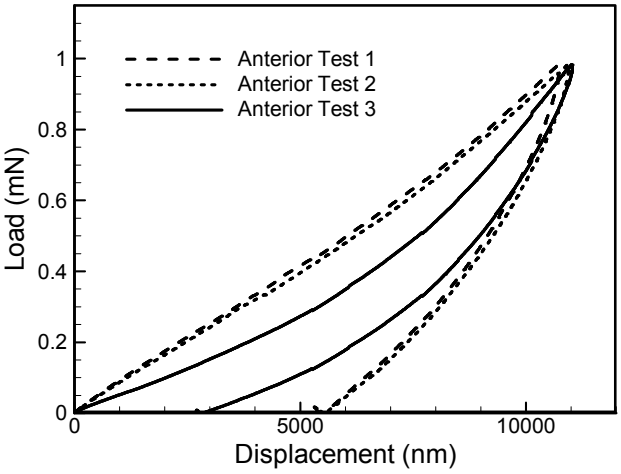
Anterior Test 1
Anterior Test 2
Anterior Test 3
Load (mN)
Displacement (nm)
0
0.2
0.4
0.6
0.8
1
0
5000
10000

(b)

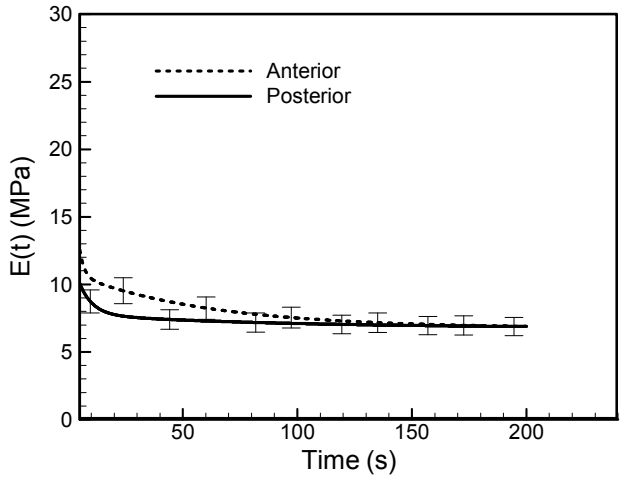

(c)

Fig. 7-5 Through-thickness tests results for wet samples. (a) Load-displacement curves for the Posterior side of TM ; (b) Load-displacement curves for the Anterior side of TM; (c) The measured $E(t)$.

For purpose of measuring the relaxation modulus, Eq. (3-10) is used to fit the load-displacement curves as shown Fig. 7-4 (a) for either a dry posterior or anterior sample. This procedure leads to the best-fit parameters in Eq. (3-10). These parameters are used to calculate the creep compliance using Eq. (3-8). The creep compliance data are then used in Eq. (6-6) to solve for the relaxation modulus as a function of time. The relaxation functions for two samples are averaged, and the average relaxation functions are represented by the generalized Maxwell model. The relaxation modulus for the dry posterior TM is determined as

$$E(t) = 176.7 + 153.5e^{-t} + 67.2e^{-0.1t} \text{ MPa}, \tag{7-9}$$

and the relaxation modulus for the dry anterior TM is

$$E(t) = 190.6 + 142.1e^{-t} + 75.2e^{-0.1t} \text{ MPa}. \tag{7-10}$$

The relaxation functions for both dry anterior and posterior TM are shown in Fig. 7-4(b). The same data analysis procedure is applied to wet posterior and anterior TM samples. After fitting Eq. (3-12) to the nanoindentation load-displacement curves as shown in Fig. 7-5, the best-fit parameters in Eq. (3-8) are determined to calculate creep compliance. The relaxation moduli are subsequently determined using Eq. (6-6). The average relaxation moduli for wet posterior and anterior TM samples are

$$E(t) = 6.8 + 7.6e^{-t} + 3.9e^{-0.1t} + 0.7e^{-0.01t} \text{ MPa}, \tag{7-11}$$

and

$$E(t) = 6.2 + 62.3e^{-t} + 3.4e^{-0.1t} + 3.6e^{-0.01t} \text{ MPa}, \tag{7-12}$$

respectively.

From the results shown in Figs. 7-4 (b) and 7-5(c), it is seen that the relaxation modulus measured for dry TM sample is much higher than that for wet samples. Moreover, the relaxation modulus data in the steady state for dry posterior and wet posterior samples are 176.7 MPa and 6.8 MPa, respectively. This indicates that the mechanical properties of TM depend highly on the moisture content. The wet eardrum used in nanoindentation had the medial side in wet condition and the lateral side in dry condition, to emulate the condition of a TM in normal physiological environment. The relaxation modulus functions for both posterior and anterior TM samples, as shown in Figs. 7-4 (b), 7-5 (c), are very close to each other, indicating that there is no significant difference of mechanical properties between the posterior and anterior sides of the TM in the through-thickness direction.

The TM tissue is in the rubbery-like state (i.e., at a temperature much higher than its glass transition temperature) in normal physiological environment. Consequently the Poisson's ratio is close to 0.5. In data analysis, the Poisson's ratio used is 0.48 for the calculation of the relaxation modulus. It should be noted that, in order to justify the application of viscoelastic contact analysis of the nanoindentation data, the deformations of samples should stay within the linearly viscoelastic regime. Since the TM is a soft membrane tissue, and the maximum displacement in nanoindentation in the through-thickness direction was around 4 μm, it is expected that the deformations in nanoindentation are well within linearly viscoelastic regime.

7.4.2 Finite element analysis of in-plane nanoindentation tests on TM

For measurements of in-plane viscoelastic properties of the TM, the configuration as shown in Fig. 7-3 (b) was used to mount a TM sample. A concentrated force was applied at the center of the thin TM sample. In actual service condition of the TM, both membrane stress and bending stress are present, as expected in the in-plane nanoindentation on the TM. Finite element method is used to simulate the in-plane nanoindentation process; An inverse problem to determine the best-fit parameters is solved in finite element analysis so that FEM results on the load-displacement data are in a good agreement with the nanoindentation load-displacement data; the best-fit parameters are then used to determine the relaxation function of the TM. The procedures for this approach are described herein. FEM analysis is first conducted to simulate the nanoindentation for a TM sample suspended on a circular orifice with the use of initial guessed values of material parameters in the model. Next, the load-displacement data

from simulation are compared with measurement data. If there is no agreement between two sets of the data, the material parameters are adjusted, and this procedure is repeated, until an agreement is reached. The best-fit parameters are then used to determine the relaxation modulus of the TM.

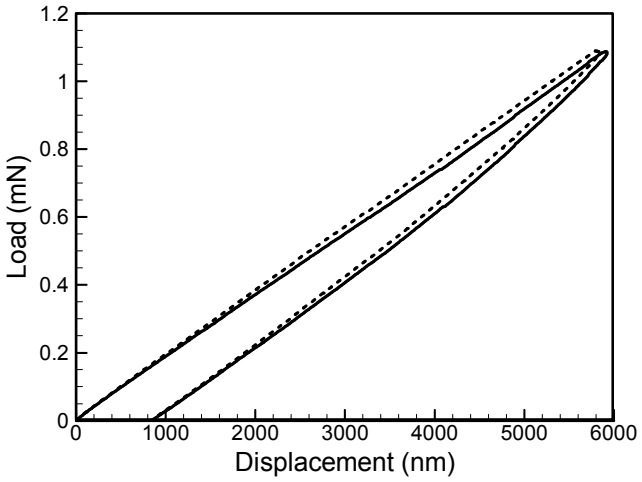

(a)

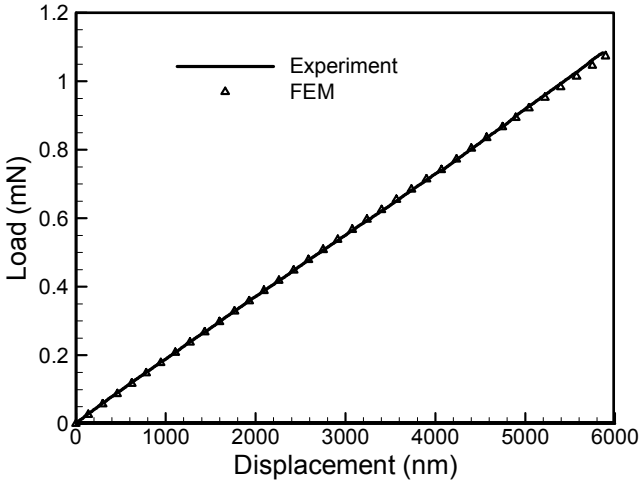

(b)

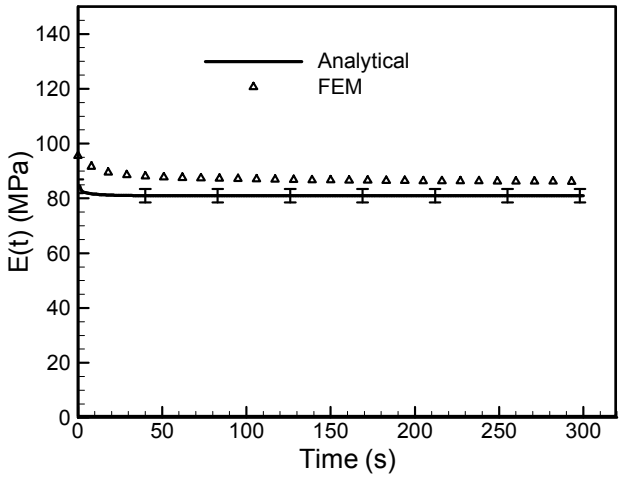

(c)

Fig. 7-6 Results for dry TMs from in-plane nanoindentation tests. (a) Load-displacement curves; (b) Correlation of load-displacement curves between finite element analysis and experiments; (c) $E(t)$ determined from the analytical solution and finite element method.

In the finite element analysis of nanoindentation on a TM sample, the ABAQUS/Standard code (Hibbitt, Karlsson & Sorensen, Inc.) was used. The finite element model for a TM sample consists of 4275 shell elements. A constant rate loading history at a rate of V_0=0.0251 mN/s was applied in nanoindentation. The relaxation modulus used in the finite element modeling is represented by the generalized Maxwell model,

$$\mu(t) = \mu_0 \left[1 - \sum_0^N \mu_i (1 - e^{-t/\tau_i}) \right], \tag{7-13}$$

where μ_0 the instantaneous relaxation modulus, μ_i are relaxation numbers (μ_i<1), and τ_i are relaxation times.

The Poisson's ratio of the TM sample is assumed as a constant value, 0.48. The bulk relaxation modulus function can be computed from shear relaxation modulus using

$$K(t) = \frac{\mu(t)}{6(1+\nu)(1-2\nu)}. \tag{7-14}$$

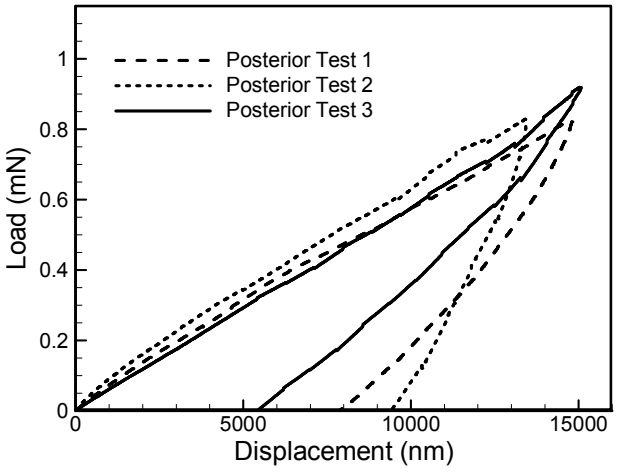

(a)

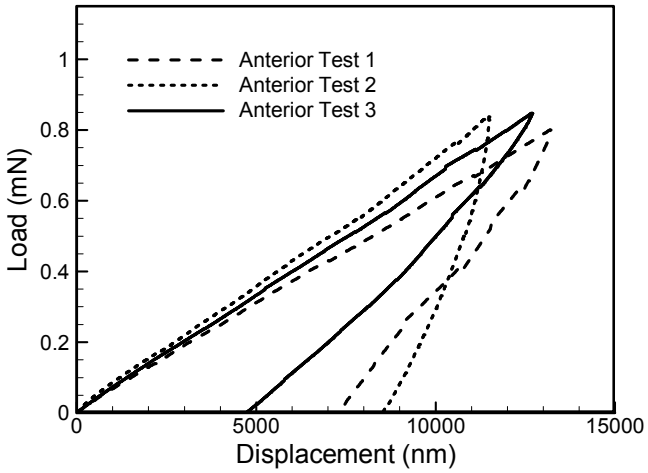

(b)

Fig. 7-7 Load-displacement curves of wet TM from in-plane indentation tests. (a) Sample from posterior side of TM; (b) Sample form anterior side of TM.

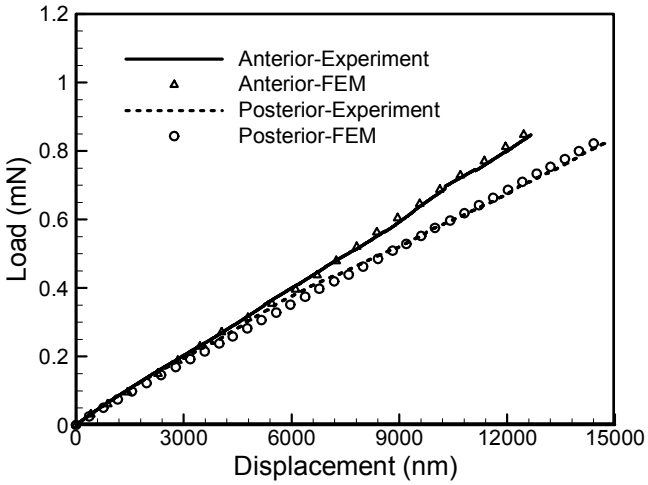

(a)

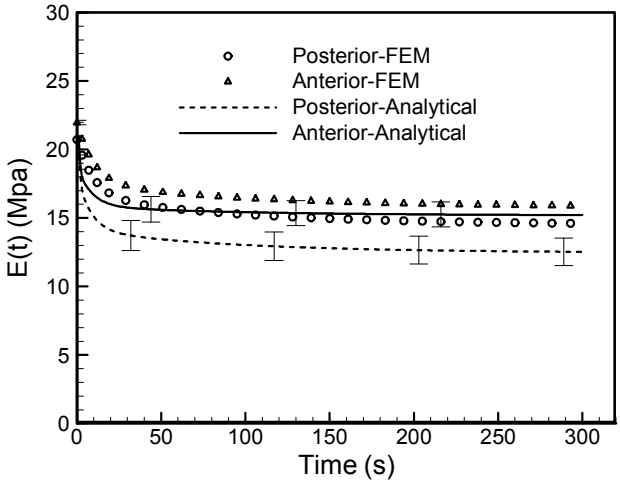

(b)

Fig. 7-8 Results for wet posterior and anterior samples from in-plane nanoindentation tests. (a) Correlation of load-displacement curves between finite element analysis and experiment; (b) $E(t)$ determined from finite element method and the analytical solution.

In-plane nanoindentation tests were conducted on both dry and wet samples. The source of samples has been described in Section 7.4.1. Fig. 7-6(a) shows two load-displacement curves of nanoindentation on dry TM samples. Figs. 7-7 (a) and 7-7 (b) show the load-

displacement curves of nanoindentation on wet posterior and anterior samples, respectively. From the comparison between load-displacement curves of dry and wet samples, it is clear that a wet sample is much softer or more stretchable than a dry sample. It should be pointed that from Figs. 7-6 (a), 7-7 (a) and 7-8(b), all load-displacement curves appear nearly linear during loading stage. However, a close observation shows that the slope changes with displacement; the divergence from linear load-displacement relation is caused by the viscoelastic behavior of the TM.

Nanoindentation processes on wet and dry TM samples are simulated using finite element analysis. For viscoelastic properties as shown in Eq. (7-13), N=2 is used in the Prony series. The parameters, μ_0, μ_i are optimized after comparing the results of load-displacement to the nanoindentation data from measurements; the procedure is iterated until the best correlation between two sets of load-displacement curves is reached. Fig. 7-6 (b) and Fig. 7-8 (a) show the results of correlations between load-displacement curves from finite element analysis and those from nanoindentation tests for the dry TM, and wet TM, respectively. The cross-correlation coefficients for the dry TM, the posterior TM and anterior TM are 0.999817, 0.999414 and 0.9991, respectively, indicating a good agreement between load-displacement data from simulations and the results from measurements. The parameters of μ_0 and μ_i at the best correlation are used to calculate the relaxation modulus. The best-fit parameters of μ_0, μ_1 and μ_2 are 7.0 MPa, 1.4 MPa, 0.7 MPa, respectively, for posterior TM, and are 7.4 MPa, 1.5 MPa, 0.6 MPa, respectively, for anterior TM, and are 290.5 MPa, 20.3 MPa, 8.7 MPa, respectively, for dry TM. Based on Eq. (7-13), uniaxial (Young's) relaxation modulus, $E(t)$, are determined as

$$E(t) = 14.5 + 4.1e^{-0.1t} + 2.1e^{-0.01t} \text{ MPa}, \quad (7\text{-}15)$$

and

$$E(t) = 15.8 + 4.4e^{-0.1t} + 1.8e^{-0.01t} \text{ MPa}, \quad (7\text{-}16)$$

for posterior TM and anterior TM, respectively.

The in-plane Young's relaxation modulus $E(t)$ for dry TM is

$$E(t) = 86.0 + 60.2.3e^{-0.1t} + 25.8e^{-0.01t} \text{ MPa}. \quad (7\text{-}17)$$

Eqs. (7-15) and (7-16) imply that the steady values of relaxation modulus are 14.5 MPa and 15.8 MPa for posterior and anterior TM, respectively. These values are on the same order of magnitude with the elastic modulus of 20 MPa measured by von Békésy (1960). The FEM results of relaxation moduli in the in-plane direction for both wet anterior and posterior TM are shown in Fig. 7-8 (b); the relaxation modulus as measured by nanoindentation for dry TM is shown in Fig. 7-6 (c). As delineated in Fig. 7-8 (b), the relaxation behavior of posterior TM and anterior TM is pronounced, especially at the beginning, while the relaxation behavior of dry TM is not noticeable. Results from finite element analysis show that the relaxation modulus for dry TM (Fig. 7-6 (c)) is much higher than that of wet TM (Fig. 7-8 (b)), indicating again that moisture in the TM plays an important role for the mechanical behavior of TM.

7.4.2 Analytical results of the Young's relaxation modulus from in-plane nanoindentation tests on TM

The analytical solution described in Section 7.2.2 is used to determine the relaxation modulus $E(t)$ of the TM in the in-plane direction using the load-displacement data from nanoindentation. The results of $E(t)$ are obtained for both dry and wet TMs. After fitting the load-displacement curves as shown in Figs. 7-6 (a), 7-7 (a), 7-7 (b) with Eq. (7-7), the parameters are extracted and used in Eq. (7-6) to determine the relaxation modulus $E(t)$ for dry TM using Eq. (7-8),

$$E(t) = 80.9 + 2.0e^{-t} + 1.9e^{-0.1t} \text{ MPa.} \tag{7-18}$$

The measured Young's relaxation modulus $E(t)$ for wet posterior TM is

$$E(t) = 12.5 + 2.6e^{-t} + 4.2e^{-0.1t} + 1.4e^{-0.01t} \text{ MPa;} \tag{7-19}$$

And $E(t)$ for wet anterior TM is

$$E(t) = 15.2 + 2.6e^{-t} + 3.1e^{-0.1t} + 0.5e^{-0.01t} \text{ MPa.} \tag{7-20}$$

The results of $E(t)$ for dry and wet TM samples are depicted in Figs. 7-6 (c) and 7-8 (b) respectively. The analytical results are compared with those measured using finite element analysis. As shown in Figs. 7-6 (c) and 7-8 (b), the analytical results of $E(t)$ are in a good agreement with $E(t)$ determined from finite elements analysis.

It is noted that in finite element analysis of in-plane nanoindentation, both bending stress and membrane stress in TM samples are considered, while in the linearly viscoelastic solution of a circular plate subjected to a concentrated force at its center, for the determination of $E(t)$ as described in Section 7.2.2 it is assumed that the membrane stress is negligible and the bending stress is predominant. The good agreement between results from analytical solution and data determined from FEM analysis indicate that the bending stress induced primarily within the collagen fibers plays a more important role than the membrane stress for the sample dimensions used in this investigation.

It is also noted that, the nanoindentation results of relaxation modulus are obtained based on the analysis of a homogeneous, isotropic viscoelastic contact mechanics problem. The human TM, however, is made of a viscoelastic composite so that it is neither homogeneous nor isotropic. Nonetheless, it is noted that the through-thickness nanoindentation invokes primarily the behavior of the material in the thickness direction so that the relaxation modulus in the thickness direction is representative of the viscoelastic property in the thickness direction. For nanoindentation on the TM clamped at the edge of a circular hole, nanoindentation displacement in the TM is primarily induced by in-plane deformation of the TM so that the in-plane viscoelastic properties play a dominant role in the nanoindentation load-displacement relation. As a first order approximation, the TM could be considered as a transversely isotropic material with the material properties identical in all in-plane directions of a TM sample. Also considering the fact that the underneath a nanoindenter, the indent impression has a dimension on the order of 10 microns so that there are many collagen fibers within an indent. Consequently, the nanoindentation results are in general a representation of the average behavior of TM. Further study is needed to determine all viscoelastic functions when anisotropic characteristics are considered.

Tale 7-1 Results of modulus (steady state) from nanoindentation measurements

	Posterior wet	Anterior wet	Posterior dry	Anterior Dry
Through-thickness modulus (steady state, MPa)	6.8	6.2	176.7	190.6
In-plane modulus, FEM (steady state, MPa)	14.5	15.8	86.0	86.0
In-plane modulus, analytical (steady state, MPa)	12.5	15.2	80.9	80.9

Table 7-1 summarizes the measured relaxation modulus of the TM at steady state using nanoindentation. The results show that the anterior and posterior sides of TM have about the same relaxation modulus in the through-thickness direction. The relaxation modulus in the in-plane direction for wet anterior TM is higher than that for wet anterior as determined from both analytical solution and finite element analysis.

7.5 Conclusions

Nanoindentation techniques were used to determine the load-displacement data representative of mechanical behavior of human TM in both the through-thickness and the in-plane directions. Theory of linear viscoelasticity has been applied to analyze the nanoindentation data. The relaxation modulus of the TM in the through-thickness direction was measured by placing a TM sample on a flat substrate while making nanoindentation into the surface of the TM sample. The relaxation modulus in the

through-thickness direction was extracted from the nanoindentation load-displacement data using an approach developed for viscoelastic materials. The relaxation modulus of TM in the in-plane direction was determined from the correlation between the finite element analysis of nanoindentation and the experiment results; the relaxation modulus in-plane direction was also measured using the analytical solution to the problem of in-plane nanoindentation on TM. A reasonably good agreement has been reached between the Young's relaxation modulus in the in-plane direction from analytical solution and that from finite element analysis. The modulus at the steady state is close to the value as determined by von Békésy (1960); The relaxation modulus of TM in wet condition is much lower than that in dry condition. The in-plane modulus at steady state is determined to be around 6 MPa for wet TM samples, and the through-thickness moduli at steady state are determined to be 177 MPa and 190 MPa for dry posterior and anterior sample, respectively. The results also show that the TM is much stiffer in the in-plane direction than in the through-thickness direction. The in-plane modulus at steady state is 14.5 MPa for the posterior TM, and is 15.8 MPa for the anterior TM sample in wet condition; the in-plane modulus at steady state is 86 MPa for dry TM sample.

CHAPTER VIII.

MEASUREMENTS OF RELAXATION MODULUS USING NANOINDENTATION

For nanoindentation, most commercial nanoindenters use force control, the applied force and the resulting displacement as a function of time are recorded for analysis to determine the material properties. With the use of force control, viscoelastic analysis will give primarily creep functions. In the analysis of stress and deformation, however, the Young's relaxation modulus is often needed. While the relaxation modulus can be converted from creep compliance, using

$$\int_0^t E(\xi)J(t-\xi) = 2(1+\nu)t \tag{8-1}$$

with E(t), J(t) and ν being Young's relaxation function, shear creep function and constant Poisson's ratio, respectively. However, this equation is ill-posed (Nikonov et al., 2005). A small error in shear creep compliance could lead to large error in relaxation modulus. In addition solving this interconversion relation requires creep data at short times, which are often not available as nanoindentation at short times corresponds to small depths at which nanoindentation data are not accurate at all (Lu et al., 2003). Consequently solving relaxation function from the creep compliance data using the interconversion relation would compromise the accuracy of the relaxation function. To characterize

the creep and relaxation behaviors of a linear viscoelastic material, the creep compliance and relaxation modulus are best advised to measure from two separate nanoindentation tests. To date, work is sparse on the nanoindentation measurement of relaxation modulus described by a general viscoelastic model. In this chapter, we present methods to measure the Young's relaxation modulus directly from nanoindentation using constant-rate displacement history. We derive equations to calculate the Young's relaxation modulus for the use of Berkovich and spherical indenters. Nanoindentation results on the Young's relation modulus will be compared with data determined from conventional measurements to examine the approach presented.

8.1. Analytical Prerequisite

In this section, equations are derived for the calculation of Young's relaxation modulus under constant-rate displacement history using either the Berkovich or spherical indenter tip. The diamond Berkovich indenter tip is modeled as a rigid conical indenter tip with a half-cone angel of 70.3° based on the cross sectional area as a function of depth same as that of conical indenter (Fischer-Cripps, 2002). For a rigid conical indenter (shown in Fig. 8-1) indenting into a linearly elastic, isotropic and homogeneous half-space, Sneddon (1965) provided the following load-displacement relation

$$P = \frac{2}{\pi(1-\nu^2)\tan\alpha} Eh^2. \tag{8-2}$$

where P is the indentation force, h the indentation depth, ν the Poisson's ratio, and E the Young's modulus; α is the angle between the half-space and conical generator (Fig. 8-1), and $\alpha = 19.7°$ for the conical indenter as a model for the Berkovich indenter.

For a spherical indenter tip indenting into a linearly elastic, isotropic and homogeneous half-space, a well-known Hertzian contact problem (Hertz, 1881), the indentation load-displacement relation is

$$P = \frac{4\sqrt{R}}{3(1-\nu^2)} E h^{3/2}, \tag{8-3}$$

where R is the radius of the spherical indenter, as shown in Fig. 8-1.

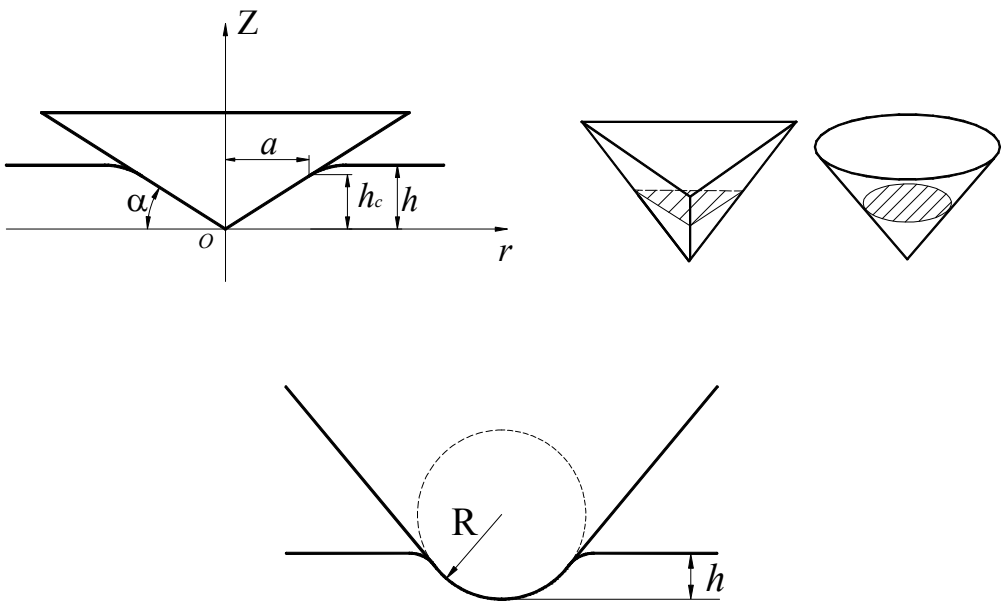

Fig. 8-1 Schematic of conical indentation and the geometries of the Berkovich, conical and spherical indenters

In general, the viscoelastic contact solution can be derived from the corresponding elastic contact problem using the corresponding principle provided that the displacement boundary does not vary with the time. However, in the case of viscoelastic contact problem using either a conical or spherical indenter, the contact area between the indenter

and the workpiece changes with time. Such varying boundary problems cannot be solved using the correspondence principle directly. To solve such varying boundary viscoelastic contact problems, Lee and Radok (1960) provided an effective approach by introducing an appropriate hereditary integral operator for situation where indentation contact area does not reduce with the increasing time. Ting (1966) gave a more general approach to solve viscoelastic contact problems, his approach can be applied to arbitrary history of contact area. The Ting approach is reduced to the Lee-Radok approach when the contact area does not increase with time. Using the Lee-Radok approach for a linearly viscoelastic, isotropic, and homogeneous material with a constant Poisson's ratio ν, the load-displacement relation follows

$$P(t) = \frac{2}{\pi(1-\nu^2)\tan\alpha}\int_0^t E(t-\xi)\frac{dh^2(\xi)}{d\xi}d\xi\,. \tag{8-4}$$

It should be noted that the contact area between the indenter and the half-space does not reduce with time (Lee and Radok, 1960, Ting, 1966).

For indentation at a constant-rate displacement history, namely,

$$h(t) = V_0 t\,, \tag{8-5}$$

with V_0 being a constant indentation velocity, Eq. (8-5) becomes

$$P(t) = \frac{4{V_0}^2}{\pi(1-\nu^2)\tan\alpha}\int_0^t E(t-\xi)\xi d\xi\,. \tag{8-6}$$

Eq. (8-6) is next re-written as

$$\int_0^t E(\xi)(t-\xi)d\xi = \frac{\pi(1-\nu^2)\tan\alpha}{4{V_0}^2}P(t)\,. \tag{8-7}$$

Using the recorded nanoindentation load-displacement data, the relaxation modulus as a function of time can be solved from Eq. (8-7). However, since at the beginning of the contact (such as when the depth is less than 50 nm) the nanoindentation load/displacement data are not accurate, due to limitation in the system as well as the initial plowing effect, Eq. (8-4) cannot be readily used for small displacements. Also solving the integral equation requires iteration from the initial results at low depths or small times, it is not suitable to apply Eq. (8-7) to the nanoindentation data to determine relaxation function. We will provide next two other approaches in an attempt to circumvent the difficulties associated with small depths of nanoindentation.

The first approach is a differentiation approach. We take the derivative of Eq. (8-7) with respect to time t,

$$\int_0^t E(\xi)d\xi = \frac{\pi(1-\nu^2)\tan\alpha}{4V_0{}^2}\frac{dP(t)}{dt}. \tag{8-8}$$

We take next another time derivative on both sides of Eq. (8-8),

$$E(t) = \frac{\pi(1-\nu^2)\tan\alpha}{4V_0{}^2}\frac{dP^2(t)}{dt^2}. \tag{8-9}$$

Eq. (8-9) can also be rearranged into

$$E(t) = \frac{\pi(1-\nu^2)\tan\alpha}{4}\frac{dP^2(t)}{dh^2}. \tag{8-10}$$

It appears that Eq. (8-10) is simple to use. However, due to again the fact that the load-displacement data from nanoindentation experiments are scattering, use of raw nanoindentation data to determine the derivative can induce errors. The errors can be reduced with the use of appropriate curve fitting technique to fit the nanoindentation data into smooth functions such as polynomial/exponential functions or neural network fitting.

Another approach is to consider the correlation between nanoindentation data and the load-displacement relation described by Eq. (8-6) with the use of appropriate viscoelastic model for the material. For the linearly viscoelastic material, we use the generalized Maxwell model for the Young's relaxation modulus

$$E(t) = E_\infty + \sum_{i=1}^{N} E_i e^{-\lambda_i t} , \tag{8-11}$$

where E_∞, E_i are relaxation numbers, λ_i are the reciprocals of relaxation times.

We substitute Eq. (8-11) into (8-6) and find

$$P(t) = \frac{4V_0^{\,2}}{\pi(1-\nu^2)\tan\alpha}\left(\frac{1}{2}E_\infty t^2 + \sum_{i=1}^{N}\left[\frac{E_i}{\lambda_i}(t-\frac{1}{\lambda_i}) + \frac{E_i}{\lambda_i}e^{-\lambda_i t}\right]\right). \tag{8-12}$$

Since $h(t) = V_0 t$, we rewrite Eq. (8-12) into

$$P = \frac{4}{\pi(1-\nu^2)\tan\alpha}\left(\frac{1}{2}E_\infty h^2 + \sum_{i=1}^{N}\left[\frac{E_i}{\lambda_i}(V_0 h - \frac{V_0^2}{\lambda_i}) + \frac{E_i}{\lambda_i}e^{-\frac{\lambda_i h}{V_0}}\right]\right). \tag{8-13}$$

After fitting Eq. (8-13) into the load-displacement curve from nanoindentation tests, the parameters such as relaxation numbers and the reciprocals of the relaxation times can be determined; these parameters can be used in Eq. (8-11) to determine the relaxation modulus.

For a spherical indenter indenting into a linearly viscoelastic, isotropic and homogeneous half-space, using the Lee-Radok (1960) method the nanoindentation load-displacement relation is

$$P(t) = \frac{4\sqrt{R}}{3(1-\nu^2)}\int_0^t E(t-\xi)\frac{dh^{3/2}(\xi)}{d\xi}d\xi . \tag{8-14}$$

Applying displacement history given in Eq. (8-5) to Eq. (8-14) leads

$$\text{to}\int_0^t E(\xi)\sqrt{t-\xi}\,d\xi = \frac{1-\nu^2}{2V_0^{3/2}\sqrt{R}}P(t)\,. \qquad (8\text{-}$$

15)We use, again, the relaxation modulus $E(t)$ represented by the generalized Maxwell model in Eq. (8-11) in Eq. (8-15), and have

$$P(t) = \frac{4}{3}\frac{V_0^{3/2}\sqrt{R}}{(1-\nu^2)}(E_\infty t^{3/2} + \sum_{i=1}^{N}\int_0^t E_i e^{-\lambda_i t}\sqrt{t-\xi}\,d\xi)\,. \qquad (8\text{-}16)$$

Considering $h(t) = V_0 t$, Eq. (8-16) becomes

$$P(t) = \frac{4}{3}\frac{\sqrt{R}}{(1-\nu^2)}(E_\infty h^{3/2} + \sum_{i=1}^{N} V_0^{3/2}\int_0^{h/V_0} E_i e^{-\lambda_i h/V_0}\sqrt{\frac{h}{V_0}-\xi}\,d\xi)\,. \qquad (8\text{-}17)$$

Since the second term on the right-hand side of Eq. (8-17) cannot be integrated analytically, an explicit relation between load and displacement cannot be obtained. Nevertheless, the relaxation function can still be determined with recourse to numerical solution of Eq. (8-17). This is conducted using an algorithm that searches iteratively for the parameters in the generalized Maxwell model in Eq. (8-11) until the load-displacement data from Eq. (8-17) correlates well with the data from nanoindentation measurements; the parameters that give the best correlation are then used in Eq. (8-11) to determine the Young's relaxation modulus $E(t)$.

8.2. Nanoindentation Measurements

An MTS Nano Indenter XP system was used in nanoindentation measurements. The nanoindenter can reach a maximum indentation depth of 500 μm and a maximum load of 500 mN. The displacement resolution is 0.2 nm and the load resolution is 50 nN. Both Berkovich and spherical indenter tips made of diamond were used. The Berkovich

indenter is modeled as a conical indenter with half-cone angel of 70.3 º; the spherical indenter has a radius of 10 μm, with schematic diagram shown in Fig. 8-1.

The materials used in these tests were polymethyl methycrylate (PMMA), polycarbonate (PC) and polyurethane (PU). The PMMA samples were made from the same PMMA plate as used in the work by Lu, et al. (1997) and by Sane and Knauss (2001). The PC specimen was the same as used in the work by Knauss and Zhu (2002). The specimens were stored in an air-tight container. Relaxation data for PMMA and PC were reported in their work. The relaxation function for PU under tensile relaxation was measured as part of this work. The glass transition temperatures are 145 ºC, 105 ºC and 42 ºC for PC, PMMA and PU, respectively. The dimensions of PMMA and PC specimens were 20mm×10mm×5mm, 20mm×20mm×6mm and 12.7mm×10mm×3.2mm, respectively. The PMMA, PC, and PU specimens were annealed at temperatures 5 ºC above their respective glass transition temperatures, and they were cooled down slowly to room temperature at a cooling rate of approximately 5 ºC /hr. Samples were then stored in an enclosed desiccator with approximately 50% relative humidity produced by placing a saturated salt solution in this enclosed environment. The specimens were then mounted on aluminum holders. All specimens had ageing times of nearly 75 hours. The relative humidity in the room was maintained at ~ 50% by the use of both humidifier and dehumidifier.

For the measurements of relaxation function for PU, we used dog-bone shaped specimens in compliance with ASTM standard D638 in uniaxial relaxation tests on an Instron 4202 screw-driven material test system. The specimens have a width of 12.7 mm, thickness of 3.2 mm, and a gauge length of 50 mm. Displacement control was used in

uniaxial relaxation tests. Images of the speckled specimen surface were acquired by a Nikon D70S 6-MP digital camera and were analyzed using the digital image correlation with the implementation of both first order and second order displacement gradients in the deformation mapping functions (Lu and Cary, 2000).

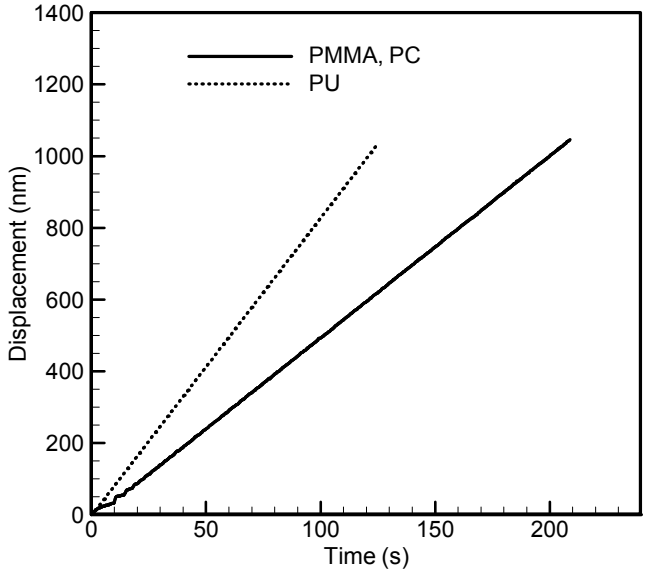

Fig. 8-2 Displacement history for nanoindentation tests of PMMA, PC and PU using Berkovich indenter tip

Nanoindentation tests on all PMMA, PC and PU specimens were conducted in air at room temperature (23 ºC). Each test did not start until the drift rate of the indenter tip had dropped below a set value (typically 0.05 nm/s) to ensure that a thermal equilibrium condition for the specimen and nanoindenter system had been reached. This procedure is necessary as the precision of the nanoindenter depends on the temperature gradient of the instrumentation. After the indenter tip had made contact with the specimen surface, a constant-rate displacement loading history was applied; both the nanoindentation load

and displacement were recorded simultaneously at a sampling rate of five data points per second.

8.3. Results and Discussions

A constant-rate displacement history, realized by controlling the load to reach set displacement value through closed-loop control, was used in all nanoindentation tests. To allow displacement to form a linear function of time, the continuous stiffness module (CSM) has to be activated in nanoindentation. Fig. 8-2 shows the prescribed displacement history used in nanoindentation tests. The resulting load-displacement data using a Berkovich indenter tip are shown in Fig. 8-3 for PMMA, PC and PU.

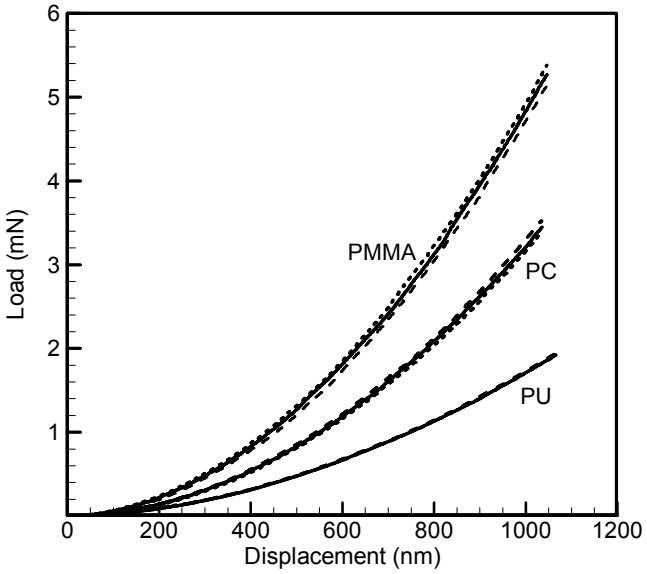

Fig. 8-3 Nanoindentation load-displacement curves for PMMA, PC and PU using Berkovich indenter tip

Since in using Eqs. (8-4) and (8-14) the contact area between indenter and workpiece cannot decrease with time, only the loading portion in the nanoindentation data was

analyzed to determine the relaxation function using the analytical approach described in Section 8.2. Fig. 8-3 shows the load-displacement curves from three tests at different locations for each specimen of PMMA, PC and PU; the consistency of data between different curves for three materials indicates that the repeatability in these nanoindentation tests was high.

We use the curve-fitting approach to fit the nanondentation load-displacement curve with a theoretical curve with the use of a set of perimeters in the generalized Maxwell model as described by Eq. (8-11) when a Berkovich indenter tip was used. The displacement rate for nanoindentation on PMMA was 5 nm/s. Using Poisson's ratio 0.3, Eq. (8-13) was used directly to fit into the nanoindentation load-displacement curve for PMMA as shown in Fig. 8-3. The fitted curve is plotted with the measurement data in Fig. 8-4; the cross-correlation coefficient between the two curves is 0.999987, indicating a good correlation between the two curves. The curve fitting process renders the best-fit parameters in Eq. (8-13). These parameters are then used in Eq. (8-11) to calculate the Young's relaxation function for PMMA as follows

$$E(t) = 2.3343 + 0.1607e^{-0.1t} + 0.2574e^{-0.01t} \text{ GPa.} \tag{8-18}$$

The relaxation function measured from nanoindentation for PMMA as expressed by Eq. (8-18) is shown in Fig. 8-5. Also plotted in Fig. 8-5 is the relaxation curve determined by Lu et al. (1997) from conventional tests for PMMA from the same batch of specimens as used in this study. The comparison between the conventional data and nanoindentation results for PMMA indicates a reasonably good agreement. The maximum discrepancy between the two sets of data is around 9.7%.

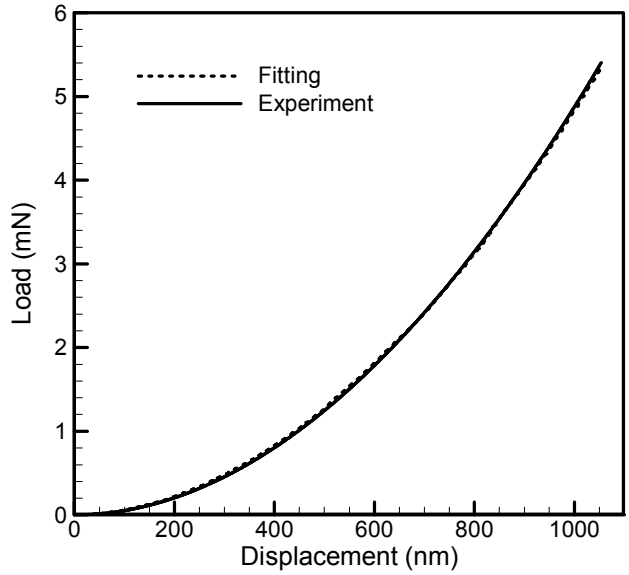

Fig. 8-4 Fitted and measured curves for PMMA using Eq. (8-13) (Berkovich indenter tip)

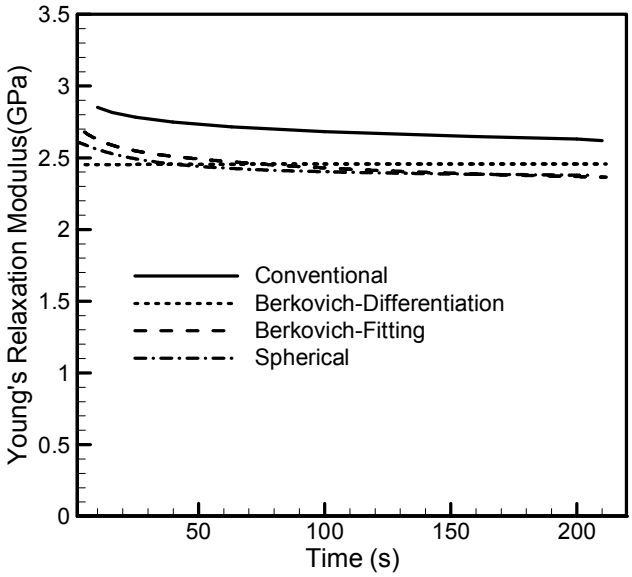

Fig. 8-5 Results of $E(t)$ for PMMA measured from different methods

Eq. (8-13) was also applied to fit into the load-displacement curve of PC as shown in Fig. 8-3. The nanoindentation displacement rate was 5 nm/s. The fitted curve, described by Eq. (8-13) is shown in Fig. 8-6, indicating nearly perfect correlation between the fitting curve

and the curve from nanoindentation test; the cross-correlation coefficient is 0.999992. The parameters used in Eq. (8-13) to obtain the fitted curve as shown in Fig. 8-6 are used in Eq. (8-11) to determine the relaxation function given as

$$E(t) = 1.4531 + 0.0681e^{-0.01t} + 0.1359e^{-0.001t} \text{ GPa.} \tag{8-19}$$

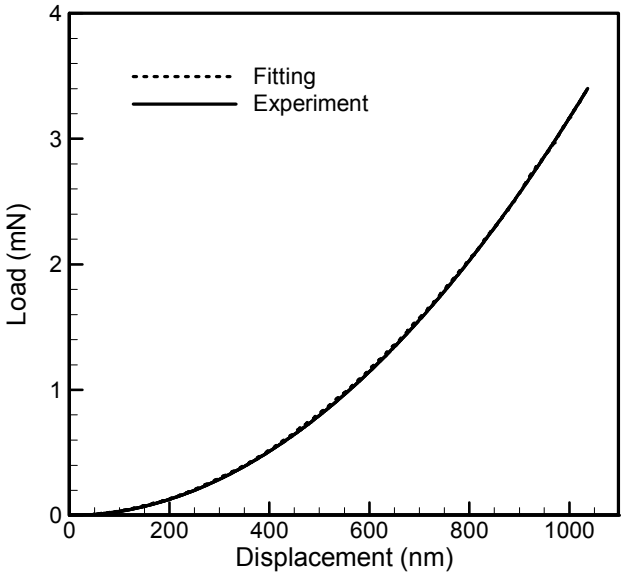

Fig. 8-6 Fitted and measured curves for PC using Eq. (8-13) (Berkovich indenter tip)

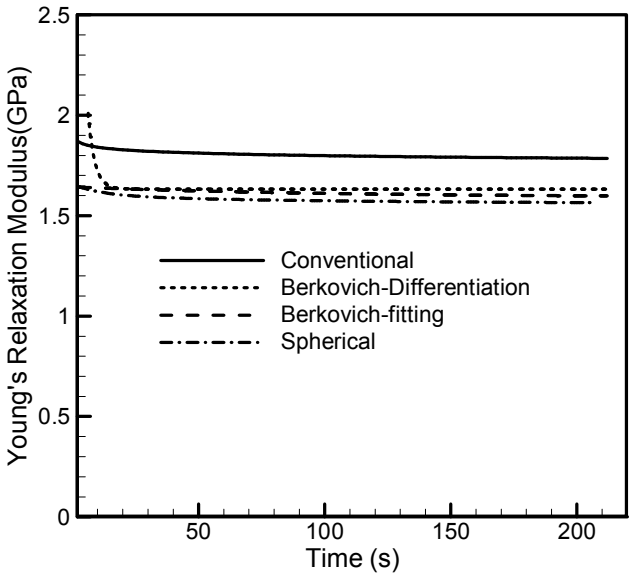

Fig. 8-7 Young's relaxation function $E(t)$ for PC measured from different methods

In the analysis of nanoindentation data for PC, the Poisson's ratio used was 0.3. The Young's relaxation modulus of PC as measured from nanoindentation is shown in Fig. 8-7. For comparison, the conventional relaxation data measured by Knauss and Zhu (2002) were also plotted in Fig. 8-7. The maximum difference between the Young's modulus measured from nanoindentation and the conventional data is 10.5%, indicating a reasonable good agreement.

The curve-fitting method was also applied to analyze the load-displacement data from Berkovich indenter to determine the Young's relaxation modulus for PU. The displacement rate for nanoindentation tests on PU was 8.55 nm/s. Fig. 8-8 shows the fitted curve for the nanoindentation load-displacement data averaged from 3 nanoindentation tests using Berkovich indenter. The cross-correlation coefficient is 0.999977 between the experimental data and the data of fitting using Eq. (8-13). The

best-fit parameters in Eq. (8-13) were substituted into Eq. (8-11) to calculate the Young's relaxation modulus as follows

$$E(t) = 0.5909 + 0.0008e^{-0.1t} + 0.2405e^{-0.01t} \text{ GPa.} \quad (8\text{-}20)$$

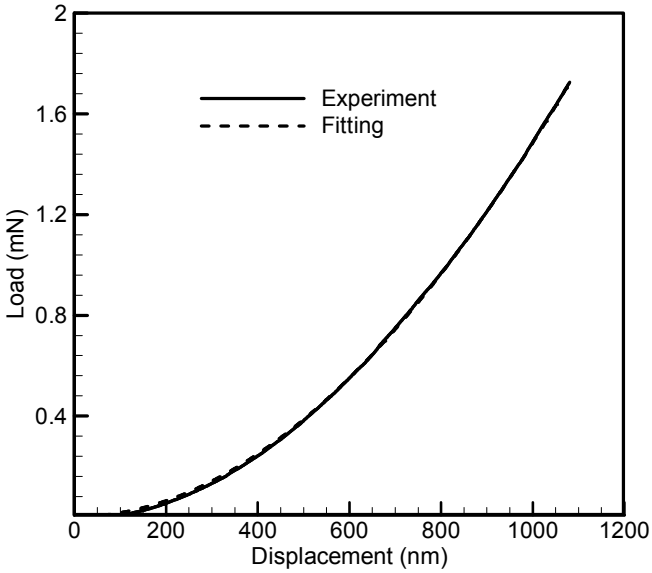

Fig. 8-8 Fitted and measured curves for PU using Eq. (8-13) (Berkovich indenter tip)

The Young's relaxation modulus curves measured by both nanoindentation (using curve-fitting approach) and conventional tests are shown in Fig. 8-9. Fig. 8-9 indicates a good agreement is reached between the data from nanoindentation tests using Berkovich and the conventional data; the maximum error is 9.5%.

Another method for measurements of Young's relaxation function, namely the differentiation method as shown in Eq. (8-10) for Berkovich indenter, was also used to calculate the relaxation modulus for PMMA, PC and PU with the load-displacement data from nanoindentation tests. Due to the fact that raw data from nanoindentation tests are normally scattered even though the curves appear smooth, it is necessary to fit the load-

displacement curves with a smooth function. Since the second-order derivative of the load is required, the computed results of relaxation modulus can depend highly on the function used for fitting the raw load-displacement data. Based on observation, the form of combined polynomial and exponential series was used for the function to fit into the load-displacement data. With the function determined from the curve-fitting process, the relaxation function can then be computed by the use of Eq. (8-10). Using the differential method, the relaxation moduli for PMMA, PC and PU were determined, and are shown in Figs. 8-5, 8-7 and 8-9, respectively.

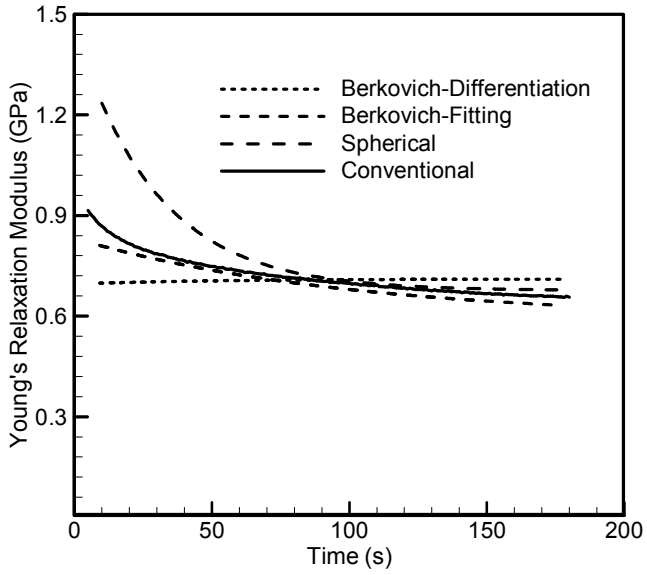

Fig. 8-9 Young's relaxation modulus $E(t)$ for PU measured from different methods

It is noted that, for results of relaxation modulus measured from nanoindentation as shown in Figs. 8-5, 8-7 and 8-9, the relaxation functions measured using the differential method tend to approach the conventional data after passing an initial time, associated with small indentation depths where nanoindentation measurements were not accurate. When indentation depth is larger, the Young's relaxation functions measured from the

differential method approach almost a constant, or simply start with almost a constant. These behaviors do not represent highly the tendency of relaxation behavior of PMMA, PC or PU. This is perhaps due to the error caused by the differentiation of the nanoindentation load data as shown in Eq. (8-10). In comparison the curve-fitting method tends to be more reliable and more accurate than the differentiation method.

In next nanoindentation measurements, a diamond spherical indenter with a tip radius of 10 μm was also used to measure relaxation modulus of the three polymers. A constant-rate displacement history was applied in all nanoindentation tests for PMMA, PC and PU. The displacement rates as measured by the nanoindenter were 4.9 nm/s, 9.7 nm/s, and 6.3 nm/s for PMMA, PC, and PU, respectively. For each polymer, the load-displacement data used for the calculation of the Young's relaxation modulus were the average of at least three nanoindentation tests at different locations. Fig. 8-10 shows the load-displacement curves for the three polymers from nanoindentation using the spherical indenter tip.

Eqs. (8-15)-(8-17) were used to analyze the load-displacement data from spherical nanoindentation. Since relaxation modulus $E(t)$ cannot be solved by differentiating Eq. (8-15), the differentiation method as used for Berkovich indenter is not applicable for spherical indenter. On the other hand, due to the difficulty involved with integration in Eq. (8-17), a closed-form relation between indentation load and displacement cannot be obtained. Consequently, a simplified equation for spherical indenter does not exist for fitting experimental load-displacement data directly to determine the Young's relaxation modulus. However, numerical solution of Eq. (8-17) can still be used to extract the relaxation function by allowing numerical load-displacement data to match the

corresponding nanoindentation data. To this end, an initial guess for these parameters, such as E_i and λ_i, was assumed, and the nanoindentation load data were numerically computed from Eq. (8-17). Next, the numerical load-displacement data were compared to the experimental data; if the correlation is not good enough then the parameters were adjusted and the process would be repeated until a good correlation, indicated by the maximization of cross-correlation coefficient between load-displacement data from Eq. (8-17) and experimental data, was reached. The Young's relaxation modulus for the three polymers determined from curve-fitting approach using spherical indenter are depicted in Fig. 8-10. The cross-correlation coefficients between numerical results of load-displacement data and experimental data are 0.999655, 0.999606, and 0.999019 for PMMA, PC and PU, respectively. Poisson's ratio of PU at room temperature is assumed to be 0.3. With the best-fit parameters used in Eq. (8-11) the Young's relaxation modulus can be determined.

The relaxation modulus data for the three polymers measured from spherical nanoindentation are shown in Figs. 8-5, 8-7 and 8-9, respectively. It is seen from these figures that the relaxation functions measured using Berkovich indenter are generally closer to conventional data than those measured using spherical indenter over relatively long time, especially for PU as shown in Fig. 8-9. The difference between the relaxation modulus measured from spherical indenter is considerably high at initial stage. However, at relatively long time, the relaxation data tend to approach the conventional values; as shown in Fig. 8-9, the error at $t = 200\ s$ is 4.2%. One possible cause for the large discrepancy in relaxation modulus at initial stage is that polyurethane has more pronounced viscoelastic effects at room temperature than both PMMA and PC, making it

difficult to control the displacement to reach constant-rate displacement history at initial stage, possibly causing pronounced hysteresis effect on the measurement though an initial constant displacement rate is nearly reached.

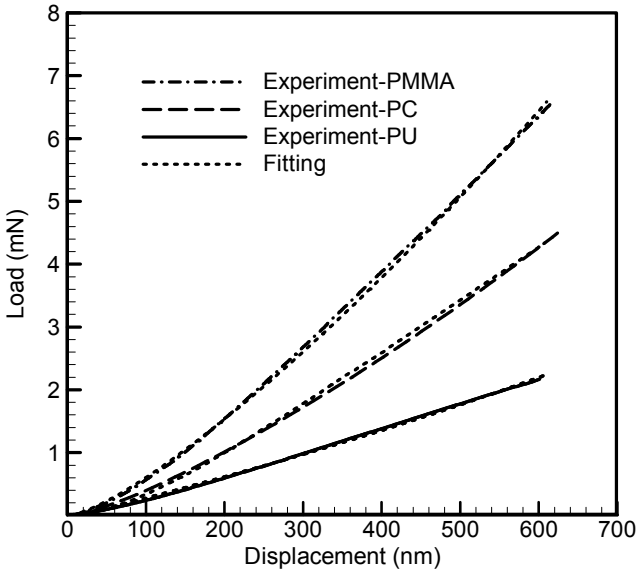

Fig. 8-10 Nanoindentation load-displacement curves for PMMA, PC and PU measured from nanoindentation tests using a spherical indenter tip, plotted with the fitted curve as described by Eq. (8-17).

It is noted that in spherical indentation, in order to apply Eq. (8-14), it is necessary to ensure that indentation displacement is far less than the radius (Giannakopoulos, 2000). The maximum displacement used in this work was less than 700 nm in all spherical nanoindentation with a tip radius of 10 μm; this ensures that the condition of small depth relative to indenter radius is satisfied. The other issue is that the linearity should be maintained, at least approximately. The use of Eq. (8-3) requires that the deformation of viscoelastic materials is within the regime of linear viscoelasticity. Lu, et al. (2003) determined the linearity limits of PMMA and PC through the visualization of indentation impression after the removal of the indenters; the limits of linearity as determined for PMMA and PC are 780 nm and 1123 nm, respectively. In this study, we used

displacement data below those limits for determination of relaxation modulus, and also the good correlations for PMMA and PC between the load-displacement curves of fitting using Eq. (8-13) and the curves from nanoindentation tests satisfied linearity requirement. For polyurethane, since the glass transition temperature is lower than that of PMMA and PC, the specimen behaves more compliant at room temperature than PMMA and PC, it is assumed that within the maximum displacement (around 1000 nm) used for analysis, the deformation would stay within the regime of linearity.

8.4. Conclusions

Methods are presented to measure the Young's relaxation modulus from nanoindentation under a constant-rate displacement history. Both the differentiation method and the curve-fitting method based on the generalized Maxwell model are developed to measure the relaxation functions by nanoindentation with the use of a rigid Berkovich indenter. For spherical nanoindentation, a curve-fitting approach was described to measure the relaxation function. Nanoindentation tests were conducted on three solid polymers, PC, PMMA and PU. The relaxation functions of the three polymers were measured using the presented methods, and were compared with the data measured from conventional tests. The comparisons show a reasonably good agreement between two sets of data for each of the three polymers, thus validating the presented methods in this chapter. The methods presented herein can avoid solving the ill-posed problem for obtaining the Young's relaxation function from the interconversion of creep compliance as measured using load-controlled nanoindentation, and have potential for the application in the measurements of relaxation modulus for viscoelastic materials in small volumes,

such as thin solid films, MEMS, and also can be applied to characterize local viscoelastic behavior of materials in which properties vary with locations, such as bones and nanocomposites.

CHAPTER IX.

SUMMARY

In this dissertation, methods for measurements of Young's modulus and hardness for elastic-plastic properties, viscoelastic functions of polymers using nanoindentation have been reviewed. The problems associated with the measurements of properties of time-dependent materials using methods developed for materials without time dependence are discussed. To address these problems, methods have been developed to measure linearly viscoelastic functions using nanoindentation. These methods are summarized herein.

(1) Methods have been proposed and validated to measure the local surface linearly viscoelastic properties in time domain from the load-displacement relation in nanoindentation, assuming the Poisson's ratio is a constant. Two bulk polymers, namely PMMA and PC, are used in the validation experiments. Based on the solution for a linearly viscoelastic half space subjected to the indentation of an indenter, the linearly viscoelastic material response is analyzed to extract the creep compliance as a function of time using both the Berkovich and spherical indenters. From nanoindentation load and displacement data, the creep functions for PMMA and PC materials were determined from the proposed methods. The load and displacement data under prescribed loading histories that include a constant rate loading and a suddenly applied step load on the material samples

was recorded, results were analyzed using the proposed methods to compute the compliance, and the compliance data were compared with conventional data for validation. The limit of linearity for each of the two polymeric materials was also determined through the observation of the indentation impressions after unloading at different loading values. The creep compliance data measured from nanoindentation have a reasonably good agreement with the data measured from conventional tension and shear tests.

(2) A method to measure the complex compliance (or modulus) in frequency domain for linearly viscoelastic materials is presented using nanoindentation with a spherical indenter. The Hertzian solution for an elastic indentation problem, in combination with a hereditary integral operator proposed by Lee & Radok (1960) for the situation of non-decreasing indentation contact area, was used to derive formulas for the complex viscoelastic functions in the frequency-domain, assuming Poisson's ratio is a constant. The formulas are most suitable for frequencies lower than a frequency limit such that the condition of non-decreasing contact area holds; they are reasonably good approximation at higher frequencies under which decreasing contact area occurs and the Ting (1966) approach for arbitrary contact area history is needed. Nanoindentation tests were conducted on both polycarbonate and polymethyl methacrylate under a harmonic indentation load superimposed on either step or constant rate indentation load, while the resulting displacement under steady state was recorded. The load and displacement data at each frequency were processed using the derived formulas to determine the viscoelastic functions in the frequency-domain. The same materials

were also tested using a Dynamic Mechanical Analysis (DMA) apparatus to determine the complex viscoelastic functions. The DMA and nanoindentation results were compared and found in very good agreement, indicating the validity of the new method presented.

(3) A method has been developed to measure both bulk and shear relaxation functions using nanoindentation. The method removed the assumption of a constant Poisson's ratio, which is a prerequisite for studies in (1) and (2). Two different nanoindenter tips, namely Berkovich and spherical indenters, were used for nanoindentation on polymers. Any two independent viscoelastic functions, such as bulk relaxation modulus and shear relaxation modulus, have different representations in the load-displacement curves obtained with these two indenters so that the two independent viscoelastic functions can be separated and determined. Two polymers, poly(vinyl acetate) (PVAc) and poly(methyl methacrylate) (PMMA) were used in nanoindentation. Nanoindentation measurements were conducted on PVAc above glass transition temperature (Tg) and on PMMA below Tg. Both shear and bulk relaxation functions determined from nanoindentation were found in a reasonably good agreement with data obtained from conventional tests, providing validation of the method presented. The new method can be applied in measurements of two independent viscoelastic functions of very small amounts of materials such as polymeric films on a substrate, heterogeneous materials such as bones, tissues, and nanocomposites.

(4) Nanoindentation used for measurements of viscoelastic properties has been applied to two different materials in small volumes: Single-Wall Carbon

Nanotube (SWNT) composite film and Tympanic Membrane (TM) film. Both in-plane and out-of-plane (through-thickness) viscoelastic properties were measured. For SWNT composite film, uniaxial (Young's) relaxation moduli in two directions were determined using the methods presented in Chapter 3 for measurement of viscoelastic properties in time domain. For TM film, aside from measuring out-of-plane modulus new methods for measuring in-plane modulus were presented which are accommodated to the film of biological tissue; the analytical solution to viscoelastic in-plane indentation problem was applied, and a method based on the correlation between results from finite element analysis (FE) and experimental data from nanoindentation tests was used to determine the in-plane properties. Results showed that data of modulus from the analytical solution are close to those from FE.

(5) Equations were derived to determine the relaxation modulus from nanoindentation tests under a displacement history with a constant rate. Both the differentiation method and the curve-fitting method based on the generalized Maxwell model are presented to measure the relaxation functions by nanoindentation with the rigid Berkovich and spherical indenters. Nanoindentation tests were conducted on three solid polymers, PC, PMMA and PU. The relaxation functions of both polymers were measured using the two presented methods, and were compared to the data measured from conventional shear tests. The comparisons show reasonably good agreement between two different series of data for PMMA, PC and PU, thus validating the presented methods in this paper. The presented methods can avoid solving the ill-posed

problem to obtain relaxation function from the conversion of creep compliance measured using load-control nanoindentation.

REFERENCES

Bhattacharya, A.K., Nix, W.D., 'Analysis of elastic and plastic deformation associated with indentation testing of thin films on substrates,' International Journal of Solids and Structure, 24, 1988, 1287-1298.

Cai, X and Bangert, H, 'Hardness measurements of thin films-determining the critical ratio of depth to thickness using FEM,' Thin Solid Films, 264, 1995, 59-71.

Chen, W., Huang, G., Lu, H., McCready, D.E., Joly, A.G. and Bovin, J., 'Utilizing nanofabrication to construct strong, luminescent materials,' Nanotechnology, 17, 2006, 2595-2601.

Cheng, L., Xia, X., Yu, W., Scriven, L.E. and Gerberich, W.W., 'Flat-punch indentation of viscoelastic material,' Journal of Polymer Science: Part B: Polymer Physics, 38, 2000, 10-22.

Cheng, Y.-T. and Cheng, C.M., 'General relationship between contact stiffness, contact depth, and mechanical properties for indentation in linear viscoelastic solids using axisymmetric indenter of arbitrary profiles,' Applied Physics Letters, 87, 2005, 111914-1- 111914-3.

Cheng, Y.T., Ni, W.Y., Cheng, C.M., 'Nonlinear analysis of oscillatory indentation in elastic and viscoelastic solids,' Physical Review Letters, 97, 2006 Art. No. 075506.

Cheng, Y.T. and Cheng, C.M., 'General relationship between contact stiffness, contact depth, and mechanical properties for indentation in linear viscoelastic solids using axisymmetric indenters of arbitrary profiles,' Applied Physical Letters, 87, 2005, Art. No. 111914.

Deng, T.H. and Knauss, W.G., 'The temperature and frequency dependence of the bulk compliance of poly(vinyl acetate),' Mechanics of Time-Dependent Materials, 1,1997, 33-49.

Doerner, M.F. and Nix, W.D., 'A method for interpreting the data from depth-sensing indentation instruments,' Journal of Material Research, 1, 1986, 601-613.

Emri, I., von Bernstorff, B.S., Cvelbar, R. and Nikonov, A., 'Re-examination of the approximate methods for interconversion between frequency- and time-dependent material functions,' Journal of Non-Newtonian Fluid Mechanics, 129, 2005, 75-84.

Fay, J., Puria, S., Decraemer, W.F., Steele, C., 'Three approaches for estimating the elastic modulus of the tympanic membrane,' Journal of Biomechanics, 38, 2005, 1807-1815.

Ficher-Cripps, A.C., Nanoindentation, Springer, 1999, 1-35.

Gan, R.Z., Feng, B., Sun, Q., 'Three-dimensional finite element modeling of human ear for sound transmission,' Annals of Biomedical Engineering 32, 2004, 847-859.

Gan, R.Z, Sun, Q., Feng, B., Wood, M.W., 'Acoustic-structural coupled finite element analysis for sound transmission in human ear – Pressure distributions,' Medical Engineering & Physics 28, 2006, 395-404.

Giannakopoulos, A.E. 'Strength analysis of spherical indentation of piezoelectric materials,' Journal of Applied Mechanics 67, 2000, 409-416.

Hammond, PT, 'Form and function in multilayer assembly: New applications at the nanoscale,' Review in: Advanced Materials 16, 2004, 1271-1293

Hertz, H., 'Über die beruhrung fester elastischer körper,' Journal für die Reine und Angewandte Mathematik, 92**,** 1881, 156-171.

Hibbitt, Karlsson & Sorensen, Inc., *ABAQUS/Standard 6.4 User's Manual*, 2004.

Hutcheson, S.A. and McKenna, G.B., 'Nanosphere embedding into polymer surfaces: a viscoelastic contact mechanics analysis,' Physical Review Letters, 94, 2005, 076103-1 - 076103-4.

Huang, G., Wang, B. and Lu, H., 'Measurements of viscoelastic functions in frequency-domain by nanoindentation,' Mechanics of Time-Dependent Materials, 8, 2004, 345-364.

Huang, G. and Lu, H., 'Measurements of two independent viscoelastic functions by nanoindentation,' Experimental Mechanics, in press, 2006.

Hunter, S.C., 'The Hertz problem for a rigid spherical indenter and a viscoelastic half-space,' Journal of Mechanics, Physics of Solids, 8, 1960, 219-234.

Hutchings R., Pethica, J.B. and Oliver, W.C 'Measurement of hardness at indentation depths as low as 20 nanometers,' Philosophical Magazine A, 48, 1983, 593-606.

King, R.B, 'Elastic analysis of some punch problems for a layered medium,' Journal of Applied Mechanics, 1987, 1657-1664.

Kirikae, I., The Structure and Function of the Middle Ear, University of Tokyo Press, Tokyo, 1960.

Koike, T., Wadea, H., and Kobayashi, T., 'Modeling of the human middle ear using the finite-element method. Journal of Acoustical Society of America,' 111, 2002, 1306-1317.

Ladak, H.M., Decraemer, W.F., Dirckx, J.J.J., and Funnell, W.R.J., 'Response of the cat eardrum to static pressure: Mobile versus immobile malleus,' Journal of Acoustical Society of America 116, 2004, 3008-3021.

Lee, S. and Knauss. W.G. 'A Note on the determination of relaxation and creep data from constant rate tests,' Mechanics of Time-Dependent Materials, 4, 2000, 1-7.

Lee, E.H. and Radok J.R.M., 'The contact problem for viscoelastic bodies,' Journal of Applied Mechanics 27, 1960, 438-444.

Li, X., Bhushan, B., 'A Review of Nanoindentation Continuous Stiffness Measurement Technique and Its Application,' Materials Characterization, 48, 2002, 11-36.

Lim, D.J., 'Structure and function of the tympanic membrane: A review,' Acta oto-rhino-laryngologica belgica, 49, 1995, 101–115.

Ling, F. F., Lai, W. M. and Lucca, D. A., Fundamental of Surface Mechanics, Springer-Verlag, New York, 2002.

Loubet, J.L., Lucas, B.N., and Oliver, W.C., 'Some measurements of viscoelastic properties with the help of nanoindentation,' San Diego Workshop on Nanoindentation, April, 1995.

Lu, H., Cary, P.D., 'Deformation measurements by digital image correlation: Implementation of a second-order displacement gradient,' Experimental Mechanics, 40, 2000, 393─400.

Lu, H, Huang, G, Wang, B, Mamedov, A. and Gupta, S., 'Characterization of the linear viscoelastic behavior of single-wall carbon nanotube/polyelectrolyte multilayer nanocomposite film using nanoindentation,' Thin Solid Films, 500, 2006, 197-202.

Lu, H., Zhang, X., and Knauss, W.G., 'Uniaxial, shear, and poisson relaxation and their conversion to bulk relaxation: studies on poly (methyl methacrylate),' Polymer Engineering and Science, 37, 1997, 1053-1064.

Lu, H., Wang, B., Ma, J., Huang, G. and Viswanathan, H., 'Measurement of creep compliance of solid polymers by nanoindentation,' Mechanics of Time-dependent Materials, 7, 2003, 189-207.

Lu, H. and Knauss, W. G., 'The role of dilatation in the nonlinearly viscoelastic behavior of pmma under multiaxial stress states,' Mechanics of Time-dependent Materials, 2, 1999, 307-334.

Lucas, B.N., Hay, J.C. and Oliver, W.C., 'Using multidimensional contact mechanics experiments to measure Poisson's ratio,' Journal of Materials Research, 19, 2004, 58-65.

Lucas, B. N., Oliver, W. C. and Swindeman, J. E., 'The dynamic of frequency-specific, depth-sensing indentation testing,' Materials Research Society Symposium, 522, 1998, 3-14.

Lui, J., Rinzler, A.G., Dai, H., Hafner, J.H., Bradley, R.K., Boul, P.J., Lu, A., Iverson, T., Shelimov, K., Huffman, C.B., Rodriguez-Macias, F., Shon, Y.S., Lee, T.R., Colbert, D.T., Smalley, R.E., 'Fullerene Pipes,' Science, 280, 1998, 1253-1256.

Ma, Z. and Ravi-Chandar, K., 'Confined compression: A stable homogeneous deformation for constitutive characterization,' Experimental Mechanics, 40, 2000, 38-45.

Mamedov, A.A., Kotov, N., Prato, M., and Guldi, D.M., 'Molecular design of single-wall carbon nanotube/polyelectrolyte multilayer composites,' Nature Material, 1, 2002, 190-194.

Menard, K. P., Dynamic Mechanical Analysis, CRC, 1999, 61-89.

Nikonov, A., Davies, A.R., Emri, I., "The Determination of Creep and Relaxation Functions from a Single Experiment", Proceedings of 5 th International Conference on Mechanics of Time Dependent Materials, Japan, October, 2005.

Odegard, G.M., Gates, T.S. and Herring, H.M., 'Characterization of Viscoelastic properties of polymeric materials through nanoindentation,' Experimental Mechanics, 45, 2005, 130-136.

Oliver, W.C., Hutchings, R. and Pethica, J.B., 'Measurement of hardness at indentation depths as low as 20 nanometers,' Microindentation Techniques in Materials Science and Engineering, ASTM 889, Blau, P. J. and Lawn, B. R (editors), 1986

Oliver, W.C. and Pharr, G.M., 'An Improved technique for determining hardness and elastic modulus using load and displacement sensing indentation experiments,' Journal of Material Research, 7, 1992, 1564-1583.

Oyen-Tiesma, M., Toivola, Y.A., and Cook, R.F., 'Load-displacement behavior during sharp indentation of viscous-elastic-plastic materials', in Fundamentals of Nanoindentation and Nanotribology II, Baker, S.P., Corcoran, S., Moody, G.N.R. and Cook, R.F. (ed.), Warrendale, PA, 2001, Q.5.1.

Pethica, J.B. and Oliver, W.C., 'Tip surface interactions in STM and AFM,' Physica Scripta, T19, 1987, 61-66.

Pharr, G.M., Oliver, W.C. and Brotzen, F.R., 'On the generality of the relationship among contact stiffness, contact area, and elastic modulus during indentation,' Journal of Material Research, 7, 1992, 613-617.

Popelar, C.F. and Liechti, K.M., 'Multiaxial nonlinear viscoelastic characterization and modeling of a structural adhesive,' Journal of Engineering Materials and Technology, 119, 1997, 205-211.

Radok, J.R.M., 'Visco-elastic stress analysis,' Quarterly of Applied Mathematics, 15, 1957, 198-202.

Riande, E., Diaz-Calleja, R., Prolongo, M.G., Masegosa, R.M. and Salom, C., Polymer Viscoelasticity-Stress and Strain in Practice, Marcel Dekker, Inc., New York, 2000.

Sane, S.B. and Knauss, W.G., 'The time-dependent bulk response of poly(methyl methacrylate),' Mechanics of Time-Dependent Materials 5, 2001, 293-324.

Sneddon, I.N., 'The relation between load and penetration in the axisymmetric Boussinesq problem for a punch of arbitrary profile,' International Journal of Engineering and Science, 3, 1965, 45-47.

Sakai, M. and Shimizu, S., 'Indentation rheometry for glass-forming materials,' Journal of Non-Crystalline Solids, 282, 2001, 236-247.

Shames, I.H. and Cozzarelli, F.A., Elastic and Inelastic Stress Analysis, Taylor & Francis, 1997, 202-239.

Shimizu, S., Yanagimoto, T. and Sakai, M., 'Pyramidal indentation load-depth curve of viscoelastic materials,' Journal of Materials Research, 14, 1999, 4075-4086.

Stauss, S., Schwaller, P., Bucaille, J.-L., Rabe, R, Rohr, Michler, J. and Blank, E., 'Determining the stress-strain behavior of small devices by nanoindentation in combination with inverse methods,' Microelectronic Engineering, 67-68, 2003, 818-825.

Syed, S.A., Wahl, K.J. and Colton, R.J., 'Nanoindentation and contact stiffness measurement using force modulation with a capacitive load-displacement transducer,' Review of Scientific Instruments, 70, 1999, 2408-2413.

Timoshenko, S., 1940. Theory of plates and shells. McGraw-Hill, New York and London.

Ting, T.C.T., 'The contact stresses between a rigid indenter and a viscoelastic half-space,' Journal of Applied Mechanics 33, 1966, 845-854.

Tschoegl, N.W., Knauss, W.G. and Emri, I., 'Poisson's ratio in linear viscoelasticity - a critical review,' Mechanics of Time-Dependent Materials, 6, 2002, 3-51.

Tsui, T.Y., Oliver, W.C. and Pharr, G.M., 'Influence of stress on the measurement of mechanical properties using nanoindentation: Part I. Experimental studies in an aluminum alloy,' Journal of Materials Research, Vol. 11, No. 3, 1996, 752-768.

Vanlandingham, M. R., Villarrubia, J. S., Guthrie, WW. F., and Meyers, G. F., 'Nanoindentation of polymers: An overview,' Macromol. Symposium, 2001, 167, 15-43.

VanLandingham, M.R., Chang, N.-K., Drzal, P.L., White, C.C., and Chang, S.-H., "Viscoelastic characterization of polymers using instrumented indentation - 1. quasi-static testing", Journal of Polymer Science B: Polymer Physics 43, 2005, 1794–1811.

VanLandingham, M.R., Chang, N.-K., Drzal, P.L., White, C.C. and Chang, S.-H., 'Viscoelastic characterization of polymers using instrumented indentation - 1. quasi-static testing,' Journal of Polymer Science B: Polymer Physics, 43, 2005, 1794–1811.

Vlassak, J.J. and Nix, W.D., 'A new bulge test technique for the determination of Young's modulus and Poisson's ratio of thin films,' Journal of Materials Research, 7, 1992, 3242-3249.

Ward, I. M., Mechanical Properties of Solid Polymers, John Wiley & Sons, 1983

Zhu, W. and Knauss, W.G., 'Nonlinear viscoelastic behavior of polycarbonate, I. Response under pure shear,' Mechanics of Time-dependent Materials, 6, 2002, 231-269.

VITA

Gang Huang

Candidate for the Degree of

Doctor of Philosophy

Thesis: MEASUREMENTS OF VISCOELASTIC PROPERTIES BY NANOINDENTATION

Major Field: Mechanical Engineering

Biographical:

Personal Data: Born in Dongyang, Zhejiang Province, P.R. China, on October 30, 1975, the son of Jiayin Huang and Jincha Guo.

Education: Graduated from Dongyang High School, Zhejiang in July, 1993. Received Bachelor of Science degree in Mechanical Engineering from Huazhong University of Science and Technology, Whuan, in June, 1997; received Master of Science degree in Mechanical Engineering from Huazhong University of Science and Technology, Wuhan, in June, 2000; completed the requirements for the Doctor of Philosophy degree with a major in Mechanical Engineering at Oklahoma State University, Stillwater, Oklahoma, in May, 2007 (thesis defended in December, 2006).

Experience: Graduate research assistant and teaching assistant at School of Mechanical and Aerospace Engineering, Oklahoma State University, January, 2002 to December, 2006.

Professional Membership: American Society of Mechanical Engineering, Society of Experimental Mechanics

Name: Gang Huang Date of Degree: May, 2007

Institution: Oklahoma State University Location: Stillwater, Oklahoma

Title of Study: MEASUREMENTS OF VISCOELASTIC PROPERTIES BY NANOINDENTATION

Pages in Study: 157 Candidate for the Degree of Doctor of Philosophy

Major Field: Mechanical Engineering

Scope and Method of Study: Nanoindentation technique was used to characterize the viscoelastic behavior of polymers. Methods were developed to measure linearly viscoelastic properties of polymers using nanoindentation. For polymers with Poisson's ratio assumed as a constant, viscoelastic functions in both time and frequency domains were determined based on the viscoelastic contact analysis of axisymmetric indentation problems. Formulas were derived to calculate the viscoelastic functions such as creep compliance and relaxation modulus using nanoindentation load-displacement data. For highly viscoelastic materials with unknown Poisson's ratio varying with time, a method is developed to measure two independent viscoelastic functions using a Berkovich indenter and a spherical indenter.

Findings and Conclusions: Methods developed in this study were validated on several viscoelastic materials, such as polymethyl methacrylate (PMMA) and polycarbonate (PC), poly(vinyl acetate) (PVAc). The viscoelastic functions measured using the developed methods agree reasonable well with the data from conventional testing methods. The methods were applied to SWNT/polyelectrolyte films and tympanic membrane. Nanoindentation based on these methods have potential for use to measure viscoelastic properties of small amounts of time-dependent materials, such as thin polymeric films, polymer components or coatings on MEMS, and they can also be used to characterize local viscoelastic behavior of materials with properties varying spatially, such as bones and nanocomposites.

ADVISER'S APPROVAL: Dr. Hongbing Lu